UNIVERSITY OF CALIFORNIA, SAN DIEGO

Systems Biology Approach to Understanding the Cellular Stress Response and Disease Mechanisms

A dissertation submitted in partial satisfaction of the
requirements for the degree of Doctor of Philosophy

in

Bioengineering

by

Sindhushree Raghunandan

Committee in charge:

Professor Shankar Subramaniam, Chair
Professor Gaurav Arya
Professor Marcos Intaglietta
Professor Rohit Loomba
Professor Shyni Varghese
Professor Sheng Zhong

2017

The Dissertation of Sindhushree Raghunandan is approved, and it is acceptable in quality and form for publication on microfilm and electronically:

_____

_____

_____

_____

_____

_____

Chair

University of California, San Diego

2017

DEDICATION

To Amma, Pappa, and Deepthi,
Thank you for your constant love and support.

To my grandparents,
For being my first teachers and role models.

TABLE OF CONTENTS

LIST OF ABBREVIATIONS

OSR	Oxidative Stress Response
OS	Oxidative Stress
HP	Hydrogen Peroxide
NAFLD	Non-Alcoholic Fatty Liver Disease
NASH	Non-Alcoholic Steatohepatitis

LIST OF TABLES AND FIGURES

ACKNOWLEDGMENTS

The work presented in this dissertation is a product of many meaningful professional collaborations and personal relationships.

I would first like to thank my advisor, Professor Shankar Subramaniam for his invaluable guidance, support, and patience throughout my doctoral studies. It has been a pleasure and a privilege to learn from such a talented scientist and kind human being. Thank you!

I would like to thank Professor Zhen Chen for being a brilliant mentor and for her guidance on the work presented in Chapter 2. I am also supremely grateful for Dr. Ebonee Williams, whose coaching has been instrumental in my personal and professional development. Additionally, I would like to thank my committee members Drs. Intaglietta, Loomba, Varghese, Arya, and Zhong for their feedback throughout the development of my dissertation.

I would like to thank all the members, past and present, of the Subramaniam Lab for their constant support, contagious curiosity, and catalytic discussions throughout my graduate studies. Thanks to Carol Kling for being a wonderful source of encouragement and expert administrative assistance.

Finally, I would like express my deepest gratitude to my family and friends who believe in me, even when I find it difficult to believe in myself. I am eternally grateful to my parents (Ramadevi Raghunandan and Raghunandan Harithas) and my grandparents (Shantha Venkataraman, Janaki Devi Krishnamurti, Karur Ramarao Venkataraman, and Doddabalapur Krishnamurti) whose commitment to seeking knowledge and unwavering belief in me has been a bottomless source of inspiration and courage in my life. I am especially grateful to my mother for being a role model of curiosity, resilience, and optimism, and my father for always believing in me and encouraging me to take the road less traveled. I would like to thank my sister, Deepthi Raghunandan, for being my coach and cheer leader and for teaching me to always be open to new

experiences. Thank you to my closest friends, Apoorva Weber, Caitlin Miller, Adelia Sabintsev, Bao Nguyen, and Priya Nayak for being fiercely loyal friends and a wonderful support system.

I would also like to acknowledge all of the co-authors of the work presented in Chapter 2 and 3. Chapter 2 is a nearly identical version of the manuscript in submission, titled "Spatiotemporal Resolution in Oxidative Stress Response in Endothelial Cells Reveals a Novel Role for HMOX-1" Sindhushree Raghunandan, Srinivasan Ramachandran, Eugene Ke1, Yifei Miao, Ratnesh Lal, Zhen Chen, Shankar Subramaniam. The author of this dissertation was the primary contributor to the work presented in this chapter. The authors would like to thank Dr. John Shyy for his generous use of the laboratory facilities and for providing, along with Dr. Shu Chien, valuable insights into shear stress responses in endothelial cells. We would like to acknowledge Dr. Janice Huss and Angie Hamilton (from the Department of Molecular & Cellular Endocrinology at City of Hope) for their technical support. Finally, we would like to acknowledge Marcy Martin, Jian Kang, and Yun-Ting Wang for their valuable insights and guidance on experimental methods.

Chapter 3 is a version of the manuscript in preparation tentatively titled "The Role of p62 and NBR1 in Liver Disease". Sindhushree Raghunandan, Shakti Gupta, Mano Maurya, Shankar Subramaniam, Maria Diaz-Meco, Jorge Moscat,. The author of this dissertation was the primary contributor to the work presented in this chapter.

VITA

2007 – 2011	University of Maryland, College Park
	Bachelor of Science, Bioengineering
2011 – 2017	University of California, San Diego
	Doctor of Philosophy, Bioengineering

TEACHING EXPERIENCE

University of California, San Diego

Teaching Assistant

BENG101: Foundations of Medical Imaging

Bioengineering Design Project

PUBLICATIONS

Duran A, Hernandez ED, Reina-Campos M, Castilla EA, Subramaniam S, **Raghunandan S**, Roberts LR, Kisseleva T, Karin M, Diaz-Meco MT, Moscat J. p62/SQSTM1 by Binding to Vitamin D Receptor Inhibits Hepatic Stellate Cell Activity, Fibrosis, and Liver Cancer. Cancer Cell. 2016

Umemura, Atsushi, Feng He, Koji Taniguchi, Hayato Nakagawa, Shinichiro Yamachika, Joan Font-Burgada, Zhenyu Zhong, Shankar Subramaniam, **Sindhu Raghunandan**, Angeles Duran, Juan F. Linares, Miguel Reina-Campos, Shiori Umemura, Mark A. Valasek, Ekihiro Seki, Kanji Yamaguchi, Kazuhiko Koike, Yoshito Itoh, Maria T. Diaz-Meco, Jorge Moscat, and Michael Karin. "P62, Upregulated during Preneoplasia, Induces Hepatocellular Carcinogenesis by Maintaining Survival of Stressed HCC-Initiating Cells." Cancer Cell 29.6 (2016)

Curtis, J. E., **Raghunandan, S.**, Nanda, H., and S. Krueger. SASSIE: A program to study intrinsically disordered biological molecules and macromolecular ensembles using experimental scattering restraints. Computer Physics Communications, 2011

Datta, S. A. K., Heinrich, F., **Raghunandan, S.**, Krueger, S., Curtis, J. E., Rein, A., and H. Nanda. HIV-1 Gag extension: conformational changes require simultaneous interaction with membrane and nucleic acid. Journal of Molecular Biology, 2011

Krueger, Susan, Jae-Ho Shin, **S. Raghunandan**, J. Curtis, Z. Kelman. "Atomistic Ensemble Modeling and Small-Angle Neutron Scattering of Intrinsically Disordered Protein Complexes: Applied to Minichromosome Maintenance Protein." Biophysical Journal, 2011

ABSTRACT OF THE DISSERTATION

Systems Biology Approach to Understanding the Cellular Stress Response and Disease Mechanisms

by

Sindhushree Raghunandan

Doctor of Philosophy in Bioengineering

University of California, San Diego, 2017

Professor Shankar Subramaniam, Chair

Cellular stress, which can be induced by multiple factors (e.g. excess reactive oxygen species, ionizing radiation, cellular dehydration, excess shearing forces etc.), can result in damage to DNA, proteins, or lipids leading to deleterious cell phenotypes. Cells are programmed to respond to stress by 1) sensing and rectifying factors that lead to cell damage, 2) repairing damage to macromolecules, and 3) appropriately regulating the cell cycle and DNA replication processes, when necessary, to accomplish (1) and (2). While acute stresses lead to the direct activation and expression of acute phase proteins, sustained stresses cause persistent dysfunctions, which then lead to the activation of complex transcriptional and epigenetic programs. The induction of the cellular stress response can result in one of three phenotypic outcomes: 1) cell death, 2) return to homeostasis, or 3) the establishment of an altered state (such as senescence or cancer). Cell fate

decisions are largely dependent the degree and duration of stress, the cell type, and ultimately the degree of damage to DNA and other macromolecules.

The primary objective of this research is to characterize response to two different types of cellular stress (oxidative stress and high-fat diet induced toxicity) using a systems biology approach and, in doing so, to identify biomarkers and response mechanisms for each type of stress. The first model of stress (i.e. oxidative stress in endothelial cells) is a study of stress response *in vitro*. The use of dose and time-dependent measurements reveal key inflection points and mechanisms of stress response. The mechanisms thus elucidated are validated through pharmacological and genetic perturbations followed by phenotypic assays that define the cell fates. The second model of stress response (i.e. a mouse model of high-fat diet induced liver toxicity) exemplifies many of the paracrine regulators of stress response. The comparison to human data reveals the potential for using mouse models in understanding human diseases. In both studies, the combined use of transcriptomic data with existing databases of protein interaction networks and transcription-factor target information provides a global perspective on stress response, which is critically important to consider when designing effective therapeutics with limited off-target effects.

CHAPTER 1 : INTRODUCTION

Cellular stress is any chemical or mechanical perturbation that directly or indirectly disrupts normal cellular functions. While isolated instances of stress can be contained and resolved, persistent or widespread cellular dysfunction drives aging and disease. As such, it is critically important to understand the nuances of cellular stress in order to characterize, treat, and prevent diseases.

1.1 Types of Stress

Stress can be broken down into two categories: mechanical and biochemical. Mechanical stress, as the name implies, includes any physical perturbation of proteins embedded in the plasma membrane or the distortion of the membrane itself. The altered structure of membrane proteins informs changes in their function. Due to the cell-cell contact structures such as adherens junctions (formed by cadherins) and focal adhesions (formed by integrins), any mechanical stress experienced by one cell can be communicated to the surrounding tissue (Chanet and Martin, 2014). Biochemical stress involves the damage of proteins, lipids, or DNA by molecular compounds (e.g. reactive oxygen, salts, heavy metals, radiation, environmental toxins) resulting in abnormal cell function (i.e. changes in metabolism, cell signaling, DNA replication etc.) (Fulda et al., 2010) (Kültz, 2005).

1.2 Anatomy of Stress Response

The anatomy of stress response is common across biochemical and mechanical stresses. The stressor is detected by sensors that are embedded in the plasma membrane or present intracellularly. Once activated, sensors interact with and modulate the activity of signal transduction proteins. Stress signals are transduced by signaling pathways such as JNK/MAPK/ERK (Kyriakis and Avruch, 2001), JAK/STAT (Rawlings et al., 2004), PI3K/AKT

(Martini et al., 2014) (Hemmings and Restuccia, 2012), TGFβ/SMAD (Weiss and Attisano, 2013) (Massagué, 2012), FAS/FADD (Flusberg and Sorger, 2015), and G-protein coupled receptors (Katritch et al., 2013) (Kroeze et al., 2003). The sequential activation of proteins transmits the signal from its origin to transcription factors or epigenetic effector proteins, which are responsible for altering gene expression (Kültz, 2005) (Sabounchi et al., 2015) (de Nadal et al., 2011).

The integrated stress response is the convergence of various stress signals (i.e. hypoxia, viral infection, glucose or amino acid deprivation, the ER unfolded protein response, or oncogene activation) on the phosphorylation of eIF2α, which decreases protein synthesis and induces ATF4 expression (Pakos-Zebrucka et al., 2016). Mitochondrial stress can also contribute to the integrated stress response (Quirós et al., 2016).

1.3 Potential Outcomes of Stress/Stress Response

The type, degree, and duration of the stress as well as nature of the stress response can guide the cell to one of many outcomes: homeostasis, apoptosis, autophagic-cell death, pyroptosis, necroptosis, necrosis, or senescence. Interestingly, the successful induction of a stress response followed by the return to homeostasis can precondition cells such that they are better equipped to respond to the same stress in the future (Acar et al., 2005) (Flusberg and Sorger, 2015) (Medzhitov et al., 2012). For example, preconditioning with death ligands (i.e. FASL and TNFα) attenuate ischemic injury (Jang et al., 2008). If the cell is unable to clear the source of stress or the resulting damage, apoptosis or necrosis is initiated.

Apoptosis is the process of programmed cell death initiated by intrinsic signals (i.e. activation of pro-apoptotic BCL2, mitochondrial cytochrome C release, and activation of caspases) or by extrinsic signals (i.e. activation of death receptors by extracellular death ligands and caspase activation). Ultimately, activated caspases result in the proteolytic cleavage of a wide array of

proteins associated cell structure, cell cycle, DNA replication/repair, and viral proteins among others, effectively halting cellular function and preventing pathogenic propagation (Fischer et al., 2003) (McIlwain et al., 2013) (Chang and Yang, 2000).

Necrosis is another process of programmed cell death that results in the release of a cell's contents into the surroundings to elicit an inflammatory response. While necrosis had previously been considered an unregulated process, recent evidence suggests that Parp1, NADPH oxidases, calpains, and receptor interacting protein kinases are involved in regulating the disintegration of the plasma membrane to facilitate the release of cellular contents (Ouyang et al., 2012) (Kanduc et al., 2002) (Berghe et al., 2014). Similarly, receptor mediated activation of RIP3K induces MLKL-mediated permeabilization of the plasma membrane in a process known as necroptosis (Tait et al., 2014).

Lesser known forms of cell death such as autophagic cell death and pyroptosis involve the activation of autophagic vacuoles and pro-inflammatory caspase-1, respectively. One potential link between autophagy and apoptosis exists in the inhibition of beclin-1 by anti-apoptotic members of the BCL2 family (i.e. BCL2 and BCLXL) (Liu and Levine, 2015) (Sinha and Levine, 2008). While specific mechanisms by which autophagy or caspse-1 initiate cell death have not yet been elucidated, they point to potentially novel avenues of crosstalk between cell death, inflammation, and autophagy (Tait et al., 2014).

Senescence is a semi-dormant cellular state in which the cell cycle is arrested (by CDKN1A/p21 or CDKN2A/p16) while certain metabolic and secretory functions are maintained (Tomimatsu and Narita, 2015). It is induced as a result of damage (i.e. DNA damage or oxidative stress) or during development. The initiation of senescence has been shown to prevent cancer progression, limit fibrosis (in the liver, kidney, cardiac muscle, and skin), protect against

atherosclerosis, prevent pulmonary hypertension among other protective functions. Contrastingly, senescence in adipocytes has been shown to promote obesity (Muñoz-Espín and Serrano, 2014) (Salama et al., 2014) (Campisi, 2013).

1.4 Paracrine Stress Signaling

Damaged tissue, marked by cell death or senescent cells can initiate the immune response in order to signal for clearance by immune cells (Rock and Kono, 2008) (Muñoz-Espín and Serrano, 2014) (Tchkonia et al., 2013) and prevent collateral damage. This process is coordinated in two phases: the non-specific response (innate immunity), which is the first line of defense, and the specific response (adaptive immunity). Damaged cells release pro-inflammatory markers such as IL1, IL6, TNFα, IL17, interferons, complement proteins, and prostaglandins (Turner et al., 2014) in order to facilitate vasodilation, increase permeability of capillaries, control tissue swelling by inducing clotting factors, initiate the migration of granulocytes/monocytes, and activation of resident macrophages. Macrophages and neutrophils are drawn to the source of chemokine signaling, where they phagocytose the dead cells to prevent the transfer of stress to the neighboring healthy cells (Erwig and Henson, 2008) and secrete ROS to kill pathogens (Chen and Junger, 2012) (Birben et al., 2012). Cell surface proteins can initiate (e.g. C1q, ICAM3, ox-LDL like moiety, calreticulin and annexin I) and prevent (e.g CD47, CD31, CD300a) clearance by immune cells. Interestingly, due to the toxic effects of ROS, the recruitment of immune cells may also cause further tissue damage and drive disease progression (Campisi et al., 2014). In such cases, where the clearance of stress leads to an amplification of tissue damage and chronic stress response, the adaptive immune response is activated. The initiation of the adaptive immune response consists of antigen presentation by damaged tissue cells or dendritic cells that have phagocytosed damaged cells (Steinman and Hemmi, 2006). Upon activation Th1 and Th2 cells secrete cytokines and

amplify the adaptive response. The activation of cytotoxic T-cells results in the targeted destruction of pathogenic or tumorigenic cells.

1.5 Systems Biology Methods in Characterizing the Cellular Stress Response

As mentioned above, the sensing of stress leads to the transduction of the stress response signal, which converges on transcriptional changes that ultimately determines the balance between pro-death and pro-survival proteins. During the course of the stress response or in conjunction with the initiation of apoptosis/senescence, the immune system can be recruited to clear marked cells. The overwhelming complexity in the combinatorial effects of stress-related sensors, transducers, and transcription factors in addition to layers of regulation introduced by paracrine signaling from multiple cell/organ types informs the application of systems biology methodology to characterize the cellular stress response. Systems Biology is the study of a biological system through unbiased measurement and characterization of its subunits (Chuang et al., 2010).

The advent of high-throughput technologies such as RNA-sequencing has provided a global perspective on transcriptional changes following the introduction of stress (de Nadal et al., 2011). The growth of text-mining to identify pleiotropic transcriptional regulatory proteins along with the careful curation of functional validation studies for those putative protein across varying cell types and disease conditions has granted a wealth of regulatory information. These findings have been summarized in databases such as TRANSFAC (Matys et al., 2006), CHEA (Lachmann et al., 2010), and ENRICHR (Kuleshov et al., 2016). Similarly, yeast-two-hybrid studies have paved the way for protein-protein interaction, which has been expanded by data-mining into mammalian protein-protein interaction networks. Finally, the recent advances characterizing epigenetic regulation inform our understanding of the transient regulation of gene expression by protein modification of histones and DNA.

Another aspect of Systems Biology is seen in the experimental design of the studies presented in this thesis. As discussed in the first chapter, use of dose- and time-dependent measurements captures the appropriate resolution necessary to identify and characterize key inflection points in stress response. In the second chapter the introduction of tissue specific ablation of key genes facilitates analysis of the coordination of stress by multiple cell types.

1.6 Gene Inactivation & Stress Response

A central strategy in assessing transcriptional programs of stress response involves the attenuation or complete inactivation of genes encoding stress-mediating proteins. In vitro studies rely on the successful transfection of siRNA to interfere with or inhibit the translation of specific mRNA associated with the gene of interest (Wilson and Doudna, 2013). The advent of the CRISPR-Cas system has advanced our ability to edit the genome resulting in an increased efficiency of gene ablation (Mohr et al., 2014). Mouse models for heterozygous or homozygous ablation of genes are generated through homologous recombination of the mutated gene. Tissue specific ablations are introduced using the Cre-LoxP system (Hall et al., 2009).

1.7 Thesis Summary

The following chapters of the thesis examine two distinct cases of stress response. Chapter 2 focuses on oxidative stress response in endothelial cells and Chapter 3 examines the role of autophagy proteins, SQSTM1 (also known as p62) and NBR1, in shaping the high-fat diet mediated progression of liver dysfunction from steatosis to cancer.

1.8 References

Acar, M., Becskei, A., and van Oudenaarden, A. (2005). Enhancement of cellular memory by reducing stochastic transitions. Nature 435, 228–232.

Berghe, T.V., Linkermann, A., Jouan-Lanhouet, S., Walczak, H., and Vandenabeele, P. (2014). Regulated necrosis: the expanding network of non-apoptotic cell death pathways. Nature Reviews Molecular Cell Biology 15, 135–147.

Birben, E., Sahiner, U.M., Sackesen, C., Erzurum, S., and Kalayci, O. (2012). Oxidative Stress and Antioxidant Defense. World Allergy Organ J 5, 9–19.

Campisi, J. (2013). Aging, cellular senescence, and cancer. Annu. Rev. Physiol. 75, 685–705.

Campisi, L., Cummings, R.J., and Blander, J.M. (2014). Death-Defining Immune Responses After Apoptosis. Am J Transplant 14, 1488–1498.

Chanet, S., and Martin, A.C. (2014). Mechanical Force Sensing in Tissues. Prog Mol Biol Transl Sci 126, 317–352.

Chang, H.Y., and Yang, X. (2000). Proteases for Cell Suicide: Functions and Regulation of Caspases. Microbiol Mol Biol Rev 64, 821–846.

Chen, Y., and Junger, W.G. (2012). Measurement of Oxidative Burst in Neutrophils. Methods Mol Biol 844, 115–124.

Chuang, H.-Y., Hofree, M., and Ideker, T. (2010). A decade of systems biology. Annu. Rev. Cell Dev. Biol. 26, 721–744.

Erwig, L.-P., and Henson, P.M. (2008). Clearance of apoptotic cells by phagocytes. Cell Death Differ. 15, 243–250.

Fischer, U., Jänicke, R.U., and Schulze-Osthoff, K. (2003). Many cuts to ruin: a comprehensive update of caspase substrates. Cell Death Differ. 10, 76–100.

Flusberg, D.A., and Sorger, P.K. (2015). Surviving apoptosis: life-death signaling in single cells. Trends Cell Biol 25, 446–458.

Fulda, S., Gorman, A.M., Hori, O., and Samali, A. (2010). Cellular stress responses: cell survival and cell death. International Journal of Cell Biology 2010.

Hall, B., Limaye, A., and Kulkarni, A.B. (2009). Overview: Generation of Gene Knockout Mice. Curr Protoc Cell Biol CHAPTER, Unit-19.1217.

Hemmings, B.A., and Restuccia, D.F. (2012). PI3K-PKB/Akt pathway. Cold Spring Harb Perspect Biol 4, a011189.

Jang, J.-H., Moritz, W., Graf, R., and Clavien, P.-A. (2008). Preconditioning with death ligands FasL and TNF-alpha protects the cirrhotic mouse liver against ischaemic injury. Gut 57, 492–499.

Kanduc, D., Mittelman, A., Serpico, R., Sinigaglia, E., Sinha, A.A., Natale, C., Santacroce, R., Di Corcia, M.G., Lucchese, A., and Dini, L. (2002). Cell death: apoptosis versus necrosis (review). International Journal of Oncology 21, 165–170.

Katritch, V., Cherezov, V., and Stevens, R.C. (2013). Structure-Function of the G-protein-Coupled Receptor Superfamily. Annu Rev Pharmacol Toxicol 53, 531–556.

Kroeze, W.K., Sheffler, D.J., and Roth, B.L. (2003). G-protein-coupled receptors at a glance. J. Cell. Sci. 116, 4867–4869.

Kuleshov, M.V., Jones, M.R., Rouillard, A.D., Fernandez, N.F., Duan, Q., Wang, Z., Koplev, S., Jenkins, S.L., Jagodnik, K.M., Lachmann, A., McDermott, M.G., Monteiro, C.D., Gundersen, G.W., Ma'ayan, A. (2016). Enrichr: a comprehensive gene set enrichment analysis web server 2016 update. Nucleic Acids Res 44, W90–W97.

Kültz, D. (2005). Molecular and evolutionary basis of the cellular stress response. Annu. Rev. Physiol. 67, 225–257.

Kyriakis, J.M., and Avruch, J. (2001). Mammalian mitogen-activated protein kinase signal transduction pathways activated by stress and inflammation. Physiol. Rev. 81, 807–869.

Lachmann, A., Xu, H., Krishnan, J., Berger, S.I., Mazloom, A.R., and Ma'ayan, A. (2010). ChEA: transcription factor regulation inferred from integrating genome-wide ChIP-X experiments. Bioinformatics 26, 2438–2444.

Liu, Y., and Levine, B. (2015). Autosis and autophagic cell death: the dark side of autophagy. Cell Death Differ. 22, 367–376.

Martini, M., De Santis, M.C., Braccini, L., Gulluni, F., and Hirsch, E. (2014). PI3K/AKT signaling pathway and cancer: an updated review. Ann. Med. 46, 372–383.

Massagué, J. (2012). TGFβ signalling in context. Nat. Rev. Mol. Cell Biol. 13, 616–630.

Matys, V., Kel-Margoulis, O.V., Fricke, E., Liebich, I., Land, S., Barre-Dirrie, A., Reuter, I., Chekmenev, D., Krull, M., and Hornischer, K. (2006). TRANSFAC® and its module TRANSCompel®: transcriptional gene regulation in eukaryotes. Nucleic Acids Research 34, D108–D110.

McIlwain, D.R., Berger, T., and Mak, T.W. (2013). Caspase functions in cell death and disease. Cold Spring Harb Perspect Biol 5, a008656.

Medzhitov, R., Schneider, D.S., and Soares, M.P. (2012). Disease tolerance as a defense strategy. Science 335, 936–941.

Mohr, S.E., Smith, J.A., Shamu, C.E., Neumüller, R.A., and Perrimon, N. (2014). RNAi screening comes of age: improved techniques and complementary approaches. Nat. Rev. Mol. Cell Biol. 15, 591–600.

Muñoz-Espín, D., and Serrano, M. (2014). Cellular senescence: from physiology to pathology. Nature Reviews Molecular Cell Biology 15, 482–496.

de Nadal, E., Ammerer, G., and Posas, F. (2011). Controlling gene expression in response to stress. Nat. Rev. Genet. 12, 833–845.

Ouyang, L., Shi, Z., Zhao, S., Wang, F.-T., Zhou, T.-T., Liu, B., and Bao, J.-K. (2012). Programmed cell death pathways in cancer: a review of apoptosis, autophagy and programmed necrosis. Cell Proliferation 45, 487–498.

Pakos-Zebrucka, K., Koryga, I., Mnich, K., Ljujic, M., Samali, A., and Gorman, A.M. (2016). The integrated stress response. EMBO Rep 17, 1374–1395.

Quirós, P.M., Mottis, A., and Auwerx, J. (2016). Mitonuclear communication in homeostasis and stress. Nat. Rev. Mol. Cell Biol. 17, 213–226.

Rawlings, J.S., Rosler, K.M., and Harrison, D.A. (2004). The JAK/STAT signaling pathway. J. Cell. Sci. 117, 1281–1283.

Rock, K.L., and Kono, H. (2008). The inflammatory response to cell death. Annu Rev Pathol 3, 99–126.

Sabounchi, S., Bollyky, J., and Nadeau, K. (2015). Review of Environmental Impact on the Epigenetic Regulation of Atopic Diseases. Curr Allergy Asthma Rep 15, 33.

Salama, R., Sadaie, M., Hoare, M., and Narita, M. (2014). Cellular senescence and its effector programs. Genes Dev. 28, 99–114.

Sinha, S., and Levine, B. (2008). The autophagy effector Beclin 1: a novel BH3-only protein. Oncogene 27, S137–S148.

Steinman, R.M., and Hemmi, H. (2006). Dendritic cells: translating innate to adaptive immunity. Curr. Top. Microbiol. Immunol. 311, 17–58.

Tait, S.W.G., Ichim, G., and Green, D.R. (2014). Die another way--non-apoptotic mechanisms of cell death. J. Cell. Sci. 127, 2135–2144.

Tchkonia, T., Zhu, Y., van Deursen, J., Campisi, J., and Kirkland, J.L. (2013). Cellular senescence and the senescent secretory phenotype: therapeutic opportunities. J. Clin. Invest. 123, 966–972.

Tomimatsu, K., and Narita, M. (2015). Translating the effects of mTOR on secretory senescence. Nat. Cell Biol. 17, 1230–1232.

Turner, M.D., Nedjai, B., Hurst, T., and Pennington, D.J. (2014). Cytokines and chemokines: At the crossroads of cell signalling and inflammatory disease. Biochim. Biophys. Acta 1843, 2563–2582.

Weiss, A., and Attisano, L. (2013). The TGFbeta superfamily signaling pathway. Wiley Interdiscip Rev Dev Biol 2, 47–63.

Wilson, R.C., and Doudna, J.A. (2013). Molecular mechanisms of RNA interference. Annu Rev Biophys 42, 217–239.

CHAPTER 2 : OXIDATIVE STRESS IN ENDOTHELIAL CELL

2.1 Abstract

Endothelial cells (ECs) form the inner lining of blood vessels and are central to sensing chemical perturbations that can lead to oxidative stress. The degree of stress is correlated with divergent phenotypes such as quiescence (at physiological conditions) and cell death or senescence (at high stress conditions). Each possible cell fate is relevant for a different aspect of endothelial function, and hence, the regulation of cell fate decisions is critically important in maintaining vascular health. In this study, we examine the oxidative stress response in human endothelial cells through longitudinal measurements. The use of dose-dependent and high throughput time-series measurements provides insights into multiple regimes of stress response. Using a systems approach, we are able to decipher molecular mechanisms across these regimes. Significantly, our study shows that HMOX1 acts as a gate keeper of cell fate decisions, playing a key role at the nexus between cell survival and death. Finally, we present novel mechanisms by which HMOX1 may orchestrate cell fate decisions in ECs.

2.2 Introduction

Endothelial dysfunction is a hallmark of many cardiovascular diseases and can be triggered by oxidative stress (Gimbrone and García-Cardeña, 2016) (He and Zuo, 2015). Endothelial cells (ECs) undergo oxidative stress in the presence of excess reactive oxygen species (ROS) such as hydrogen peroxide (HP), superoxide, and hydroxyl radicals. ROS are produced by endogenous sources (mitochondria, peroxisomes, lipoxygenases, NADPH oxidases, and Cytochrome P450) or by exogenous factors (immune cells, ultraviolet light, inflammatory cytokines, ionizing radiation, chemotherapeutics, or environmental toxins) (Finkel and Holbrook, 2000) (Taniyama and Griendling, 2003). When present in excess, ROS can cause significant damage to cellular

macromolecules, disrupt cellular signaling, and lead to multi-faceted endothelial dysfunction, ranging from imbalanced redox signaling, impaired nitric oxide bioavailability, pro-inflammatory response, to cell cycle disruption and cell death. Persistent endothelial dysfunction and the extravasation of lipoproteins and monocytes into the sub-endothelial space is the first in a series of steps that leads to the formation of plaque and subsequently, more serious cardiovascular events (Zhou et al., 2013) (Winn and Harlan, 2005) (Huynh et al., 2011).

The change in activity of cell signaling pathways, gene expression changes and proteins that directly or indirectly moderate the response to damage by ROS is known as the oxidative stress response (OSR). In ECs, this involves the coordinated efforts by multiple signaling pathways (e.g. ATM/p53, NFκB, NRF2/KEAP1, PI3K/Akt etc.) (Liang et al., 2017) that initiate changes in the cell's structure and function culminating in the final phenotype (i.e. return to homeostasis, apoptosis, necrosis, or senescence). NRF2/KEAP1 signaling is able to reestablish basal redox status by inducing the expression of key antioxidant enzymes such as heme oxygenase-1 (HMOX1) (Kobayashi and Yamamoto, 2006) (Trachootham et al., 2008). NFκB signaling molecules directly or indirectly sense ROS and subsequently coordinate changes to the redox and inflammatory status (Morgan and Liu, 2011). PI3K/AKT signaling regulates the phosphorylation of eNOS and therefore nitric oxide (NO) availability, which is critically important for endothelial homeostasis (Tousoulis et al., 2012).

When oxidative stress overwhelms the protective responses arising from these pathways, apoptosis may be induced, resulting in increased endothelial permeability (Zhou et al., 2013) (Winn and Harlan, 2005) (Huynh et al., 2011). Caspase-dependent apoptosis involves the ROS-mediated (Elmore, 2007) activation of death receptors (FAS, TRAIL etc.), mitochondrial cytochrome c release, or cytotoxicity resulting in the degradation of DNA by endonucleases

(Chandra et al., 2000). Alternatively, the resistance to cell death can be established by anti-apoptotic factors such as protective members of the BCL2 family or the Inhibitors of Apoptosis (IAP) family of proteins (Portt et al., 2011). If the resistance to apoptosis is accompanied by cell cycle arrest, ECs can enter a quiescent or senescent state (Salminen et al., 2011). While quiescence is a reversible and relatively dormant cell state, senescence is an irreversible arrest accompanied by continued cellular activity (Kuilman et al., 2010) (Toussaint et al., 2002) (Muñoz-Espín and Serrano, 2014) (Chen et al., 2008) (Chen et al., 2008). Endothelial cell fate decisions are critically important for determining vascular phenotypes. Quiescent cell cycle arrest is established during physiological conditions (Yu et al., 2001), apoptosis facilitates vascular development and remodeling (Mallat and Tedgui, 2000) (Dimmeler and Zeiher, 2000) and EC proliferation is induced during angiogenesis and vascular repair (Aydogan et al., 2015). Interestingly, many pro-apoptotic ligands (such as FASL and TNFα) have been shown to concurrently activate pro-death and pro-survival mechanisms allowing cells to exist at the nexus between cell fates (Flusberg and Sorger, 2015) (Secchiero et al., 2004) (Secchiero et al., 2003) (Cantarella et al., 2014). Ultimately, the decision between cell death and survival is determined by a combination of extrinsic variability (i.e. differences in cell microenvironment) and intrinsic variability (i.e. differences in how the stress is processed due to genetic and epigenetic differences between cells) (Flusberg and Sorger, 2015). In ECs, heterogeneity in cell fate decisions among neighboring cells can disrupt the monolayer and result in dramatic consequences for vascular health and function. While signaling pathways involved in the OSR and cellular pathways involved in cell fate decisions are well defined, these results are based on static models across various cell types and stress conditions providing limited temporal endothelial specific insight.

Heme oxygenase-1 (HMOX1), an antioxidant enzyme activated by oxidative stress, is a central regulator of endothelial function and cell fate. The protective role of HMOX1 has primarily been attributed to its enzymatic activity in regulating concentrations of heme, CO, Fe2+, and Biliverdin, which influence inflammation, redox status, expression of monocyte adhesion factors, and proliferation of ECs (Yachie et al., 1999) (Soares et al., 2002) (Brouard et al., 2000) (Soares et al., 2004) (Brouard et al., 2002) (Seldon et al., 2007) (Silva et al., 2006) (Kim et al., 2007) (Balla et al., 1991) (Balla et al., 1993) (Gozzelino et al., 2010) (Romanoski et al., 2011). Non-enzymatic activities of HMOX1 have also been shown to regulate the redox status and the expression of transcription factors associated with the OSR (Hori et al., 2002) (Lin et al., 2007) (Dulak and Jozkowicz, 2014). While the activation of HMOX1 has been observed as early as 2 hours post stress (Reichard et al., 2007) (Chan et al., 2011) and in late-stage disease models (Deshane et al., 2005), the role of this enzyme in the transition from early to late endothelial dysfunction has not been explored.

In this study, we provide a systems level analysis of the OSR in human umbilical vein endothelial cells (HUVECs) treated with hydrogen peroxide (HP). By using dose-dependent and high throughput time-series measurements we have identified three phases of stress response that are consistent with known hallmarks of vascular disease. Next, we identify key players at the nexus of cell function and dysfunction and identify HMOX1 as a central regulator of this transition. Further examination and perturbation of the transition from the early/acute stress response to the later/chronic stress response demonstrates the role of HMOX1 as the gatekeeper of cell fate decisions. We explore novel mechanisms by which HMOX1 coordinates stress signals affecting multiple cellular locations, culminating in the final decision between survival and apoptosis.

2.3 Materials and Methods

Cell Culture

Pooled Human Umbilical Vein Endothelial Cells (HUVECs) were purchased from ATCC (PCS-100-013, Lot#60279032) and Cell Applications (200p-05n). HUVECs were cultured in media supplemented with an endothelial cell growth kit from ATCC (PCS-100,041). Cells used in this study were between passages 4 and 7. The hydrogen peroxide used to treat cells was 30% ACS grade from Thermo Fisher (#7722-84-1) and diluted in ice cold PBS.

siRNA Knockdown Experiments

ATCC HUVECs were cultured to 50-60% confluence before being transfected with Lipofectamine RNAimax (Thermo Fisher, CAT# 13778150). Then, 48 hours after the start of transfection, cells were treated with HP. Six hours after the addition of HP cells were collected for analysis (phase contrast imaging, qPCR, RNAseq, or MitoStressTest). Each knockdown experiment included Scrambled-Untreated, Scrambled-Treated, and Knockdown-Treated groups.

Table 2.1 siRNA sequences and catalog numbers

Gene	Target Sequence	Accession Number	Catalog Number
HMOX1	CAGGCAATGGCCTAAACTTCA	NM_002133	-
ATF3	CTGGGTGGTACCCAGGCTTTA	NM_001030287	-
Negative Control	-	-	1022076

Sample Preparation for RNAseq: Timecourse Experiment

ATCC HUVECs were cultured to near confluence and treated with 0.5 mM HP in duplicate. Samples were collected at 0 (control), 1, 2, 4, 6, 8, 10, 12, 14, and 16 hour time points. Total RNA was purified and concentrated using the Zymo Quick-RNA mini prep and RNA Clean & Concentrator kits (Zymo Research, #R1054 and #1015). Samples were sequenced on the Illumina HiSeq system (at the Salk Institute for Biological Studies).

Sample Preparation for RNAseq: Knockdown Experiment

ATCC HUVECs were cultured and transfected with scrambled control or si-HMOX1 according to the Lipofectamine RNAiMAX protocol (13778075; Thermo Fisher, Waltham, MA). After induction with HP, total RNA was isolated in duplicate using the Zymo Direct-zol RNA MiniPrep Kit (R2050). Samples were submitted to the UC San Diego Genomics Core for stranded mRNA library preparation and sequencing on the Illumina HiSeq4000 system. Scrambled siRNA without HP treatment was used as a control to test the effect of HP treatment. Similarly, Scrambled siRNA with HP treatment was used as a control to test the effect of the HMOX1 knockdown on the response to HP treatment.

RNA-sequencing Analysis

Both sequencing dataset include 50 base-pair single end reads (The exact number of reads sequenced per sample and the uniquely mapped alignment percentage is summarized in FIG2.S1S1). The quality of the reads was verified using FastQC (Andrews, 2010). Next, Omicsoft Sequence Aligner 2 (OSA2) (Hu et al., 2012) was used to align the reads to the Human.B37.3 reference genome build using the Ensembl R66 gene model resulting in gene counts. DESeq2 was used for differential expression analysis (Love et al., 2014). After identifying differentially expressed genes (DEGs), additional p-value ($p < 0.01$) and fold-change ($|\text{fold-change}| > 1.3$) cutoffs were implemented. Kyoto Encyclopedia of Genes and Genomes (KEGG) pathway (Kanehisa and Goto, 2000) (Kanehisa et al., 2016) (Kanehisa et al., 2017) enrichment analysis was conducted using the list of DEGs at each time point, assuming a hyper-geometric distribution to calculate p-values. Enrichment of gene ontologies was also explored using DAVID (Huang et al., 2009). Transcription factor-target interactions were identified using the TRANSFAC database (Matys et al., 2006). Agglomerative hierarchical clustering was performed using the flashClust() function in R in order to cluster normalized gene counts (Langfelder and Horvath, 2012).

Plate Assays

For the CCK8, Casp3/7, and GSH/GSSG plate assays, cells were seeded at ~5,000 cells per well including blank and negative controls. Each plate assay had 4 technical replicates per dose. Fresh media was exchanged after 24 hours, and cells were further incubated for 12 hours before induction with different concentrations of HP. For the CCK8, HUVECs were seeded in black walled, transparent bottom, 96-well plates (Greiner bio-one) in 100 µl of full growth media. For the Caspase Glo 3/7 and GSH/GSSG assays, HUVECs were seeded in white walled, opaque, 96-well plates (Greiner bio-one) in 100 µl of full growth media.

CCK-8 Assay

The CCK8 viability assay was used as a measure of dehydrogenase activity, which is a marker of cell viability and proliferation. 10 µl of CCK-8 reagent (#CK04-11, Dojindo; Rockville, MD) was added to each well at the end of 6, 12, 24, and 48 hours of induction. Absorbance values were measured at 450 nm on Tecan Safire M200 plate reader at 37° C. This experiment was repeated three times with four technical replicates per dose; the average blank value was subtracted from each treatment average and compared against negative control (untreated cells) and expressed as percent toxicity. (n = 3 (P3-P5); for each repeat of the experiment includes four time points and four replicates for each dose of HP per time point)

Caspase-Glo 3/7 Assay

Caspase activity was measured with Caspase-Glo 3/7 reagent (G8090, Promega; Madison, WI) at 12 hours after induction. Four technical replicates per dose; luminescence values were measured on Tecan Safire M200 plate reader at RT and expressed as a percentage of the positive control (10uM staurosporine). (n = 1 (P5), four technical replicates per HP dose)

GSH/GSSG-Glo Assay

GSH/GSSG-Glo kit (V6611, Promega; Madison, WI) was used to assay the ratio of oxidized (GSSG) to reduced (GSH) glutathione. At the end of the induction time, 50 µl of Luciferin generating agent was added and incubated for 30 min at RT with intermittent shaking followed by the addition of 100 µl of luciferin detection reagent after which luminescence was measured on Tecan Safire M200 plate reader. This experiment included four technical replicates per HP dose, vehicle control, and no-cell control; the average background measurement (from the no-cell control) was subtracted from the average luminescence measurement for all other treatment groups and represented as a percentage of the untreated/vehicle control as per manufacturer's instructions. (n = 1 (P5), four technical replicates per HP dose).

Cell-Tox Green Assay

HUVECs were assayed for cell toxicity with Cell-Tox reagent (G8742, Promega; Madison, WI) at the end of 12 and 24 hours of induction by microscopy. Inomycin (0.5uM) was added to positive controls at the time of seeding. Reagent was added at 30 min before the assay time and incubated at RT. Fluorescence was measured at 490 nm excitation and emission at 530 nm on Olympus IX71 fluorescence microscope (n = 2, two technical replicate per HP dose).

Cell Cycle Analysis

ATCC HUVECs were cultured and treated with 0 or 0.5mM HP for 24 hours. At the end of the treatment time, cell density was adjusted to 106 cells in 0.5 ml PBS, and transferred to 4.5 ml of ice cold ethanol overnight for fixing. Subsequently, cell suspension was spun down (300g at 4°C for 10 min) and ethanol was decanted. Cell pellet was washed in 5 ml of PBS and incubated with 0.5 ml of staining solution (FxCycle PI-RNAse, LifeTechnologies) for 30 min in dark before analyzing in flow cytometer (BD-FACScan). 10,000 events were collected for each sample and their histograms were plotted for data visualization and analysis. This experiment as repeated twice.

The percentage of cells in each phase with 0 and 0.5mM treatment was compared across the two biological replicates using a Students two-tailed t-test ($p < 0.05$ was considered significant).

Autophagy Assay

Cyto-ID (Enzo life sciences, USA) is an autophagy detection kit that selectively stains autophagic vacuoles without non-specific lysosome staining. HUVECs grown on glass bottom dishes treated with 0 or 0.5mM of HP for ≥ 24 h were stained with Cyto-ID as recommended by the manufacturer. After staining, cells were washed in wash buffer supplemented with 5% FBS and imaged in wash buffer. Autophagic vacuoles were imaged with excitation at 463 nm and emission at 534nm. (n = 1, two technical replicate per treatment condition)

Mitochondrial Network Integrity

HUVECs plated on glass bottom Petri dishes (MatTek Corp.) at 5000 cells/cm2 were allowed to reach 70% confluence before induction with 0 and 0.5, 0.6 and 0.7 mM HP for 12 and 24 h. Cells were stained with MitoTraker Deep Red FM dye (10 nM) mixed with Hoechst 33342 (0.75 µg/ml) (LifeTechnologies, USA) in fresh warm media for 45 min at 37º C. Cells were washed in warm media and imaged in warm HBSS on environment controlled chamber on IX71 microscope. 3-5 random fields were chosen for 100x imaging. Acquisition parameters were optimized for control cells and same parameters were used for acquiring all treatment groups. 3D stacks (X,Y,Z) for each channel (Blue & Red) were obtained and combined in Metamorph Imaging software. Images were analyzed in ImageJ software. To visualize the mitochondrial network, their distribution and size, high pass filter (edge detection) was applied. Maximum intensity projection was applied to determine total intensity of mitochondrial stain. (n = 2, two technical replicate per treatment condition).

Mitochondrial Membrane Potential Assay

Cells grown on glass bottom dishes were treated with different concentrations of HP for 12h, subsequently incubated with 5 µM JC-1 (Biotium, USA) diluted in fresh warm media for 30 min at 37° C. After this, cells were gently washed with 2 volumes of fresh media 2 times- each for 3 min and imaged immediately on IX71 equipped with environmental chamber. For JC-1 monomers and aggregates, an excitation and emission wavelengths of 485/535 and 560/595 nm, respectively were used. Mitochondrial membrane depolarization is indicated by green fluorescent monomers (unhealthy/apoptotic cells) and healthy mitochondria are indicated by red fluorescent aggregates. Ratios of monomers/aggregates (green/red ratio) indicate the overall health of mitochondria in the treatment group. Images were analyzed in ImageJ using a macro that automatically segment and quantify green and red fluorescence. (Biological replicate: n = 2; two technical replicate per HP dose)

Quantitative PCR

RNA was isolated from cells using Trizol (Thermo Fisher, 15596018). Total RNA was reverse transcribed using the Clontech Prime Script RT Master Mix (RR036B) followed by qPCR with SYBR Green (Bio-Rad); qPCR was run on the Bio-Rad CFX-96 realtime system. Beta-Actin was used as the internal control when calculating the delta-deta Ct/relative expression level. Student's two-tailed unpaired t-test was used to determine significant changes between fold-changes in relative expression (delta-delta Ct).

Table 2.2 qPCR primer pairs

Gene	Forward Primer	Reverse Primer
MT-ND3	GCGGCTTCGACCCTATATCC	AGGGCTCATGGTAGGGGTAA
MT-ATP6	TCCCTCTACACTTATCATCTTCAC	GACAGCGATTTCTAGGATAGTC
IGF1R	CCTGCACAACTCCATCTTCGTG	CGGTGATGTTGTAGGTGTCTGC
EGFR	TATGTCCTCATTGCCCTCAACA	CTGATGATCTGCAGGTTTTCCA
RBBP5	GTGGACCCTATTGCTGCCTTCT	CCATCAAGGAGGTTTGGACTGC
KDM6A	AGCGCAAAGGAGCCGTGGAAAA	GTCGTTCACCATTAGGACCTGC
PPM1D	GTGGTCATCATTCGGGGCAT	CATCCTTCGGGTCATCCTGAA
HMOX1	AAGACTGCGTTCCTGCTCAAC	AAAGCCCTACAGCAACTGTCG
ATF3	CCTCTGCGCTGGAATCAGTC	TTCTTTCTCGTCGCCTCTTTT
B-ACTIN	GCACCACACCTTCTACAATG	ATCACGATGCCAGTGGTAC
GAPDH	CTCCTCACAGTTGCCATGTA	GTTGAGCACAGGGTACTTTATTG

Quantifying Mitochondrial Respiration (Seahorse MitoStress Test XFe24)

Mitochondrial function was assessed using the MitoStress Test (XFe24, Agilent). After 48 hours of transfection, endothelial cells were trypsinized, resuspended, and plated into the XFe 24-well plate at a density of 30,000 cells/well. The cells were allowed to grow overnight before being treated with HP. Five hours after treatment, the cell culture media was removed and replaced with the Agilent base media (102353-100, Agilent; Santa Clara, CA) supplemented with D-glucose (5.5mM) and L-glutamine (0.68mM) before being incubated in a non-CO2 incubator for 1 hour. Oligomycin, FCCP, and Antimycin/Rotenone were loaded into ports A, B, and C respectively of the cartridge at the following concentrations: Oligomycin (1uM), FCCP (2uM), and Ant/Rot (0.5uM). All oxygen consumption measurements were normalized by cell count or protein concentration (BCA Protein Quantification). This experiment was repeated three times (n = 3, P5-7). All measurements in each experiment were normalized by the average basal respiration for the scrambled untreated control group. Next, the three basal measurements were averaged for each treatment group (Scrambled-NT, Scrambled-HP, siHMOX1-HP). Similarly, the three measurements made after each drug were averaged. Then, mitochondrial function parameters were calculated as follows:

ATP production = Avg Basal – Avg Oligo

Proton Leak = Avg Oligo – Avg Rot/AA

Spare Capacity = Avg FCCP – Avg Basal

Non-Mitochondrial OCR = Avg Rot/AA

After repeating these calculations for each of the three experiments, the paired student's t-test was used to compare Scrambled-HP vs. Scrambled-NT and siHMOX1-HP vs. Scrambled-HP across all three experiments. A threshold of $p < 0.05$ was used to identify significant changes.

2.4 Results

Dose and Time-Dependent Response to Oxidative Stress in HUVECs

In order to explore cellular response to oxidative stress, we explored the mechanisms that follow HP-induced stress in HUVECs. We examined the dose-dependent response of ECs under oxidative stress using three functional readouts (i.e., caspase 3/7 activation, viability, and antioxidant capacity) to characterize different aspects of cellular response as a function of HP dose.

To determine the appropriate dose and time window to characterize the OSR, dose response and time series measurements were carried out using CCK-8 assay that measures cell viability by assessing dehydrogenase activity. Across all time points, cell viability decreased with increasing dose of HP. About 50% of cells remain viable between 0.5-0.55 mM (FIG2.1A). Doses beyond 0.6 mM drastically reduced cell viability. To verify that 0.5 mM HP establishes effective oxidative stress, the ratio of reduced to oxidized glutathione (GSH/GSSG), a specific measure of cellular redox potential was measured. At 0.5 mM HP, the antioxidant capacity is reduced by 50% (FIG2.1B). There is an inverse relationship between the HP concentration and the antioxidant capacity ($R^2 = 0.9005$). In addition to damaging proteins and DNA, ROS also disrupt the integrity of lipid membranes. Cell toxicity was measured to ensure that the induction dose does not result in drastic cell death as it affects the quality of genomic material for gene expression studies. Cell-Tox green assay showed increasing toxicity (number of green cells) with dose. Minimal cell death (~ 10%) was observed at 0.5 mM compared to positive control (inomycin) (FIG2.1C) at 12 hours after induction. Also, caspase3/7 assays showed dose dependent increase in activity up to 0.5 mM (~30% of staurosporine treated positive controls, FIG2.1B), with no caspase activity beyond 0.65 mM HP, suggesting activation of caspase dependent cell death mechanisms at low doses and caspase independent mechanisms (necrosis) at higher doses.

Overall, these assays established that 0.5 mM HP induces oxidative stress and places the cell at the transition of cell function and dysfunction.

To characterize the mechanism of stress response at the nexus between cell function and cell dysfunction, HUVECs were treated with 0.5 mM HP and total RNA was collected at 0, 1, 2, 4, 6, 8, 10, 12, 14, and 16 hours post treatment for RNA-sequencing. The number of differentially expressed genes (DEGs) at each time point is shown in FIG2.1E. There was a dramatic increase in the number of DEGs from 1 to 4 hours to ~6000 genes. The number of DEGs gradually decreased from 4-16 hours to ~3500 genes.

KEGG pathway enrichment was examined for each time point to identify the key processes that are active across the time-course. FIG2.1F shows significantly enriched pathways and the –log(p-value) for each pathway across time. Early time-points (i.e. 1-4 hours) were highly enriched for TNFα, MAPK, TGFβ, NFκB, PI3K/Akt, and FOXO signaling along with KEGG pathways related to cytokine-cytokine receptor interaction and oxidative phosphorylation. At 4 hours, p53 signaling was maximally enriched. Finally, from 4-16 hours, pathways associated with cell cycle, DNA replication, and DNA repair were enriched.

Hierarchical clustering of the normalized gene counts was performed to identify distinct phases of the OSR (FIG2.1G). Neighboring time-points are clustered together. At a tree height cut-off of ~30, three distinct clusters emerge: 0-2 hour defined the “early” cluster, 4-6 hour formed the “mid/transitional” cluster, and 8-16 hour formed the “late” cluster.

Additional functional analyses (FIG2.S3) suggest that treatment with 0.5mM HP resulted in decreased mitochondrial membrane potential and disintegration of the mitochondrial network surrounding the nucleus (FIG2.S3-C&D). Furthermore, there is a decrease in the percentage of cells in the S phase ($p = 0.07$) and an increase in the percentage of cells in the G2/M phase ($p <$

0.05) (FIG2.S3A). Finally, there is an increase in autophagic vacuoles in response to HP treatment (FIG2.S3B).

Taken together, the dose- (FIG 1A-C) and time-dependent (FIG2.1D-E) response to oxidative stress suggest a nexus between cell function and dysfunction; this nexus is characterized by three distinct phases (early, mid, and late). The initial activation of classical OSR in the early phase is later accompanied by regulation of cell cycle, DNA replication, and DNA repair pathways.

A Temporal Model of Oxidative Stress Response in Endothelial Cells

Significantly enriched ($p < 0.05$) genes and pathways were identified from time-series RNA-sequencing and used to construct a temporal model of the OSR (FIG2.2). The direction of pathway and gene regulation is specified: blue indicates down-regulation and red indicates up-regulation (the exact fold-change and p-values are summarized in FIG2.S2). We observed that the introduction of oxidative stress caused the expression of genes associated with mitochondrial damage and p53 activation in the first hour. Mitochondrial damage was characterized by the consistent down-regulation of key mitochondrial transcripts associated with the electron transport chain (ETC) subunits and ATP synthase from 1-16 hours. At hour 2, potent cell cycle inhibitors (CDKN1A (p21) and GADD45A) were up-regulated and remained up-regulated until 16 hours. This resulted in the strong down-regulation of cell cycle genes (cyclins, CDKs, etc.) from 4-16 hours. Interestingly, DNA replication and repair genes were also strongly down-regulated from 4-16 hours.

We observed a balance between pro- and anti-apoptotic gene programs. The resistance to apoptosis is maintained by strong up-regulation of inhibitor of apoptosis family members BIRC2 and BIRC3. Anti-apoptotic BCL family members BCL2L1 and BCL2L2 were also strongly up-regulated across the time course. Pro-apoptotic factors such as BRCA1, CASP8 and caspase

inducing factors such as TRADD and FADD were down-regulated across time. Finally, up-regulation of TGFβ family members SMAD6 and SMAD7 also supported the resistance to apoptosis. On the other hand, pro-apoptotic factors such as FAS, CHOP, NR4A1, BAK1, and BAX were strongly up-regulated across time (FIG2.2).

Pro-inflammatory processes such as NFκB signaling and expression of cytokines and chemokines were up-regulated from 2-16 hours. Interestingly, inhibitors of NFκB (NFKBIA, NFKBIB) are also up-regulated across the time course. Also, ICAM1 which is known to recruit and facilitate pro-inflammatory monocyte extravasation was up-regulated from 2-16 hours. Similarly, SELE is up-regulated from 2-8 hours but switches to down-regulation from 10-12 hours.

NFE2L2, a critical transcription factor involved in the OSR is up-regulated from 2-8 hours and again at 12-14 hours. Similarly, KLF2, a stress response transcription and central regulator of endothelial function, was up-regulated in the first 4 hours and then switched to down-regulation. Interestingly, downstream stress response processes such as the expression of antioxidants is down-regulated from 4-14 hours. Key autophagy proteins such as LC3A and PIK3C3 were up-regulated from 2-16 hours while other autophagic proteins such as ATG4C were down-regulated from 4-10 hours. Lysosomal activity increased over time with a majority of lysosome hydrolases being up-regulated at 16 hours. From 6-16 hours, we also observed a slight increase in mTOR activity as indicated by up-regulation of up-stream activators of mTORC1, RRAGB and RHEB.

HMOX1: A Key Regulator

Since the switch in phenotype occurred from 4-6h as indicated by the hierarchical clustering and functional analysis, transcription factors induced in the first hour that may participate in facilitating the switch from 4-6 hours were identified. Of the top 10 transcription

factors that were up-regulated in the first hour, four were JUN family transcription factors: FOSB, ATF3, FOS and JUNB (FIG2.3A).

To explore the mechanistic consequence of JUN activation, the top 10 up-regulated JUN family targets were identified using the TRANSFAC database (Matys et al., 2006) (FIG2.3B). From this list, two gene candidates (i.e. HMOX1 and ATF3) were selected based on the following criteria: 1) regulation of oxidative stress-related processes (Gozzelino et al., 2010) (Han et al., 2008) (Tanaka et al., 2011) (Yoshida et al., 2008) and 2) association with endothelial apoptosis (Kawauchi et al., 2002) (Soares et al., 2002). Additionally, it is important to note that the role of HMOX1 and ATF3 in the transition from acute to chronic stress response has previously not been explored (FIG2.3C). The knockdown experiment included three main treatment groups: 1) scrambled-untreated (hereafter scrambled-NT), 2) scrambled-treated (hereafter scrambled-HP), and 3) knockdown-treated (hereafter knockdown-HP). We observed no significant differences in cell count between the scrambled siRNA and siHMOX1 transfected cells prior to the addition of HP. Forty-eight hours after transfection, Groups 2 and 3 were treated with HP for 6 hours before cells were imaged. FIG2.3D shows the relative expression of ATF3 and HMOX1 in the three experimental groups. The comparison of scrambled-HP versus scrambled-NT displays the effect of the treatment; we observed a decrease in cell count and slight change in cell morphology. Comparing the scrambled-HP sample to each individual knockdown + HP group revealed that the greatest change in cell count and morphology occurred after HMOX1 knockdown.

HMOX1: A Global Regulator of Cell Function

The global role of HMOX1 in orchestrating the response to oxidative stress in the transitional regime between acute and chronic stress was examined by high-throughput transcriptomic analysis. Measurement of HMOX1 expression by qPCR in each treatment group is

shown in FIG2.3D; the comparison of the first two groups indicated degree of HMOX1 induction upon HP treatment (~4-fold), while comparison of the second two groups quantified the knockdown efficiency (~80%). After alignment with OSA2, gene counts were used for differential expression analysis; the number of differentially expressed genes are summarized in FIG2.4A.

Key processes that were affected by HP treatment in the time-course data were examined in the context of the knockdown (FIG2.4B). Many processes which were up-regulated by HP treatment alone were down-regulated in HMOX1 deficient cells when treated with HP and vice versa. For example, mitochondrial transcripts MT-ATP6, MT-ND3, and MT-CYB were all strongly down-regulated upon HP treatment. However, after the knockdown, these transcripts were up-regulated in response to HP treatment. Similarly, genes associated with inflammation, autophagy, transcription, ER stress, the antioxidant response, and the cell cycle switch their direction of regulation in response to HP when HMOX1 expression was decreased. In fact, there were 2892 genes (with $p < 0.05$) that were consistently regulated in the time-course and knockdown experiments (i.e. were up regulated in both 6h vs. 0h and Scrambled-HP vs. Scrambled-NT or were down regulated in both 6h vs. 0h and Scrambled HP vs. Scrambled-NT); 51% of these DE genes switched their direction of regulation upon HMOX1 knockdown in response to HP treatment (FIG2.4C).

After performing GO and KEGG enrichment of the 51% of switching genes, we found three spatial categories: nucleus, cell surface, and mitochondria (FIG2.4D). Nuclear pathways included spliceosome, histone demethylase activity, nuclear pore, and DNA directed RNA polymerase activity. Cell surface pathways included cell-cell adherens junction and antigen processing and presentation. Finally, the mitochondrial pathways included oxidative phosphorylation and respiratory chain related GO terms. Pathways and processes that were

significantly enriched in the knockdown data were also enriched ($p < 0.05$) at various time-points across the time-course data (FIG2.4D). Mitochondrial pathways were enriched earlier in the time course whereas nuclear and cell surface processes were enriched across the time course.

Taken together, these data suggest the global impact of HMOX1 on regulating the functional response to oxidative stress.

Novel Mechanisms of HMOX1 in Regulating the OSR

Upon further exploration of the location specific effects of HMOX1 knockdown, we found key mitochondrial transcripts, cell surface receptors, and nuclear regulatory genes that switch their direction of expression upon HP treatment when HMOX1 is silenced (all relevant fold-change and p-values are summarized in FIG2.S4). At the cell surface, EGFR and IGF1R were up-regulated with HP treatment alone and down-regulated in HMOX1 deficient HUVECs (FIG2.5B).

Mitochondrial transcripts that encode subunits of the ETC were down-regulated upon HP treatment alone and up-regulated in HMOX1 deficient HUVECs (FIG2.5D). To gauge the functional consequence of this transcriptional switch, we performed the Seahorse Mito Stress Test to quantify mitochondrial respiration. Consistent with the transcriptional switch, measurement of the oxygen consumption rate in the scrambled-NT, scrambled-HP, and siHMOX1-HP groups indicated a decrease in ATP production upon HP treatment alone, which was rescued in response to HP treatment in the HMOX1 knockdown group (FIG2.5E).

Finally, we showed that key histone modification genes (KDM6A, RBBP5, and PPM1D) were up-regulated upon HP treatment and down-regulated upon HP treatment in HMOX1 deficient HUVECs (FIG2.5F & FIG2.5G). Additionally, we have identified long non-coding RNAs (lncRNAs) that switched their direction of regulation (i.e. up- to down- or vice versa) in response to HP treatment upon HMOX1 deficiency (FIG2.5H).

Taken together, these results highlight novel organelle-specific HMOX1-mediated mechanisms of cell protection in response to oxidative stress.

2.5 Discussion

Endothelial dysfunction and cell death are central to the progression of vascular diseases (Libby et al., 2011) (Gimbrone and García-Cardeña, 2016) (Madamanchi et al., 2005). The monolayer of endothelial cells that forms a barrier between blood flow and the surrounding tissue allows selective molecules and immune cells to cross into the sub-endothelial space. Under chronic stress, gaps in the endothelium allow uninhibited extravasation of immune cells and lipoproteins, contributing to the persistent pro-inflammatory state that supports the formation of plaque (Galbraith et al., 1998). Endothelial dysfunction and cell death can be triggered by many mechanical (Chiu and Chien, 2011) (Chien, 2008) (Ajami et al., 2017) and chemical (Deanfield et al., 2007) (Hadi et al., 2005) cues. As the first line of defense facing the circulating toxins in the blood, ECs are primed to sense and respond to subtle chemical perturbations such as oxidative stress (Deanfield et al., 2007) (Pennathur and Heinecke, 2007).

In this study we have characterized the response to oxidative stress in ECs using a systems biology approach and, in doing so, we have identified gatekeepers at the nexus of cell fate decisions.

Dose Dependent OSR in ECs

One of the key features of vascular disease is eNOS uncoupling, which results from the oxidation of nitric oxide; this process is dependent on the amount of ROS available (i.e. the degree of oxidative stress) (Elahi et al., 2009). We have shown in this study that cell viability and anti-oxidant capacity of HUVECs decrease while cell toxicity and apoptotic signaling increase with

0.1-0.5 mM HP treatment. Beyond 0.5 mM HP, cell toxicity increases more dramatically and apoptotic signaling begins to decay, suggesting that beyond this concentration, the cells begin to undergo necrosis (FIG2.1A-D). Previous studies have shown similar trends in apoptosis, cell viability, cell toxicity, and redox status upon treatment with HP (Zhou et al., 2013) (Csordas et al., 2006) (Wen et al., 2013) (Gong et al., 2010) (Clément et al., 1998) (Xu et al., 2013) (van Gorp et al., 1999) (Nadeev et al., 2015) (Messner et al., 2012). Considering that beyond 0.5 mM HP the antioxidant capacity, cell viability, apoptotic signaling, and membrane integrity are severely degraded, ~0.5 mM HP is the point of cell fate transition.

Time Dependent OSR in ECs and Hallmarks of Vascular Disease

The transition from cell function to dysfunction is temporally mediated by transcriptional changes. In order to characterize transcriptional programs that facilitate the transition from EC function to dysfunction, we examined the longitudinal response to oxidative stress. Our dose-response analysis in conjunction with the longitudinal study revealed the tipping point of endothelial function allowing us to focus on factors that initiate cell dysfunction. Furthermore, our use of high-throughput time series measurements allowed us to distinguish three clear phases of stress response and provide a systems level perspective on the endothelial-specific OSR (FIG2.1E-G).

By looking at the global response to oxidative stress at the nexus of cell function and dysfunction we have been able to show the EC-specific crosstalk between multiple anti-apoptotic mechanisms. It is also important to note that we observe the up-regulation of pro-apoptotic signals (FIG2.2). Parallel activation of survival and death pathways allows sensing of the stress response and immediate clearance of cells that have incomplete or insufficient repair mechanisms (Flusberg and Sorger, 2015) (Gross et al., 1999). Additionally, senescent endothelial cells are known to be

susceptible to spontaneous or stress induced apoptosis (Donato et al., 2015) (SEALS et al., 2011) (Zhang et al., 2002). Also, studies have shown that cells that recover from stress initiate protective measures for future instances of stress resulting in disease tolerance (Flusberg and Sorger, 2015) (Medzhitov et al., 2012) (Jang et al., 2008). This may explain why pro- and anti-apoptotic genes are concurrently activated in the progression from acute to chronic stress response. Interestingly, the induction of apoptosis has been shown to cause caspase-mediated disruption of adherens junctions in vitro (Bannerman et al., 1998) and caspases also have non-canonical roles in inflammation (Martinon and Tschopp, 2004). Therefore, even if the anti-apoptotic signaling prevents cell death and preserves endothelial barrier function, the activation of pro-apoptotic signals could indirectly increase endothelial permeability and inflammation. The concurrent activation of pro- and anti-apoptotic processes highlights the heterogeneity of stress response at the nexus of cell function and dysfunction.

In our model, we find that cell cycle and DNA replication is strongly inhibited by p21 and GADD45A from 4-16 hours (FIG2.2, FIG2.S3); this is in line with previous findings (Gao et al., 2009) (Zhan, 2005) (Niehrs and Schäfer, 2012) (Moskalev et al., 2012) (Tamura et al., 2012). In addition to cell cycle arrest, our data reveals that hallmarks of endothelial senescence, such as up-regulation of pro-inflammatory cytokines, monocyte adhesion factors, and autophagy along with down-regulation of NOS3, are present in a sustained manner throughout our time course. This is in line with previous reports of endothelial senescence (Lum and Roebuck, 2001) (Tian and Li, 2014). Therefore, at the nexus of cell function and dysfunction, decreased replicative potential and activation of senescence supports key pillars of endothelial dysfunction such as decreased NO, increased cytokines, and increased monocyte adhesion.

Finally, examination of key transcription factors associated with the OSR in ECs indicates that while NFE2L2 is up-regulated its target antioxidant genes (i.e. CAT, PRDX3, TXNRD2) are down-regulated from 4-16h. Given that KLF2 activates NFE2L2 (Fledderus et al., 2008), the switch in regulation of KLF2 from up- to down-regulation may contribute to the down-regulation of NFE2L2-mediated antioxidant gene expression. Also, KLF4 up-regulation from 1-16 hours, may be critical in maintaining the up-regulation of THBD in order to reduce thrombin levels and inhibit pro-thrombogenic signaling (Sangwung et al.) (Jiang et al., 2014). (FIG2.2)

Taken together our data suggests that the inhibition of antioxidant gene expression and activation of senescent, pro-inflammatory, and chemoattractant gene expression promote progression of acute stress to endothelial dysfunction. Interestingly, while resistance to apoptosis in healthy ECs would protect the barrier functionality of the endothelium, persistence of this "protective" factor under significant oxidative stress shields dysfunctional ECs from being cleared and contributes to the chronic stress state typical of vascular disease.

HMOX1: A Master Regulator

While HMOX1 has been shown to influence many cellular functions, these studies span many different stress conditions and cell types and mostly provide a "snapshot" of HMOX1 regulated cellular function at a fixed time point (Kim et al., 2011) (Gozzelino et al., 2010). Given that 51% of genes switch their direction of regulation upon HP treatment in HMOX1-deficient cells (FIG2.4C), it is clear that HMOX1 has a dramatic effect on gene expression highlighting the substantial influence of this enzyme on the endothelial OSR. KEGG and GO enrichment of the 51% of switching genes reveal three spatial clusters: the nucleus, mitochondria and the cell surface (FIG2.4D). Interestingly, the protein encoded by HMOX1 is located at the cell surface, mitochondria, and nucleus (Dunn et al., 2014). In order to identify novel mechanisms of HMOX1

function, we identified switching genes that had not previously been associated with HMOX1 at each of the enriched locations.

At the cell surface, we found that HP treatment-induced EGFR and IGF1R was significantly dampened in HMOX1 deficient HUVECs (FIG 5B). Consistent with our findings, it has been reported that the addition of HP increases the gene expression and protein concentration of EGFR (in murine melanoma cells) and the gene expression of IGF1R (in VSMCs) in vitro (Hyoudou et al., 2006) (Du et al., 2001). Our study demonstrates the induction of EGFR and IGF1R expression by HP in ECs and highlights the positive correlation between HMOX1 expression and the expression of these two genes (FIG2.5B). Studies indicating the increased apoptosis of ECs upon EGFR inhibition (Bruns et al., 2000) supports our finding that HMOX1-deficient cells treated with HP resulting in decreased EGFR expression (FIG2.5B) is associated with increased cell death (FIG2.3). Similarly, low IGF-1 (which can also be simulated by decreased expression of the IGF1 receptor as seen in the HMOX1-deficient HUVECs treated with HP (FIG2.5D)) is associated with increased endothelial apoptosis/dysfunction and cardiovascular risk (Conti et al., 2004). Additionally, it has been shown that growth factor signaling results in the phosphorylation of pro-apoptotic proteins, protecting the cell from death (Winn and Harlan, 2005). Taken together, the expression of EGFR and IGF1R (that informs the signaling flux through these receptors) influences decisions of cell fate in ECs. As such, targeted studies exploring the mechanism by which HMOX1 influences the expression of these receptors and the functional consequence of those changes would illuminate potential therapeutic targets for endothelial dysfunction and vascular diseases.

We and others have shown that HP treatment in HMOX1-competent HUVECs causes the down-regulation of mitochondrial encoded electron transport chain (ETC) subunits (Karnewar et

al., 2016); interestingly, we show that this is reversed in HMOX1 deficient HUVECs (FIG2.5D). Consistently, we observed that the increased expression of genes associated with mRNA degradation (e.g. SUPV3L1, CNOT6L/4, and DCP1A/B) in HMOX1-competent cells treated with HP is reversed in HMOX1 deficient HUVECs (data not shown). Furthermore, the decreased expression of protein translation and processing genes (e.g. DARS2, FARS2, MRPL16, MRPL17, SPG7) is reversed in HMOX1 deficient HUVECs in response to HP treatment. Taken together, the increased expression of HMOX1 upon HP treatment is accompanied by increased mRNA degradation and decreased protein processing, which likely results in the decreased expression of ETC subunits and attenuates synthesis of ETC proteins. The reversal of this expression profile in HMOX1 deficient cells suggests that HMOX1 protects against mito-ROS mediated cell death by inhibiting expression or protein assembly of the ETC. Our characterization of mitochondrial respiration in HMOX1-competent and HMOX1-deficient HUVECs suggests that the observed transcriptional changes associated with mitochondrial mRNA and protein processing may have lasting functional consequences. Indeed, our functional analysis of mitochondrial respiration indicates that, consistent with the ETC subunit gene expression, ATP production is significantly decreased upon HP treatment alone and partially rescued upon HP treatment in HMOX1-deficient ECs (FIG2.5E). Previous studies have shown that mitochondrial HMOX1 affects the flux through the ETC by regulating the availability of free heme and CO (Heinemann et al., 2008) (Almeida et al., 2015) (Zuckerbraun et al., 2007) (FIG2.5C). Upon HP treatment, decreased expression of ETC subunits and down-regulation of post-transcriptional and post-translational regulators inhibits mitochondria activity and prevents mitochondrial-ROS mediated pro-death and pro-inflammatory processes. However, in HMOX1 deficiency, this protective mechanism is lost and increased mitochondrial ROS likely promote dysfunction and death. While the role of HMOX1 in

maintaining the redox potential of the mitochondria has been observed, our work provides novel mechanisms for therapeutic intervention to address dysfunctional ECs in vascular disease.

Finally, while the localization of HMOX1 to the nucleus, its decreased enzymatic activity upon nuclear entry, and its potential role in regulating transcription have been suggested (Biswas et al., 2014) (Lin et al., 2007) (Dulak and Jozkowicz, 2014), the role of HMOX1 in epigenetic regulation have not yet been described. We show, for the first time, that HMOX1 deficiency alters the expression of many histone modification genes and lnc-RNAs (FIG2.5F-H). While it has been shown that oxidative stress initiates histone modification influencing HMOX1 expression (Chervona and Costa, 2012), there is no evidence of HMOX1 levels influencing the expression and activity of histone modification genes. Furthermore, lnc-RNAs have been implicated in various aspects of the OSR (Kim et al., 2017) (Huang et al., 2016). These novel aspects suggest that HMOX1-regulated endothelial response to oxidative stress can influence not only transcriptional control but also epigenetic modulations. However, their regulation by HMOX1 is yet to be explored.

In summary, our longitudinal analysis of the OS response in EC has elucidated dynamical mechanisms that are invoked leading to cell fate decisions. At higher doses of OS, as shown in literature extensively and based on our studies, ECs go towards cell death through apoptotic and necrotic mechanisms. At low doses, the cells use recovery mechanisms including, redox enzymes involved in removing free radical species, induction of DNA repair mechanisms through transcription and cell protective mechanisms at the interface of genotoxic and metabolic stress. At a critical dose that lies between cell recovery and death, lie the mechanisms that poise the cell either towards recovery or death. Our temporal studies of response at this dose points to a multitude of cellular responses including several of the cell protective mechanisms that suspend the cell at

the interesting nexus between cell survival and death. Most importantly, our study reveals a master regulator, HMOX1, which appears to play a key role regulating the spatiotemporal response in EC to OS. Whether the novel mechanisms of HMOX1 presented here occur either by the decoupling of its enzymatic and non-enzymatic activities or as a combination of the two requires further analysis. Our study also points to interesting avenues for designing therapeutics to deal with OS response, which is important for vascular dysfunction and disease.

2.6 Acknowledgements

Chapter 2 is a nearly identical version of the manuscript in submission, titled "Spatiotemporal Resolution in Oxidative Stress Response in Endothelial Cells Reveals a Novel Role for HMOX-1" Sindhushree Raghunandan, Srinivasan Ramachandran, Eugene Ke1, Yifei Miao, Ratnesh Lal, Zhen Chen, Shankar Subramaniam. The author of this dissertation was the primary contributor to the work presented in this chapter. This work was supported by NIH grants U01 CA200147 (SS), U01 CA198941(SS), U19 AI090023(SS), R01 HL106579(SS), R01HL108735(SS), R01 HD084633(SS), R01 DK109365(SS), NIH/NHLBI K99/R00HL122368 (ZC) and NSF-STC grant 0939370(SS). The authors would like to thank Dr. John Shyy for his generous use of the laboratory facilities and for providing, along with Dr. Shu Chien, valuable insights into shear stress responses in endothelial cells. We would like to acknowledge Dr. Janice Huss and Angie Hamilton (from the Department of Molecular & Cellular Endocrinology at City of Hope) for their technical support. Finally, we would like to acknowledge Marcy Martin, Jian Kang, and Yun-Ting Wang for their valuable insights and guidance on experimental methods.

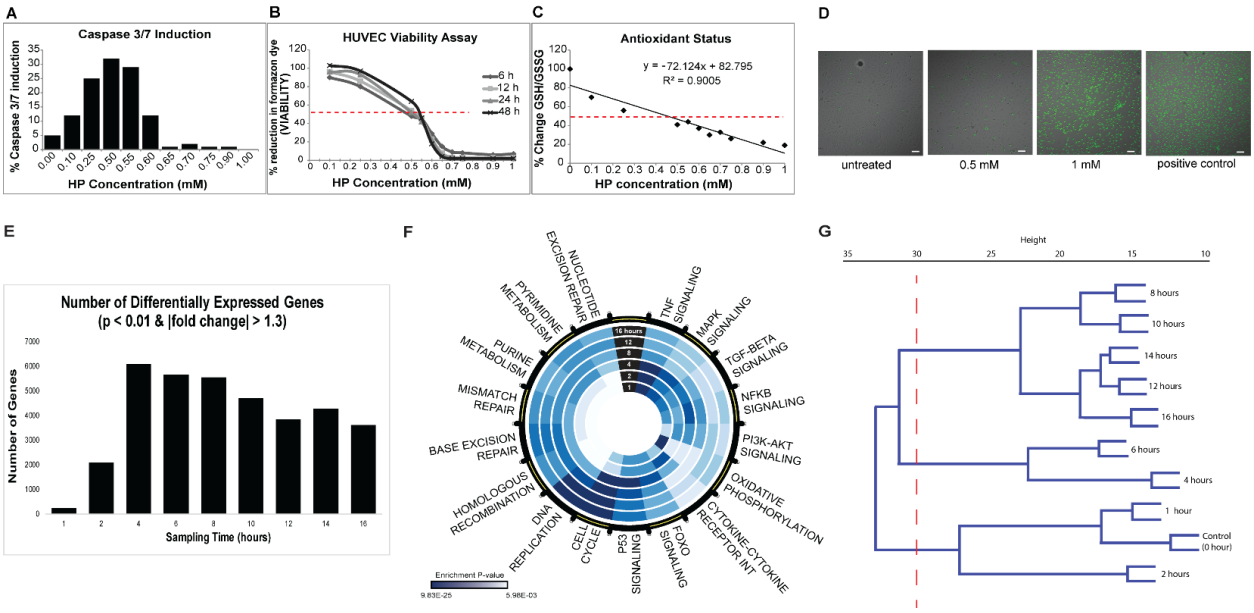

Figure 2.1 A Dose- and Time-Dependent Analysis of H2O2 Induced Oxidative Stress in HUVECs.

(A-D) HUVECs were treated with 0-1mM HP and functional measurements were made to characterize the dose-dependent response to oxidative stress. (E-G) Next, HUVECs were treated with 0.5mM HP in duplicate and mRNA samples, collected at 0, 1, 2, 4, 6, 8, 10, 12, 14, and 16 hours post-treatment, were sequenced in order to characterize the time-dependent response to oxidative stress. A) Caspase 3 and 7 was measured as indicator of apoptotic status. Caspase activity is reported as percent of positive control (10uM staurosporine) at 12 hours post treatment. B) Dehydrogenase activity was measured as proxy for cell viability. Blank adjusted measurements are reported as percentage of the negative control (untreated cells) at 6, 12, 24, and 48 hours post treatment. C) GSH/GSSG ratio measured as an indicator of redox status and reported as percent change with respect to untreated samples D) Cyto-Tox Green assay: amount of green staining is proportional to cytotoxicity. Scale bar: 20µm. E) The number of differentially expressed genes at each time point post HP treatment with respect to control (0 hour); DE genes were identified by a p-value cutoff of 0.01 and a |fold-change| cutoff of 1.3. F) Significantly enriched KEGG pathways. Each ring of the circle represents one time-point, where the inner-most ring represents 1 hour and the outer-most ring represents 16 hours. Dark blue indicates highly significant p-values, whereas light-blue represents less significant p-values. G) Hierarchical clustering dendrogram of normalized gene counts from each time point.

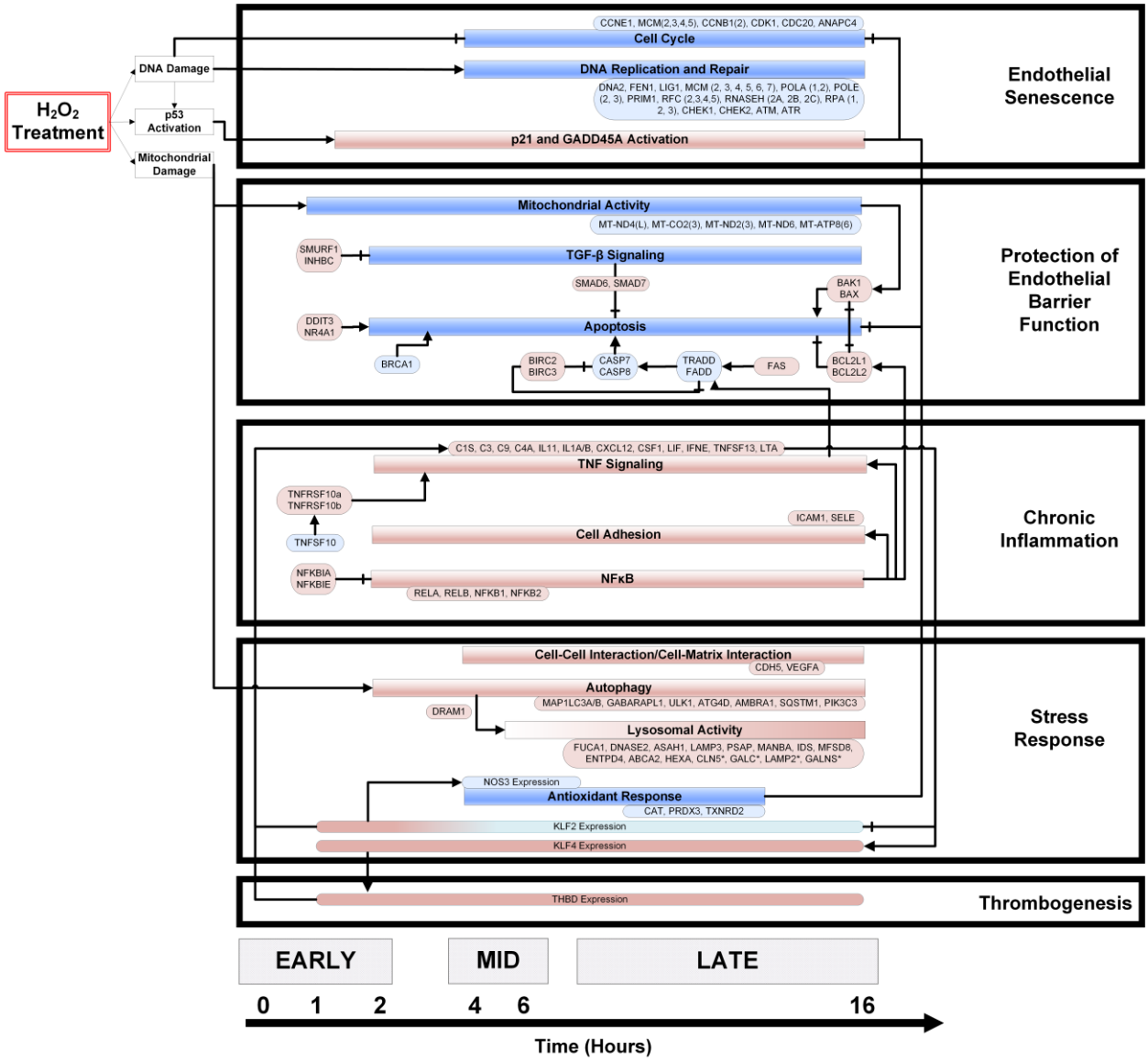

Figure 2.2 A Temporal Model of HP Induced Oxidative Stress in HUVECs.
HUVECs were treated with 0.5mM HP in duplicate and mRNA samples (from 0-16h) were sequenced. Significantly regulated genes and cellular processes ($p < 0.05$) were used to construct a temporal model depicting the time-course of oxidative stress response. The boxes colored in blue and red represent down- and up-regulated genes or processes, respectively. The axis at the bottom of the figure indicates the time at which various processes become significantly regulated. Positive regulation is depicted by an arrow head and negative regulation is indicated by a flat line. Vascular phenotypes associated with each group of genes/processes (i.e. endothelial senescence, protection of endothelial barrier function, chronic inflammation, stress response, and thrombogenesis) are indicated to the right of the temporal model. The log2(fold-change) values for the genes specified in this model are summarized in the supplementary material (FIG S2)

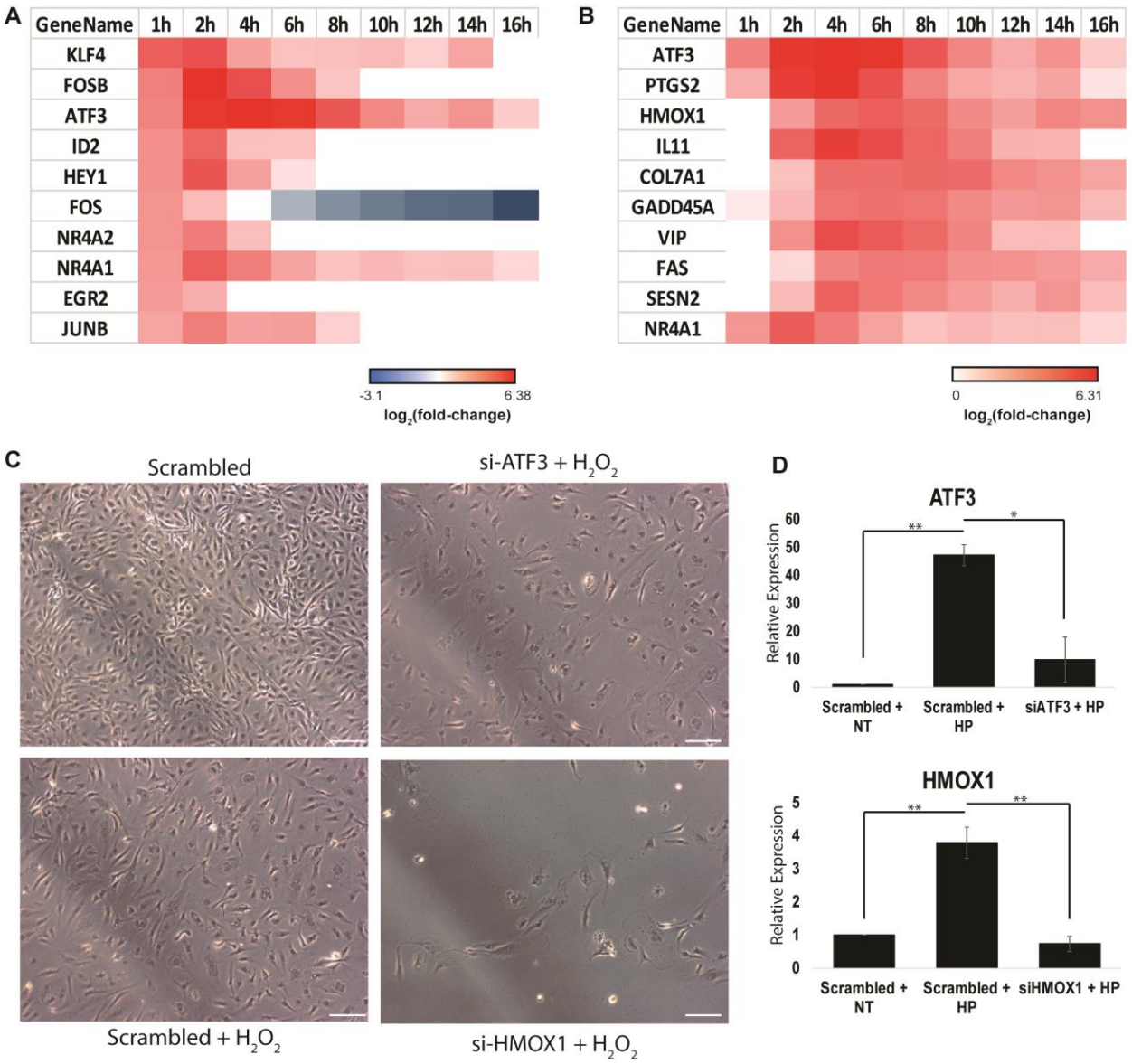

Figure 2.3 HMOX1 is a key regulator of cell fate in HUVECs upon HP treatment.
Significant transcription factor-target interactions were identified to determine key gatekeepers of cell fate and function. A) Top 10 up-regulated transcription factors at 1 hour post HP treatment. B) The top 10 up-regulated gene targets of JUN family transcription factors. All JUN targets differentially expressed at at least one time point were identified and ranked by average fold-change across all time points. C) Two genes were selected from B) for a siRNA screen experiment: ATF3 and HMOX1. After 48 hours of transfection and 6 hours of HP treatment HUVECs were imaged using phase contrast microscopy (the images shown are the representative images taken from 3 repeats of the experiment; scale bars indicate 100µm) D) Mean fold-change + S.E.M. are shown by qPCR for ATF3 (n = 2) and HMOX1 (n = 3). $p < 0.01$ is indicated by ** , $p < 0.05$ is indicated by *.

Figure 2.4 HMOX1 is a global regulator of cell function in HUVECs upon HP treatment. RNA collected from scrambled-NT, scrambled-HP, and siHMOX1-HP samples groups (n= 2 per group) was submitted for RNA-seq. A) The number of differentially expressed genes between Scrambled-HP vs. Scrambled-NT (i.e. indicating the effect of the HP treatment) and between siHMOX1-HP vs. Scrambled-HP (i.e. indicating the effect of the HMOX1 knockdown in response to HP treatment). B) Log2(fold-change) of genes associated with mitochondrial function, inflammatory/immune response, autophagy, transcription, ER stress, antioxidant response, and cell cycle in the time-course data (to the left of the black bar) and in the knockdown experiment (to the right of the black bar). C) The Venn diagram indicates the number of overlapping differentially expressed genes between the time-course experiment and the knock-down experiment (i.e. the 6h vs. 0h comparison of the time-course data, the scrambled-HP vs. scrambled-untreated comparison of the knockdown data, and the siHMOX1-HP vs. scrambled-HP comparison of the knockdown data; $p < 0.05$). The table indicates the number and percentage of overlapping genes that switch direction of expression upon HP treatment in HMOX1 deficient HUVECs. D) KEGG and GO enrichment analysis of the overlapping genes that switch their direction of regulation upon HP treatment in HMOX1 deficient HUVECs. Enrichment of pathways in the time-course data is also shown. The color of cell indicates significance of p-value (the lighter the shade the less significant and the darker the shade the more significant the p-value). The enriched KEGG pathways and GO terms were grouped into three spatial categories as specified in the first column of the table.

A

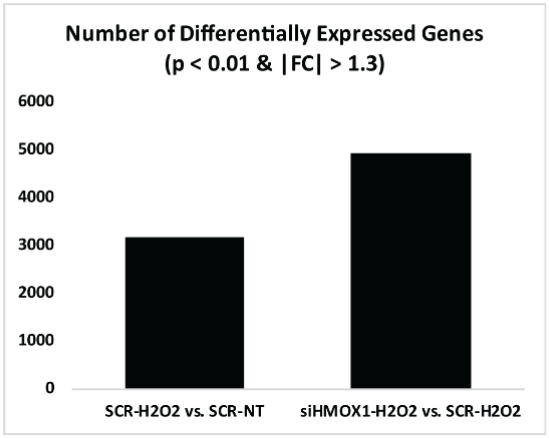

C

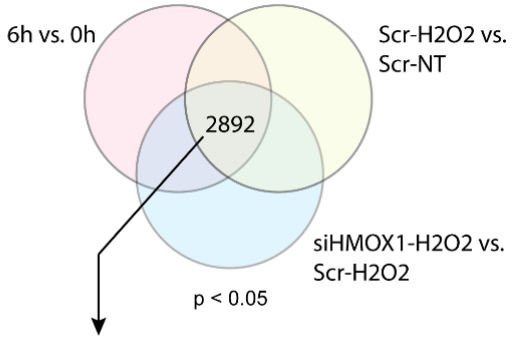

Regulation in 6h v. 0h	Regulation in Scr-H2O2 vs. ScrNT	Regulation in siHMOX1-H2O2 vs. Scr-H2O2	# DE Genes	Percent of Total DE Genes
↑	↑	↓	869	51%
↓	↓	↑	597	

B

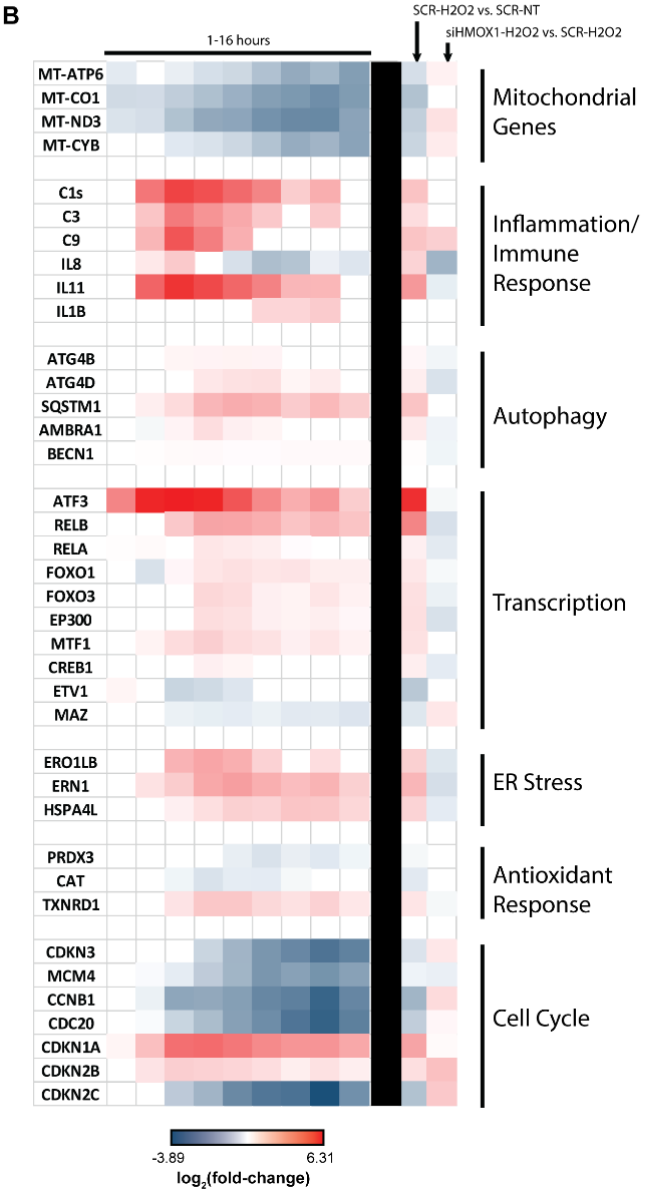

D

Cellular Location	KEGG Pathway/GO Term	siHMOX1-H2O2 vs. SCR-H2O2	P-Value 1h	2h	4h	6h	8h	10h	12h	14h	16h
Nucleus	hsa03040:Spliceosome	1.19E-04									
	GO:0032452~histone demethylase activity	3.97E-04									
	GO:0005643~nuclear pore	8.23E-04									
	GO:0003899~DNA-directed RNA polymerase activity	2.55E-02									
Cell Surface	GO:0005913~cell-cell adherens junction	1.35E-03									
	GO:0019886~antigen processing and presentation	6.55E-03									
Mitochondria	GO:0070469~respiratory chain	1.65E-05									
	hsa00190:Oxidative phosphorylation	8.55E-04									
	GO:0005743~mitochondrial inner membrane	1.27E-03									
	GO:0008137~NADH dehydrogenase (ubiquinone) activity	3.30E-03									
	GO:0005747~mitochondrial respiratory chain complex I	1.38E-02									
	GO:0032981~mitochondrial respiratory chain complex I assembly	4.10E-02									

1.49E-12 4.81E-02
Enrichment p-value

Figure 2.5 HMOX1 deficiency perturbs the OSR at the cell surface, nucleus, and mitochondria.

Differentially expressed genes and pathways in each cellular location were examined in order to identify novel targets of HMOX1 regulation. A) Network diagram depicting HMOX1 activity at the cell surface. B) Fold-change of EGFR and IGF1R expression by qPCR in scrambled-NT, scrambled-HP, and siHMOX1-HP samples. C) Network diagram depicting HMOX1 activity in the mitochondria. D) Fold change of MT-ND3 and MT-ATP6 expression by qPCR in scrambled-NT, scrambled-HP, and siHMOX1-HP samples. E) The MitoStress Test (Seahorse XFe24) was used to quantify functional changes in mitochondrial function. The line-graph shows a representative oxygen consumption rate (pmol/min/cell) for one of the three biological repeats of this experiment (n = 3); 1µM Oligomycin was added at ~20 minutes followed by 2µM FCCP at ~50 minutes and finally 0.5µM Rot/AA at ~80 minutes. The background subtracted mean OCR + SEM across two to four technical replicates for scrambled-NT (blue line), scrambled-HP (red line), and siHMOX1-HP (green line) is shown. The bar-graph to the right indicates the ATP production across all three experiments; all oxygen consumption rate measurements in each experiment were normalized to the basal respiration rate of the Scrambled-NT group. Then, the average measurement after each injection for each treatment group was used to calculate the OCR associated with ATP production. The mean ATP production as a percentage of basal respiration + S.E.M. across all three experiments is shown. $p < 0.05$ (*). F) Network diagram indicating lnc-RNAs and histone modification genes affected by HMOX1 expression. G) Fold change of KDM6A, RBBP5, and PPM1D expression by qPCR in scrambled-NT, scrambled-HP, and siHMOX1-HP samples. H) Log2(fold-change) of lnc-RNAs from the time-course experiment and the knockdown experiment indicating the switch in expression upon HMOX1 deficiency. $p < 0.05$ are shaded; $p > 0.05$ are blank. Log2(fold-change) and p-values for genes described in panels A, C, and F are summarized in FIG S4. For all qPCR data presented: mean + SEM from at least 3 biological replicates (n_bio > 3) is shown; Students unpaired t-test was used to determine p-values: $p < 0.05$ (*), $p < 0.01$ (**), and $p < 0.001$ (***).

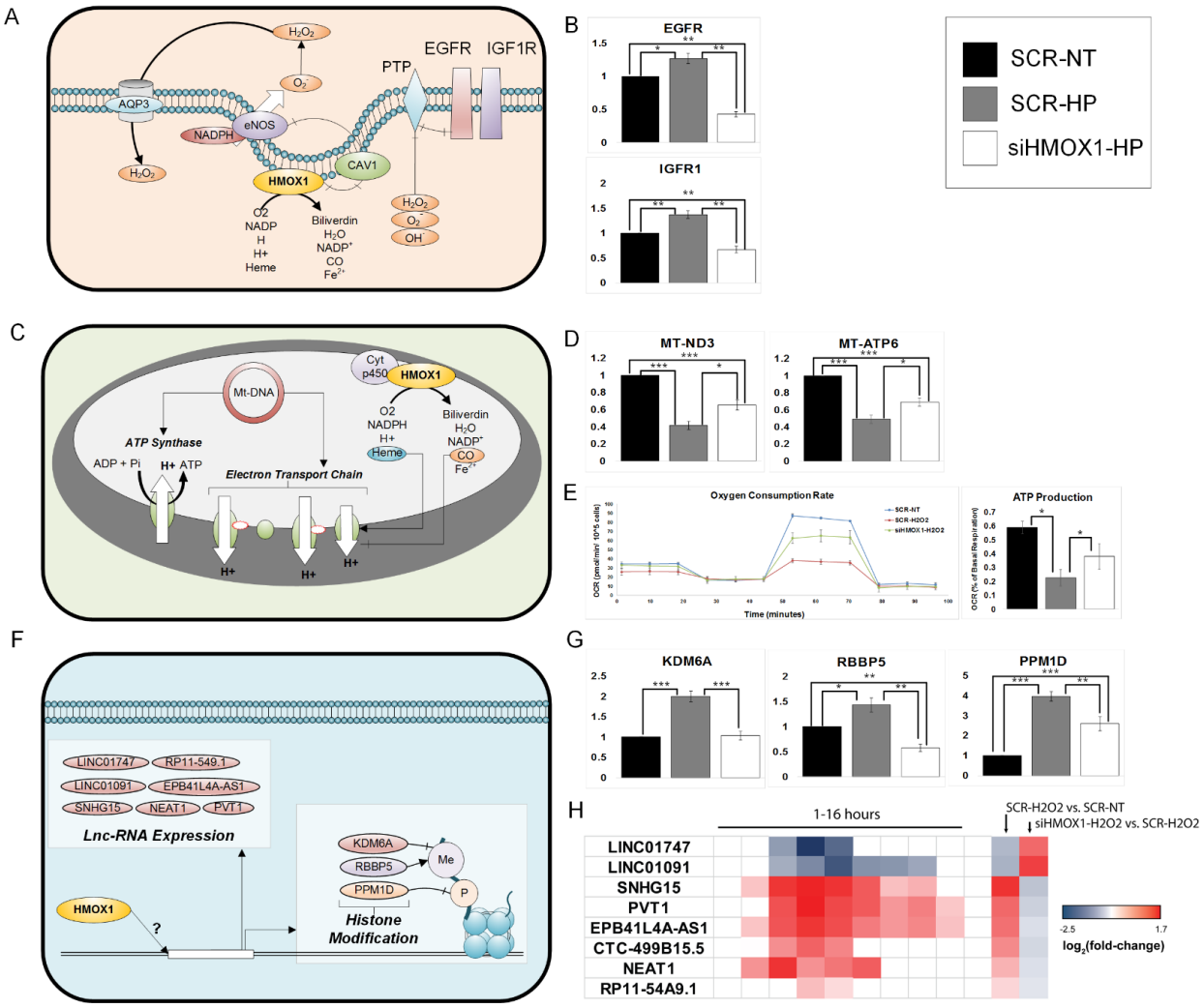
A
B
C
D
E
F
G
H
EGFR
IGF1R
PTP
AQP3
eNOS
NADPH
CAV1
HMOX1
Biliverdin
SCR-NT
SCR-HP
siHMOX1-HP
MT-ND3
MT-ATP6
Mt-DNA
Cyt p450
ATP Synthase
Electron Transport Chain
Oxygen Consumption Rate
ATP Production
Time (minutes)
LINC01747
RP11-549.1
LINC01091
EPB41L4A-AS1
SNHG15
NEAT1
PVT1
Lnc-RNA Expression
KDM6A
RBBP5
PPM1D
Me
P
Histone Modification
KDM6A
RBBP5
PPM1D
1-16 hours
SCR-H2O2 vs. SCR-NT
siHMOX1-H2O2 vs. SCR-H2O2
LINC01747
LINC01091
SNHG15
PVT1
EPB41L4A-AS1
CTC-499B15.5
NEAT1
RP11-54A9.1
log2(fold-change)

A

	Replicate 1		Replicate 2	
	Total read#	Uniquely mapped read%	Total read#	Uniquely mapped read%
control	22088557	83.9122	23782479	84.0059
1h	19739474	83.7663	22057285	83.6304
2h	19386750	84.0874	24870187	82.984
4h	14557529	84.2354	22377555	82.2981
6h	15434799	84.6441	17578932	83.9786
8h	17224818	83.691	23413820	84.0869
10h	17626853	83.3105	16690048	85.1201
12h	17909366	84.8559	18843315	85.2262
14h	20310499	86.1189	20790570	85.5375
16h	15039794	82.271	18047435	84.5686

B

	Replicate 1		Replicate 2	
	Total read#	Uniquely mapped read%	Total read#	Uniquely mapped read%
Scrambled-NT	23464850	87.6069	18695249	68.7756
Scrambled + H2O2	15574457	88.4159	27920902	88.1699
siHMOX1 + H2O2	26549836	87.5914	25304702	87.56

C

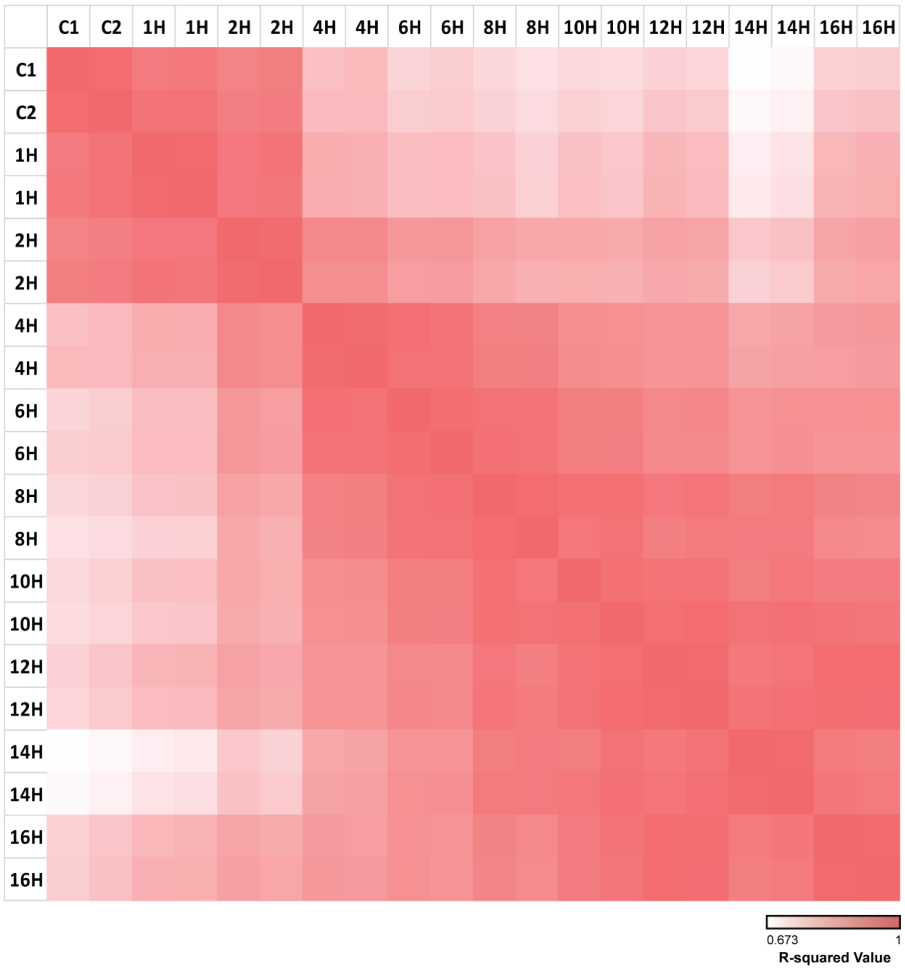

Figure 2.S1 Summary of data quality (read, alignment, and replicate quality)
A) All samples in the time-series experiment had ~20 million reads; the average uniquely mapped alignment percentage was ~84.11%. B) All samples in the knockdown experiment had ~23 million reads; the average uniquely mapped alignment percentage was ~85% C) The R2 value was calculated for all pairwise comparisons between samples in the time-series experiment using raw gene counts from the OSA2 output. The legend indicating the range of R2 values is shown at the bottom left of the heatmap.

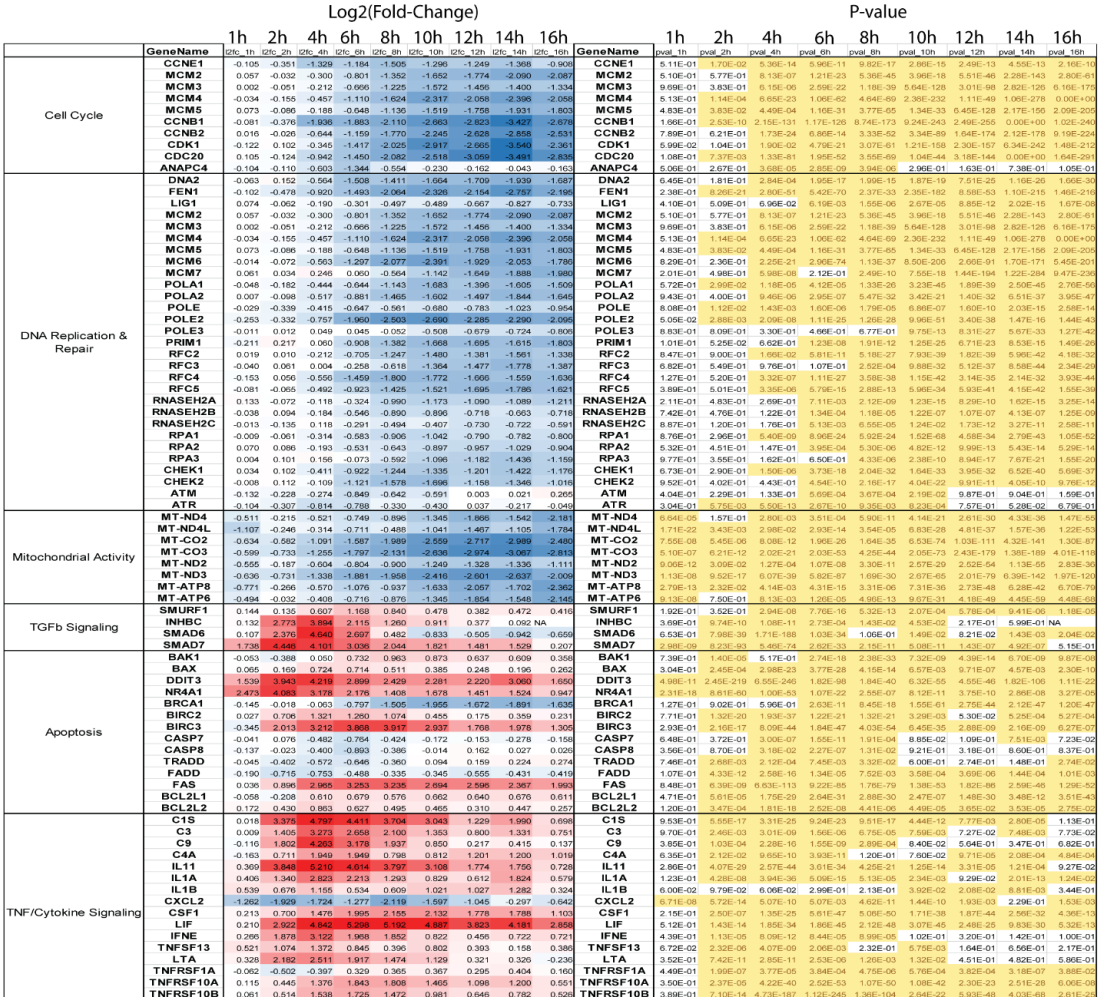

Figure 2.S 2 Summary of log2(fold-change) and p-values for genes included in Figure 2.2
Red indicates up-regulation, blue indicates down-regulation. Yellow coloring of the tiles on the right indicate significant p-values ($p < 0.05$). Pathways and processes corresponding to those mentioned in Figure 2 are listed in the first column.

Figure 2.S3 Phenotypic Validation of Temporal Model of OSR.
HUVECs were treated with 0 or 0.5mM HP and phenotypic measurements were taken to verify the functional consequences of the transcriptomic changes in response to oxidative stress. A & B) HUVECs treated with 0 and 0.5mM HP were analyzed in a flow cytometer. 10,000 events were collected for each sample and their histograms were plotted. The first peak represents the distribution of cells in the G0/G1 phase (M1), the second peak represents cells in the S phase (M2), and the third peak represents cells in the G2/M phase (M3). The average percentage of cells in G0/G1, S, and G2/M phases in control (dark gray) and 0.5mM (light gray) treated samples; error bars indicate standard deviation of the average calculated across two biological repeats of the experiment. P-values labeled above each group; $p < 0.05$ indicated by *. C) HUVECs treated with 0 and 0.5mM HP were stained with Cyto-ID. Autophagic vacuoles are stained in green in 0mM (left) and 0.5mM (right) treated cells were imaged with excitation at 463nm and emission at 534nm.Scale bar indicates 10 μm. D) HUVECs treated with 0 and 0.5mM HP were stained with MitoTraker Deep Red FM dye. 3-5 random fields were chosen for 100x imaging. Images were analyzed in ImageJ software. To visualize the mitochondrial network, their distribution and size, high pass filter (edge detection) was applied. Maximum intensity projection was applied to determine total intensity of mitochondrial stain. The image on the left shows untreated cells and the image on the right shows 0.5 mM HP treated cells. Scale bars, shown at the bottom right corner of each image represent 5μm. E & F) HUVECs were treated with 0 and 0.5mM HP; 12 hours after induction, HUVECs were incubated with 5 μM JC-1. For JC-1 monomers and aggregates, an excitation and emission wavelengths of 485/535 and 560/595 nm, respectively were used. Images were analyzed in ImageJ using a macro that automatically segment and quantify green and red fluorescence. Mitochondrial membrane depolarization is indicated by green fluorescent monomers (green section of bar graph) and healthy mitochondria are indicated by red fluorescent aggregates (red section of bar graph). Ratios of monomers/aggregates (green/red ratio, blue section of bar graph) indicate the overall health of mitochondria in control and treated HUVECs. Scale bar: 10 μm.

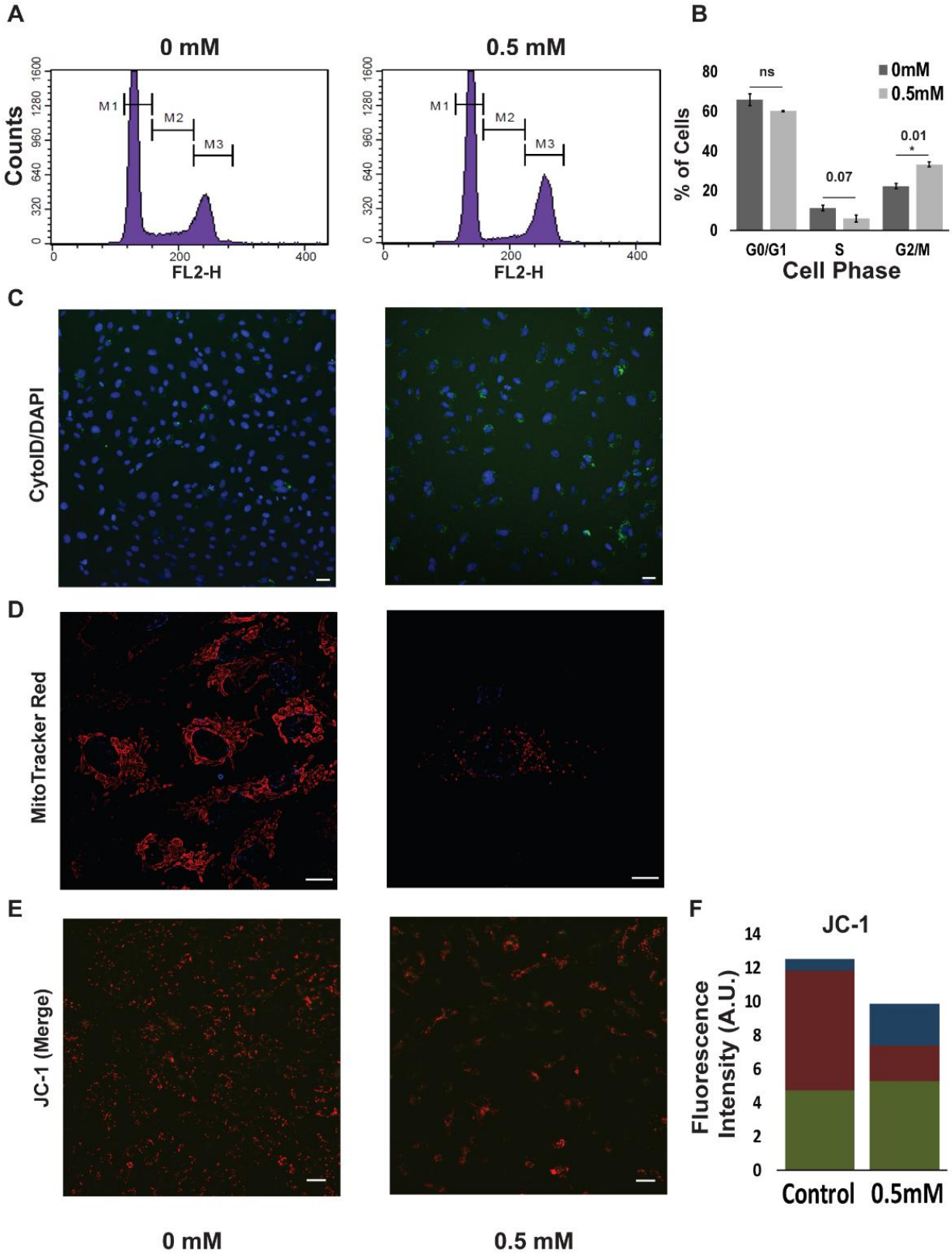
A
0 mM
0.5 mM
Counts
M1
M2
M3
FL2-H
B
ns
0.07
0.01
*
0mM
0.5mM
% of Cells
G0/G1
S
G2/M
Cell Phase
C
CytoID/DAPI
D
MitoTracker Red
E
JC-1 (Merge)
F
JC-1
Fluorescence Intensity (A.U.)
Control
0.5mM
0 mM
0.5 mM

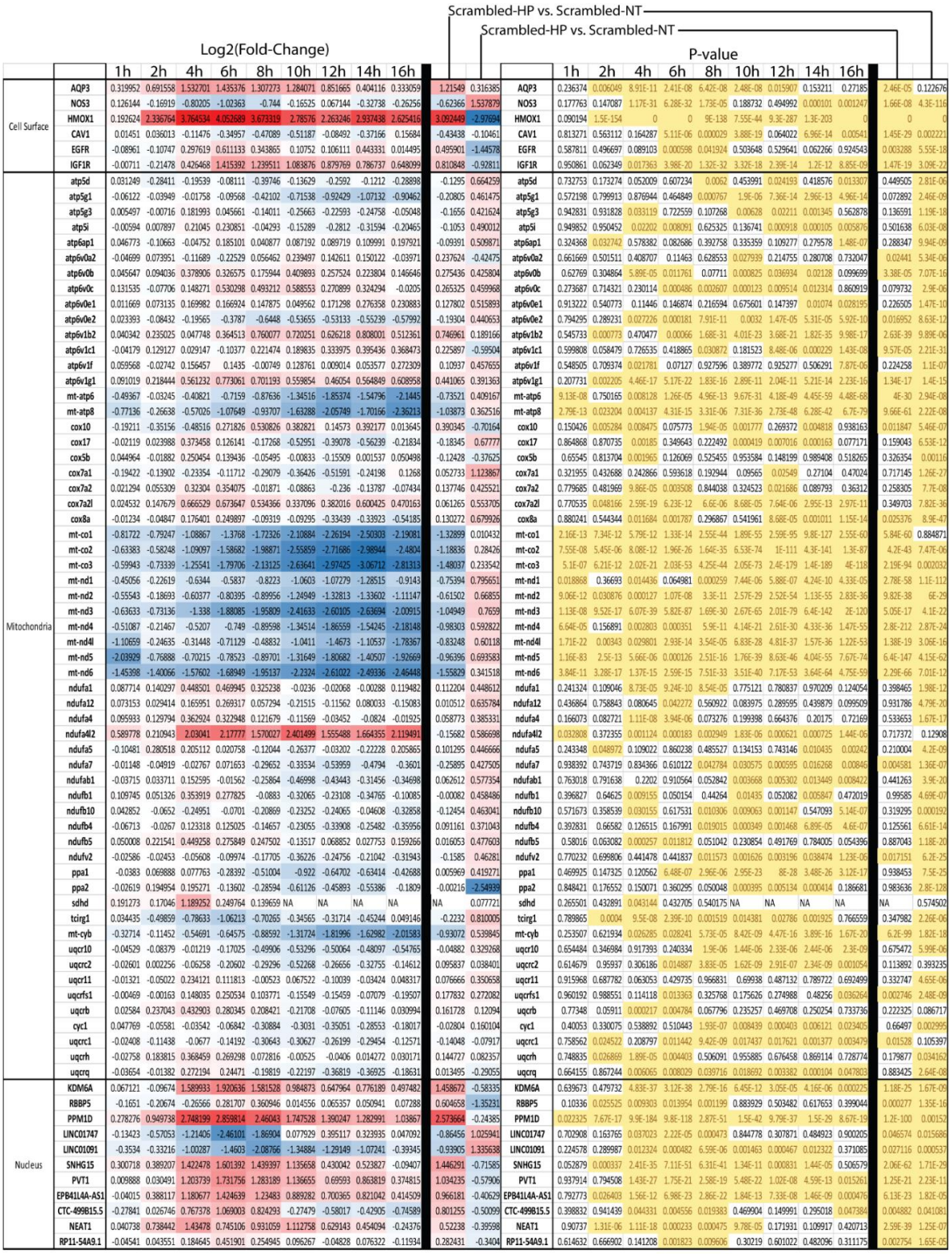

Figure 2.S4 Summary of log2(fold-change) and p-values for genes included in Figure 2.5
Red indicates up-regulation, blue indicates down-regulation. Yellow coloring of the tiles on the right indicate significant p-values ($p < 0.05$). Cellular locations mentioned in FIG 5 are listed in the first column.

2.7 References

Ajami, N., Gupta, S., Maurya, M., Nguyen, P., Yi-Shaun Li, J., Shyy, J., Chen, Z., Chien, S., and Subramaniam, S. (2017). Systems biology analysis of longitudinal functional response of endothelial cells to shear stress. PNAS.

Almeida, A.S., Figueiredo-Pereira, C., and Vieira, H.L.A. (2015). Carbon monoxide and mitochondria-modulation of cell metabolism, redox response and cell death. Front Physiol 6, 33.

Andrews, S. (2010). FastQC: A quality control tool for high throughput sequence data. Reference Source.

Aydogan, V., Lenard, A., Denes, A.S., Sauteur, L., Belting, H.-G., and Affolter, M. (2015). Endothelial cell division in angiogenic sprouts of differing cellular architecture. Biol Open 4, 1259–1269.

Balla, G., Jacob, H.S., Eaton, J.W., Belcher, J.D., and Vercellotti, G.M. (1991). Hemin: a possible physiological mediator of low density lipoprotein oxidation and endothelial injury. Arterioscler. Thromb. 11, 1700–1711.

Balla, J., Jacob, H.S., Balla, G., Nath, K., Eaton, J.W., and Vercellotti, G.M. (1993). Endothelial-cell heme uptake from heme proteins: induction of sensitization and desensitization to oxidant damage. Proc. Natl. Acad. Sci. U.S.A. 90, 9285–9289.

Bannerman, D.D., Sathyamoorthy, M., and Goldblum, S.E. (1998). Bacterial lipopolysaccharide disrupts endothelial monolayer integrity and survival signaling events through caspase cleavage of adherens junction proteins. J. Biol. Chem. 273, 35371–35380.

Biswas, C., Shah, N., Muthu, M., La, P., Fernando, A.P., Sengupta, S., Yang, G., and Dennery, P.A. (2014). Nuclear heme oxygenase-1 (HO-1) modulates subcellular distribution and activation of Nrf2, impacting metabolic and anti-oxidant defenses. J. Biol. Chem. 289, 26882–26894.

Brouard, S., Otterbein, L.E., Anrather, J., Tobiasch, E., Bach, F.H., Choi, A.M., and Soares, M.P. (2000). Carbon monoxide generated by heme oxygenase 1 suppresses endothelial cell apoptosis. J. Exp. Med. 192, 1015–1026.

Brouard, S., Berberat, P.O., Tobiasch, E., Seldon, M.P., Bach, F.H., and Soares, M.P. (2002). Heme oxygenase-1-derived carbon monoxide requires the activation of transcription factor NF-kappa B to protect endothelial cells from tumor necrosis factor-alpha-mediated apoptosis. J. Biol. Chem. 277, 17950–17961.

Bruns, C.J., Solorzano, C.C., Harbison, M.T., Ozawa, S., Tsan, R., Fan, D., Abbruzzese, J., Traxler, P., Buchdunger, E., Radinsky, R., Fidler, I.J. (2000). Blockade of the epidermal growth factor receptor signaling by a novel tyrosine kinase inhibitor leads to apoptosis of endothelial cells and therapy of human pancreatic carcinoma. Cancer Res. 60, 2926–2935.

Cantarella, G., Di Benedetto, G., Ribatti, D., Saccani-Jotti, G., and Bernardini, R. (2014). Involvement of caspase 8 and c-FLIPL in the proangiogenic effects of the tumour necrosis factor-related apoptosis-inducing ligand (TRAIL). FEBS J. 281, 1505–1513.

Chan, K.H., Ng, M.K.C., and Stocker, R. (2011). Haem oxygenase-1 and cardiovascular disease: mechanisms and therapeutic potential. Clin. Sci. 120, 493–504.

Chandra, J., Samali, A., and Orrenius, S. (2000). Triggering and modulation of apoptosis by oxidative stress. Free Radical Biology and Medicine 29, 323–333.

Chen, J., Patschan, S., and Goligorsky, M.S. (2008). Stress-induced premature senescence of endothelial cells. Journal of Nephrology 21, 337.

Chervona, Y., and Costa, M. (2012). The control of histone methylation and gene expression by oxidative stress, hypoxia and metals. Free Radic Biol Med 53, 1041–1047.

Chien, S. (2008). Effects of Disturbed Flow on Endothelial Cells. Ann Biomed Eng 36, 554–562.

Chiu, J.-J., and Chien, S. (2011). Effects of disturbed flow on vascular endothelium: pathophysiological basis and clinical perspectives. Physiological Reviews 91, 327–387.

Clément, M.-V., Ponton, A., and Pervaiz, S. (1998). Apoptosis induced by hydrogen peroxide is mediated by decreased superoxide anion concentration and reduction of intracellular milieu. FEBS Letters 440, 13–18.

Conti, E., Carrozza, C., Capoluongo, E., Volpe, M., Crea, F., Zuppi, C., and Andreotti, F. (2004). Insulin-like growth factor-1 as a vascular protective factor. Circulation 110, 2260–2265.

Csordas, A., Wick, G., and Bernhard, D. (2006). Hydrogen peroxide-mediated necrosis induction in HUVECs is associated with an atypical pattern of caspase-3 cleavage. Experimental Cell Research 312, 1753–1764.

Deanfield, J.E., Halcox, J.P., and Rabelink, T.J. (2007). Endothelial function and dysfunction: testing and clinical relevance. Circulation 115, 1285–1295.

Deshane, J., Wright, M., and Agarwal, A. (2005). Heme oxygenase-1 expression in disease states. Acta Biochim. Pol. 52, 273–284.

Dimmeler, S., and Zeiher, A.M. (2000). Endothelial cell apoptosis in angiogenesis and vessel regression. Circ. Res. 87, 434–439.

Donato, A.J., Morgan, R.G., Walker, A.E., and Lesniewski, L.A. (2015). Cellular and Molecular Biology of Aging Endothelial Cells. J Mol Cell Cardiol 89, 122–135.

Du, J., Brink, M., Peng, T., Mottironi, B., and Delafontaine, P. (2001). Thrombin regulates insulin-like growth factor-1 receptor transcription in vascular smooth muscle: characterization of the signaling pathway. Circ. Res. 88, 1044–1052.

Dulak, J., and Jozkowicz, A. (2014). Novel Faces of Heme Oxygenase-1: Mechanisms and Therapeutic Potentials. Antioxidants & Redox Signaling 20, 1673–1676.

Dunn, L.L., Midwinter, R.G., Ni, J., Hamid, H.A., Parish, C.R., and Stocker, R. (2014). New Insights into Intracellular Locations and Functions of Heme Oxygenase-1. Antioxid Redox Signal 20, 1723–1742.

Elahi, M.M., Kong, Y.X., and Matata, B.M. (2009). Oxidative stress as a mediator of cardiovascular disease. Oxid Med Cell Longev 2, 259–269.

Elmore, S. (2007). Apoptosis: a review of programmed cell death. Toxicologic Pathology 35, 495–516.

Finkel, T., and Holbrook, N.J. (2000). Oxidants, oxidative stress and the biology of ageing. Nature 408, 239–247.

Fledderus, J.O., Boon, R.A., Volger, O.L., Hurttila, H., Ylä-Herttuala, S., Pannekoek, H., Levonen, A.-L., and Horrevoets, A.J. (2008). KLF2 primes the antioxidant transcription factor Nrf2 for activation in endothelial cells. Arteriosclerosis, Thrombosis, and Vascular Biology 28, 1339–1346.

Flusberg, D.A., and Sorger, P.K. (2015). Surviving apoptosis: life-death signaling in single cells. Trends Cell Biol 25, 446–458.

Galbraith, C.G., Skalak, R., and Chien, S. (1998). Shear stress induces spatial reorganization of the endothelial cell cytoskeleton. Cell Motil. Cytoskeleton 40, 317–330.

Gao, M., Guo, N., Huang, C., and Song, L. (2009). Diverse roles of GADD45α in stress signaling. Current Protein and Peptide Science 10, 388–394.

Gimbrone, M.A., and García-Cardeña, G. (2016). Endothelial Cell Dysfunction and the Pathobiology of Atherosclerosis. Circ. Res. 118, 620–636.

Gong, G., Qin, Y., Huang, W., Zhou, S., Yang, X., and Li, D. (2010). Rutin inhibits hydrogen peroxide-induced apoptosis through regulating reactive oxygen species mediated mitochondrial dysfunction pathway in human umbilical vein endothelial cells. European Journal of Pharmacology 628, 27–35.

van Gorp, R.M., Broers, J.L., Reutelingsperger, C.P., Bronnenberg, N.M., Hornstra, G., van Dam-Mieras, M.C., and Heemskerk, J.W. (1999). Peroxide-induced membrane blebbing in endothelial cells associated with glutathione oxidation but not apoptosis. American Journal of Physiology-Cell Physiology 277, C20–C28.

Gozzelino, R., Jeney, V., and Soares, M.P. (2010). Mechanisms of cell protection by heme oxygenase-1. Annual Review of Pharmacology and Toxicology 50, 323–354.

Gross, A., McDonnell, J.M., and Korsmeyer, S.J. (1999). BCL-2 family members and the mitochondria in apoptosis. Genes Dev. 13, 1899–1911.

Hadi, H.A., Carr, C.S., and Al Suwaidi, J. (2005). Endothelial Dysfunction: Cardiovascular Risk Factors, Therapy, and Outcome. Vasc Health Risk Manag 1, 183–198.

Han, E.-S., Muller, F.L., Pérez, V.I., Qi, W., Liang, H., Xi, L., Fu, C., Doyle, E., Hickey, M., and Cornell, J. (2008). The in vivo gene expression signature of oxidative stress. Physiological Genomics 34, 112–126.

He, F., and Zuo, L. (2015). Redox Roles of Reactive Oxygen Species in Cardiovascular Diseases. Int J Mol Sci 16, 27770–27780.

Heinemann, I.U., Jahn, M., and Jahn, D. (2008). The biochemistry of heme biosynthesis. Arch. Biochem. Biophys. 474, 238–251.

Hori, R., Kashiba, M., Toma, T., Yachie, A., Goda, N., Makino, N., Soejima, A., Nagasawa, T., Nakabayashi, K., and Suematsu, M. (2002). Gene transfection of H25A mutant heme oxygenase-1 protects cells against hydroperoxide-induced cytotoxicity. J. Biol. Chem. 277, 10712–10718.

Hu, J., Ge, H., Newman, M., and Liu, K. (2012). OSA: a fast and accurate alignment tool for RNA-Seq. Bioinformatics 28, 1933–1934.

Huang, D.W., Sherman, B.T., and Lempicki, R.A. (2009). Systematic and integrative analysis of large gene lists using DAVID bioinformatics resources. Nat Protoc 4, 44–57.

Huang, T.-S., Wang, K.-C., Li, J.Y.-S., Chang, T.-Y., Subramaniam, S., Shyy, J., Wang, H.-W., and Chien, S. (2016). Role of lncRNAs in Regulating Endothelial Function. FASEB J 30, 1028.9-1028.9.

Huynh, J., Nishimura, N., Rana, K., Peloquin, J.M., Califano, J.P., Montague, C.R., King, M.R., Schaffer, C.B., and Reinhart-King, C.A. (2011). Age-Related Intimal Stiffening Enhances Endothelial Permeability and Leukocyte Transmigration. Sci Transl Med 3, 112ra122.

Hyoudou, K., Nishikawa, M., Kobayashi, Y., Umeyama, Y., Yamashita, F., and Hashida, M. (2006). PEGylated catalase prevents metastatic tumor growth aggravated by tumor removal. Free Radic. Biol. Med. 41, 1449–1458.

Jang, J.-H., Moritz, W., Graf, R., and Clavien, P.-A. (2008). Preconditioning with death ligands FasL and TNF-alpha protects the cirrhotic mouse liver against ischaemic injury. Gut 57, 492–499.

Jiang, Y.-Z., Jiménez, J.M., Ou, K., McCormick, M.E., Zhang, L.-D., and Davies, P.F. (2014). Hemodynamic disturbed flow induces differential DNA methylation of endothelial Kruppel-Like Factor 4 promoter in vitro and in vivo. Circ. Res. 115, 32–43.

Kanehisa, M., and Goto, S. (2000). KEGG: kyoto encyclopedia of genes and genomes. Nucleic Acids Res. 28, 27–30.

Kanehisa, M., Sato, Y., Kawashima, M., Furumichi, M., and Tanabe, M. (2016). KEGG as a reference resource for gene and protein annotation. Nucleic Acids Res. 44, D457-462.

Kanehisa, M., Furumichi, M., Tanabe, M., Sato, Y., and Morishima, K. (2017). KEGG: new perspectives on genomes, pathways, diseases and drugs. Nucleic Acids Res. 45, D353–D361.

Karnewar, S., Vasamsetti, S.B., Gopoju, R., Kanugula, A.K., Ganji, S.K., Prabhakar, S., Rangaraj, N., Tupperwar, N., Kumar, J.M., and Kotamraju, S. (2016). Mitochondria-targeted esculetin alleviates mitochondrial dysfunction by AMPK-mediated nitric oxide and SIRT3 regulation in endothelial cells: potential implications in atherosclerosis. Sci Rep 6, 24108.

Kawauchi, J., Zhang, C., Nobori, K., Hashimoto, Y., Adachi, M.T., Noda, A., Sunamori, M., and Kitajima, S. (2002). Transcriptional Repressor Activating Transcription Factor 3 Protects Human Umbilical Vein Endothelial Cells from Tumor Necrosis Factor-α-induced Apoptosis through Down-regulation ofp53 Transcription. Journal of Biological Chemistry 277, 39025–39034.

Kim, C., Kang, D., Lee, E.K., and Lee, J.-S. (2017). Long Noncoding RNAs and RNA-Binding Proteins in Oxidative Stress, Cellular Senescence, and Age-Related Diseases. Oxid Med Cell Longev 2017, 2062384.

Kim, K.M., Pae, H.-O., Zheng, M., Park, R., Kim, Y.-M., and Chung, H.-T. (2007). Carbon monoxide induces heme oxygenase-1 via activation of protein kinase R-like endoplasmic reticulum kinase and inhibits endothelial cell apoptosis triggered by endoplasmic reticulum stress. Circ. Res. 101, 919–927.

Kim, Y.-M., Pae, H.-O., Park, J.E., Lee, Y.C., Woo, J.M., Kim, N.-H., Choi, Y.K., Lee, B.-S., Kim, S.R., and Chung, H.-T. (2011). Heme Oxygenase in the Regulation of Vascular Biology: From Molecular Mechanisms to Therapeutic Opportunities. Antioxid Redox Signal 14, 137–167.

Kobayashi, M., and Yamamoto, M. (2006). Nrf2–Keap1 regulation of cellular defense mechanisms against electrophiles and reactive oxygen species. Advances in Enzyme Regulation 46, 113–140.

Kuilman, T., Michaloglou, C., Mooi, W.J., and Peeper, D.S. (2010). The essence of senescence. Genes & Development 24, 2463–2479.

Langfelder, P., and Horvath, S. (2012). Fast R Functions for Robust Correlations and Hierarchical Clustering. J Stat Softw 46.

Liang, Y., Li, J., Lin, Q., Huang, P., Zhang, L., Wu, W., and Ma, Y. (2017). Research Progress on Signaling Pathway-Associated Oxidative Stress in Endothelial Cells. Oxid Med Cell Longev 2017, 7156941.

Libby, P., Ridker, P.M., and Hansson, G.K. (2011). Progress and challenges in translating the biology of atherosclerosis. Nature 473, 317–325.

Lin, Q., Weis, S., Yang, G., Weng, Y.-H., Helston, R., Rish, K., Smith, A., Bordner, J., Polte, T., Gaunitz, F., Dennery, P.A. (2007). Heme oxygenase-1 protein localizes to the nucleus and activates transcription factors important in oxidative stress. J. Biol. Chem. 282, 20621–20633.

Love, M.I., Huber, W., and Anders, S. (2014). Moderated estimation of fold change and dispersion for RNA-Seq data with DESeq2. Genome Biology 15, 550.

Lum, H., and Roebuck, K.A. (2001). Oxidant stress and endothelial cell dysfunction. Am. J. Physiol., Cell Physiol. 280, C719-741.

Madamanchi, N.R., Vendrov, A., and Runge, M.S. (2005). Oxidative stress and vascular disease. Arterioscler. Thromb. Vasc. Biol. 25, 29–38.

Mallat, Z., and Tedgui, A. (2000). Apoptosis in the vasculature: mechanisms and functional importance. Br J Pharmacol 130, 947–962.

Martinon, F., and Tschopp, J. (2004). Inflammatory caspases: linking an intracellular innate immune system to autoinflammatory diseases. Cell 117, 561–574.

Matys, V., Kel-Margoulis, O.V., Fricke, E., Liebich, I., Land, S., Barre-Dirrie, A., Reuter, I., Chekmenev, D., Krull, M., and Hornischer, K. (2006). TRANSFAC® and its module TRANSCompel®: transcriptional gene regulation in eukaryotes. Nucleic Acids Research 34, D108–D110.

Medzhitov, R., Schneider, D.S., and Soares, M.P. (2012). Disease tolerance as a defense strategy. Science 335, 936–941.

Messner, B., Frotschnig, S., Steinacher-Nigisch, A., Winter, B., Eichmair, E., Gebetsberger, J., Schwaiger, S., Ploner, C., Laufer, G., and Bernhard, D. (2012). Apoptosis and necrosis: two different outcomes of cigarette smoke condensate-induced endothelial cell death. Cell Death Dis 3, e424.

Morgan, M.J., and Liu, Z. (2011). Crosstalk of reactive oxygen species and NF-κB signaling. Cell Res 21, 103–115.

Moskalev, A.A., Smit-McBride, Z., Shaposhnikov, M.V., Plyusnina, E.N., Zhavoronkov, A., Budovsky, A., Tacutu, R., and Fraifeld, V.E. (2012). Gadd45 proteins: relevance to aging, longevity and age-related pathologies. Ageing Research Reviews 11, 51–66.

Muñoz-Espín, D., and Serrano, M. (2014). Cellular senescence: from physiology to pathology. Nature Reviews Molecular Cell Biology 15, 482–496.

Nadeev, A.D., Kudryavtsev, I.V., Serebriakova, M.K., Avdonin, P.V., Zinchenko, V.P., and Goncharov, N.V. (2015). [DUAL PROAPOPTOTIC AND PRONECROTIC EFFECT OF HYDROGEN PEROXIDE ON HUMAN UMBILICAL VEIN ENDOTHELIAL CELLS]. Tsitologiia 57, 909–916.

Niehrs, C., and Schäfer, A. (2012). Active DNA demethylation by Gadd45 and DNA repair. Trends in Cell Biology 22, 220–227.

Pennathur, S., and Heinecke, J.W. (2007). Oxidative stress and endothelial dysfunction in vascular disease. Curr. Diab. Rep. 7, 257–264.

Portt, L., Norman, G., Clapp, C., Greenwood, M., and Greenwood, M.T. (2011). Anti-apoptosis and cell survival: a review. Biochim. Biophys. Acta 1813, 238–259.

Reichard, J.F., Motz, G.T., and Puga, A. (2007). Heme oxygenase-1 induction by NRF2 requires inactivation of the transcriptional repressor BACH1. Nucleic Acids Res 35, 7074–7086.

Romanoski, C.E., Che, N., Yin, F., Mai, N., Pouldar, D., Civelek, M., Pan, C., Lee, S., Vakili, L., and Yang, W.-P. (2011). Network for Activation of Human Endothelial Cells by Oxidized Phospholipids A Critical Role of Heme Oxygenase 1. Circulation Research 109, e27–e41.

Salminen, A., Ojala, J., and Kaarniranta, K. (2011). Apoptosis and aging: increased resistance to apoptosis enhances the aging process. Cell. Mol. Life Sci. 68, 1021–1031.

Sangwung, P., Zhou, G., Nayak, L., Chan, E.R., Kumar, S., Kang, D.-W., Zhang, R., Liao, X., Lu, Y., Sugi, K., Fujioka, H., Shi, H., D, Lapping, S.D., Ghosh, C.C., Higgins, S.J., Parikh, S.M., Jo, H., Jain, M.K. KLF2 and KLF4 control endothelial identity and vascular integrity. JCI Insight 2.

SEALS, D.R., JABLONSKI, K.L., and DONATO, A.J. (2011). Aging and vascular endothelial function in humans. Clin Sci (Lond) 120, 357–375.

Secchiero, P., Gonelli, A., Carnevale, E., Milani, D., Pandolfi, A., Zella, D., and Zauli, G. (2003). TRAIL promotes the survival and proliferation of primary human vascular endothelial cells by activating the Akt and ERK pathways. Circulation 107, 2250–2256.

Secchiero, P., Zerbinati, C., Rimondi, E., Corallini, F., Milani, D., Grill, V., Forti, G., Capitani, S., and Zauli, G. (2004). TRAIL promotes the survival, migration and proliferation of vascular smooth muscle cells. Cell. Mol. Life Sci. 61, 1965–1974.

Seldon, M.P., Silva, G., Pejanovic, N., Larsen, R., Gregoire, I.P., Filipe, J., Anrather, J., and Soares, M.P. (2007). Heme oxygenase-1 inhibits the expression of adhesion molecules associated with endothelial cell activation via inhibition of NF-kappaB RelA phosphorylation at serine 276. J. Immunol. 179, 7840–7851.

Silva, G., Cunha, A., Grégoire, I.P., Seldon, M.P., and Soares, M.P. (2006). The antiapoptotic effect of heme oxygenase-1 in endothelial cells involves the degradation of p38 alpha MAPK isoform. J. Immunol. 177, 1894–1903.

Soares, M.P., Usheva, A., Brouard, S., Berberat, P.O., Gunther, L., Tobiasch, E., and Bach, F.H. (2002). Modulation of endothelial cell apoptosis by heme oxygenase-1-derived carbon monoxide. Antioxid. Redox Signal. 4, 321–329.

Soares, M.P., Seldon, M.P., Gregoire, I.P., Vassilevskaia, T., Berberat, P.O., Yu, J., Tsui, T.-Y., and Bach, F.H. (2004). Heme oxygenase-1 modulates the expression of adhesion molecules associated with endothelial cell activation. J. Immunol. 172, 3553–3563.

Tamura, R.E., de Vasconcellos, J.F., Sarkar, D., Libermann, T.A., Fisher, P.B., and Zerbini, L.F. (2012). GADD45 proteins: central players in tumorigenesis. Current Molecular Medicine 12, 634.

Tanaka, Y., Nakamura, A., Morioka, M.S., Inoue, S., Tamamori-Adachi, M., Yamada, K., Taketani, K., Kawauchi, J., Tanaka-Okamoto, M., and Miyoshi, J. (2011). Systems analysis of ATF3 in stress response and cancer reveals opposing effects on pro-apoptotic genes in p53 pathway. PLoS One 6, e26848.

Taniyama, Y., and Griendling, K.K. (2003). Reactive oxygen species in the vasculature: molecular and cellular mechanisms. Hypertension 42, 1075–1081.

Tian, X.-L., and Li, Y. (2014). Endothelial cell senescence and age-related vascular diseases. J Genet Genomics 41, 485–495.

Tousoulis, D., Kampoli, A.-M., Tentolouris, C., Papageorgiou, N., and Stefanadis, C. (2012). The role of nitric oxide on endothelial function. Curr Vasc Pharmacol 10, 4–18.

Toussaint, O., Remacle, J., Dierick, J.-F., Pascal, T., Frippiat, C., Royer, V., Magalhacs, J.P., Zdanov, S., and Chainiaux, F. (2002). Stress-induced premature senescence: from biomarkers to likeliness of in vivo occurrence. Biogerontology 3, 13–17.

Trachootham, D., Lu, W., Ogasawara, M.A., Valle, N.R.-D., and Huang, P. (2008). Redox regulation of cell survival. Antioxidants & Redox Signaling 10, 1343–1374.

Wen, Y.-D., Wang, H., Kho, S.-H., Rinkiko, S., Sheng, X., Shen, H.-M., and Zhu, Y.-Z. (2013). Hydrogen sulfide protects HUVECs against hydrogen peroxide induced mitochondrial dysfunction and oxidative stress. PLoS One 8, e53147.

Winn, R.K., and Harlan, J.M. (2005). The role of endothelial cell apoptosis in inflammatory and immune diseases. J. Thromb. Haemost. 3, 1815–1824.

Xu, M.-C., Shi, H.-M., Wang, H., and Gao, X.-F. (2013). Salidroside protects against hydrogen peroxide-induced injury in HUVECs via the regulation of REDD1 and mTOR activation. Molecular Medicine Reports 8, 147–153.

Yachie, A., Niida, Y., Wada, T., Igarashi, N., Kaneda, H., Toma, T., Ohta, K., Kasahara, Y., and Koizumi, S. (1999). Oxidative stress causes enhanced endothelial cell injury in human heme oxygenase-1 deficiency. J. Clin. Invest. 103, 129–135.

Yoshida, T., Sugiura, H., Mitobe, M., Tsuchiya, K., Shirota, S., Nishimura, S., Shiohira, S., Ito, H., Nobori, K., Gullans, S.R., Akiba, T., Nitta, K. (2008). ATF3 protects against renal ischemia-reperfusion injury. J. Am. Soc. Nephrol. 19, 217–224.

Yu, J., Tian, S., Metheny-Barlow, L., Chew, L.J., Hayes, A.J., Pan, H., Yu, G.L., and Li, L.Y. (2001). Modulation of endothelial cell growth arrest and apoptosis by vascular endothelial growth inhibitor. Circ. Res. 89, 1161–1167.

Zhan, Q. (2005). Gadd45a, a p53-and BRCA1-regulated stress protein, in cellular response to DNA damage. Mutation Research/Fundamental and Molecular Mechanisms of Mutagenesis 569, 133–143.

Zhang, J., Patel, J.M., and Block, E.R. (2002). Enhanced apoptosis in prolonged cultures of senescent porcine pulmonary artery endothelial cells. Mech. Ageing Dev. 123, 613–625.

Zhou, X., Yuan, D., Wang, M., and He, P. (2013). H2O2-induced endothelial NO production contributes to vascular cell apoptosis and increased permeability in rat venules. Am. J. Physiol. Heart Circ. Physiol. 304, H82-93.

Zuckerbraun, B.S., Chin, B.Y., Bilban, M., d'Avila, J. de C., Rao, J., Billiar, T.R., and Otterbein, L.E. (2007). Carbon monoxide signals via inhibition of cytochrome c oxidase and generation of mitochondrial reactive oxygen species. FASEB J. 21, 1099–1106.

CHAPTER 3 : HIGH FAT DIET INDUCED LIVER CANCER

3.1 Abstract

The liver is highly complex organ responsible for detoxifying the blood as well as producing proteins (e.g. vitamins, hormones etc) and clotting factors that are circulated throughout the body. It also plays a critical role in orchestrating metabolic functions of the intestines (by producing and secreting bile acid for lipid absorption), adipose tissue (where excess food and energy processed by the liver are stored as lipid vesicles), and muscle tissue (to which the liver is the main source of glucose). Additionally, the liver synthesizes and secretes complement proteins, which are important effector molecules in the innate and adaptive immune response. Finally, the liver is the only organ that is able to regenerate upon severe stress/damage. Taken together, the liver not only filters toxic substances from blood but is highly involved in both anabolic and catabolic processes, which results in constant turnover of cellular stress. Also, because the liver generates components (such as amino acids, vitamins, coagulation factors etc.) that are used by other tissues in the body, there is a tremendous amount of systemic feedback that regulate the liver. So, it is important to consider the role of hepatic and systemic stress response in the development of liver cancer. It is also important to note that p62, a key player in selective autophagy, is overexpressed in cancers and has been found in the Mallory-Denk bodies that are characteristic of hepatocellular carcinoma (HCC). The objective of this study is to understand the role of p62 and NBR1 (a structurally similar protein) in mediating high-fat diet induced stress in the development of liver dysfunction and disease. To this end liver samples from total and conditional (hepatocyte specific) knockout mouse models of p62 and NBR1 were sequenced and the transcriptional signature of each knockout condition was examined.

3.2 Introduction

The prevalence of non-alcoholic fatty liver disease (NAFLD) is 25% worldwide (Younossi et al., 2016). The initial stages of hepatic fat accumulation leading to NAFLD (known as simple steatosis), progresses to non-alcoholic steatohepatitis (NASH) due to the increased inflammatory and oxidative stress in response to the accumulated fat. Persistence in the inflammatory and immune response results in the advancement to cirrhosis, which involves fibrosis and the formation of scar tissue. Finally, oxidative and replicative stress drives DNA damage, genomic instability, oncogenic transformation, and progression to hepatocellular carcinoma (HCC) (Lewis and Mohanty, 2010) (Cohen et al., 2011) (Reuter et al., 2010). Taken together, it is clear that the progression of liver disease is founded on three pathophysiological features: metabolic dysregulation/steatosis, activation of the immune response, and fibrosis.

The liver is a central regulator of metabolism; it is able to coordinate energy storage (during fed states) or energy utilization (during fasting states) (Rui, 2014). In cases of obesity or insulin resistance, which are comorbidities of NAFLD (Paschos and Paletas, 2009) (Younossi et al., 2016), the persistent secretion of fatty acids (FAs) by adipose tissue is stored by the liver as triglycerides resulting in steatosis. Additionally, NAFLD is characterized by increased de novo lipogenesis as well as decreased FA oxidation and lipoprotein secretion, which maintains the steatotic phenotype (Koo, 2013) (Kawano and Cohen, 2013). An excess supply of FAs results in increased oxidative stress and inflammation (Soardo et al., 2011), resulting in liver dysfunction (Poli et al., 1987) (Dowman et al., 2010). The response to increased FAs is coordinated by the direct sensing of FAs by SREBPs and PPARs (Pettinelli et al., 2011) (Desvergne et al., 2006) (Fatehi-Hassanabad and Chan, 2005) or by the regulation of these transcription factors by up-

stream kinases such as mTORC1 (Laplante and Sabatini, 2012). Due to the crosstalk between transcription factors that coordinate glucose and lipid metabolism (Lu et al., 2014) (Bechmann et al., 2012), any dramatic changes in hepatic lipid content also influences glucose metabolism. This is critically important since, under starvation, the liver is the main source of glucose for the organism.

Upon liver injury, neighboring hepatocytes proliferate to fill the void left by the apoptotic hepatocytes; this process is accompanied by a modest generation of ECM components. The aberrant generation of excess ECM, however, is known as fibrosis and is regulated by hepatic stellate cells (HSCs) (Bataller and Brenner, 2005). HSCs are activated by intracellular ROS, TLR signaling by gut-derived bacterial components, or cytokines released by neighboring immune and parenchymal cells (Elpek, 2014). Once activated, HSCs break down perinuclear droplets of retinyl esters and produce ECM components, such as collagen, integrin, laminin etc., in order to remodel the surrounding ECM (Bataller and Brenner, 2005) (Elpek, 2014). The synthesis of collagen is primarily regulated by TGFβ in an autocrine and paracrine fashion (Elpek, 2014). While the activation of matrix-metalloprotinases (MMPs) limits the degree of ECM remodeling, the expression of MMP inhibitors (i.e. TIMPs) in later stages of liver disease facilitates the chronic and unchecked propagation of fibrosis (Pellicoro et al., 2014) (Iredale et al., 2013). Cytokines generated by HSCs activate neighboring and circulating immune cells (Weiskirchen and Tacke, 2014), resulting in a positive feedback loop that maintains the pro-fibrogenic activities of HSCs. Additionally, bone-marrow derived circulating fibroblasts, portal fibroblasts, as well as hepatocytes can acquire HSC like phenotypes, amplifying the pro-fibrogenic signal (Elpek, 2014). This chronic activation of pro-fibrogenic signaling drives the progression to HCC by perturbing hepatocyte differentiation, proliferation, and polarity (Gissen and Arias, 2015) (Radisky et al.,

2007). Additionally, by facilitating angiogenesis (Elpek, 2015), fibrosis promotes the progression from tumorigenesis to HCC.

The hepatic immune response participates in clearance of dysfunctional hepatocytes and circulating toxins. Hepatocytes and activated stellate cells secrete cytokines (Dong et al., 1998) (Rowell et al., 1997) (Weiskirchen and Tacke, 2014) to activate resident macrophages (Kupffer cells) as well as recruit circulating leukocytes and, in chronic stress conditions, adaptive immune cells. Damaged or tumorigenic hepatocytes present damage associated antigens or tumor antigens to their surface using the major histocompatibility complex proteins (Herkel et al., 2003), which are recognized by the activated innate or adaptive immune cells. Another effector function of the immune response that is activated under hepatic stress is the complement system (Shen et al., 2014), which has been shown to regulate inflammation, anti-tumor mechanisms, and liver regeneration (Pio et al., 2013) (Reis et al., 2017) (Rensen et al., 2009) (Bilzer et al., 2006) (DeAngelis et al., 2006) (DeAngelis et al., 2012) (Min et al., 2016). A persistent availability of damage signals or the inability of the immune response to clear the damage results in a chronic stress state that drives the progression to HCC (Robinson et al., 2016). Whether metabolic dysregulation, immune response, and fibrosis occur in succession (i.e. the "double-hit" hypothesis) or in parallel is unclear (Berlanga et al., 2014).

Mallory Denk bodies (MDBs), which are aggregates of misfolded or toxic proteins are a hallmark of HCC; MDBs have been found to include SQSTM1/p62, an autophagy regulator and signaling scaffold (Lahiri et al., 2016) (Moscat and Diaz-Meco, 2009) (Zatloukal et al., 2002) (Stumptner et al., 2007) (Stumptner et al., 1999) (Long et al., 2017). Interestingly, the ablation of p62 gene expression in mice results in insulin resistance and mature-onset obesity (Rodriguez et

al., 2006), contributing to the progression from NAFLD to HCC (Moscat and Diaz-Meco, 2012). Its diverse set of protein binding domains allows p6 to integrate and coordinate various processes such as insulin signaling, adipogenesis, BAT thermogenesis, energy/nutrient balance, autophagy, apoptosis, oxidative stress, and inflammation (Long et al., 2017). By functional similarity (Dash et al., 2016), NBR1 may also participate in the progression from NAFLD to HCC. It has also been shown that NBR1-mediated MEKK3/JNK signaling results in adipose tissue inflammation and obesity (Hernandez et al., 2014).

While high-throughput analysis of liver and plasma samples taken from patients in each stage of liver disease has aided in biomarkers discovery (Gorden et al., 2015), the molecular mechanism of disease progression has not yet been clarified. Additionally, the role of p62 and NBR1 in the progression of liver disease are not fully elucidated. In this study, we provide a systems level analysis of the effect of high-fat diet on DEN treated mice that are deficient in p62, NBR1, or both (double-knockout). The comparison of total mouse knockouts to hepatocyte specific knockouts highlights the role of these proteins in several cell/tissue types in coordinating the progression to HCC.

3.3 Materials and Methods

Mouse Models & Phenotypic Characterization

Knockout mouse models were generated by Dr. Jorge Moscat and Dr. Maria Diaz-Meco at the Sanford Burnham Prebys Medical Discovery Institute (La Jolla, CA) (Durán et al., 2004) (Müller et al., 2013) (Yang et al., 2010). The treatment protocol and the phenotypic characterization of each knockout cohort at the end of the experiment was performed by the Moscat and Diaz-Meco groups. All mice were given 25mg/kg of DEN at 2 weeks and then fed a high-fat

diet (HFD) from 6-36 weeks, after which they were sacrificed. At the time of sacrifice, mouse weight, liver weight, tumor number, number of tumors less than 3mm, and number of tumors greater than 3 mm were recorded. Once the mice were sacrificed, the success of the gene knockouts was confirmed by PCR. The following phenotypes were also recorded: degree of fibrosis (Sirius Red Stain), concentration of triglycerides in liver tissue, concentration of plasma ALT, and finally, expression of Collagen, αSMA, TGFβ, and TNFα (by qPCR). All animal protocols were approved by IACUC and SBP Medical Discovery Institute.

RNA-sequencing

The mRNA was prepared from tissue samples from each knockout mouse in biological triplicate using the NucleoSpin RNA Kit (Macherey-Nagel). There were 54 samples in total, 3 biological replicates from each of the following knockout groups:

Table 3.1 Abreviations Used for Knockout Groups

	Knockout Mouse Model	Abbreviation Used
TOTAL KNOCKOUTS	Wild Type	WT
	$p62^{-/-}$	p62KO
	$NBR1^{-/-}$	NBR1KO
	$(p62\text{-}NBR1)^{-/-}$	DKO (double knock out)
ALB-CRE KNOCKOUTS (hepatocyte specific knockout)	$p62^{f/f}$	p62ff
	$p62^{\Delta hep}$	p62ffAC
	$NBR1^{\Delta hep}$	NBR1ffAC
	$(p62\text{-}NBR1)^{f/f}$	pNff
	$(p62\text{-}NBR1)^{\Delta hep}$	pNffAC

Once the mRNA samples were prepared, the NEBNext Ultra Directional RNA Library Prep Kit for Illumina with polyA enriched RNA was used to prepare the sequencing library. The sequencing was done on an Illumina HiSeq2000 system. The sequencing data consists of 100 base-pair, paired end reads. The RNAseq data for HSCs isolated from the p62 total knockout mouse

model was downloaded from NCBI GEO (GSE78760). Only the vehicle treated WT and p62 knockout samples were used in our analysis.

For each RNAseq datasets the following workflow was used for quality assurance, alignment, and differential expression analysis. FASTQC was used to check the quality of the reads (Andrews, 2010). Omicsoft Sequence Aligner (Hu et al., 2012) was used to align reads to reference genome Mouse.B37 using genome build Ensembl.R66, and output gene counts for each sample. DESEq2 (Love et al., 2014) was implemented using a $p < 0.01$ and $|\text{fold-change}| > 1.3$ cutoffs to identify differentially expressed (DE) genes for each knockout condition.

Human data reported in a study by Gordon et. al. was incorporated into our analysis to determine the consistency of the mouse models to human disease (Gorden et al., 2015). This dataset includes human liver biopsies from patients with different degrees of liver dysfunction: normal (n = 31), steatosis (n = 17), steatohepatitis (n = 20), and cirrhosis (n = 20). Each disease cohort (setatosis, steatohepatitis, and cirrhosis) were compared individually to the normal cohort by pairwise ANOVA (genes with $p < 0.01$ were considered differentially expressed).

Functional Analyses

Kyoto Encyclopedia of Genes and Genomes or KEGG (Kanehisa and Goto, 2000) (Kanehisa et al., 2016) (Kanehisa et al., 2017) pathway enrichment analysis was done using the list of differentially expressed genes from each knockout condition assuming a hypergeometric distribution to calculate p-values. The pathways with enrichment p-values < 0.05 were compared between knockout groups. Transcription factor-target analysis was done using the 2017 TRANSFAC database (Matys et al., 2006).

3.4 Results

In order to explore the role of p62 and NBR1 in high-fat diet mediated HCC, we have analyzed high-throughput transcriptomic measurements from liver tissue taken from p62KO, NBR1KO, DKO, p62ffAC, and pNffAC mice. The comparison of gene expression profiles for total and hepatocyte-specific knockouts provides insight into the mechanisms by which p62 and NBR1 influence paracrine signaling between the liver and other metabolic organs.

Phenotypic Characterization

All knockout mice were treated with DEN (a carcinogen) at 2 weeks and fed a high-fat diet until 36 weeks. The phenotypic data collected is summarized in Table 3.1. The p62KO group presented the most severe disease phenotypes: HCC grade tumors that are larger than 3mm, increased bridging fibrosis, ALT levels, TNFα expression, triglyceride levels, and elevated markers of stellate cell activation. NBR1KO mice presented no phenotypic differences from WT mice. Interestingly, the DKO mice presented a mixed phenotype. While the DKO presented an increase in adenomas compared to WT, a majority of their tumors were less than 3mm. They exhibited no increases in markers of liver inflammation (i.e. ALT and TNFα) or stellate cell activation. However, the DKO mice did have elevated triglyceride levels. The hepatocyte specific knockout groups depicted a very different trend. Both the p62ffAC and the pNffAC groups showed a decrease in the number of tumors and an increase in TNFα expression levels. The p62ffAC was marked by an increase in triglyceride levels. Also, there was a decrease in plasma ALT levels in the pNffAC. The NBR1ffAC showed no dramatic change in phenotype compared to the wildtype.

Table 3.2 Summary of Phenotypic Traits of Each Knockout Group

	p62KO v WT	**NBR1KO v WT**	**DKO v WT**	**p62ffAC v p62ff**	**NBR1ffAC v NBR1ff**	**pNffAC v pNff**
Tumor Grade	HCC	Adenoma	Adenoma	-	-	-
Tumor Number	Increased (> 3mm)	No change	Increased (< 3mm)	Decreased	No change	Decreased
Fibrosis	Increased bridging fibrosis	No change	No change			
ALT	Increased	No change	No change	No change	No change	Decreased
TNFα	Increased	No change	No change	Increased	No change	Increased
Steatosis (TG)	Increased	No change	Increased	Increased	-	No change
Stellate Cell Activation (collagen, α-Sma)	Increased	No change	No change	No change	-	-

Differential Expression & Functional Enrichment

Messenger RNA extracted from liver tissue samples taken from each of the wildtype and knockout mouse models and was prepared for RNAseq. The number of differentially expressed (DE) genes for each knockout condition is shown in FIG3.1A. There were significantly more DE genes in the p62KO (3625 genes) and DKO (2710 genes) than there were for the NBR1KO (263 genes). For the hepatocyte-specific knockout models, p62ffAC (873 genes) had roughly twice the number of DE genes as pNffAC (428 genes). Since there were so few DE genes and pathways for NBR1KO, it was not included in downstream analyses. The use of p62ff or pNff as the wildtype group for NBR1ffAC resulted in 906 and 1139 DE genes, respectively (data not shown); since the

large number of DE genes was inconsistent with lack of phenotypic changes, the NBR1ffAC was not included in any further analysis or comparisons.

KEGG pathway enrichment for the DE genes in each knockout condition is shown in the last column of FIG3.1A. Significantly enriched KEGG pathways ($p < 0.05$) were grouped into functional categories for each knockout condition: 1) metabolic, 2) structural, 3) cancer-related, 4) signaling, 5) immune/inflammation-related, 6) cell-cycle/DNA replication, and 7) other (FIG3.1B). The largest functional category in every knockout group was metabolic pathway regulation (i.e. 61% in p62KO, 45% in DKO, 53% in p62ffAC, and 40% in pNffAC). While there was a decrease in the percentage of metabolic pathways (from 61% to 45%), there was an increase in the percentage of signaling (6% to 14%) and immune pathways (6% to 13%) in the DKO compared to the p62KO. Similarly, in the hepatocyte-specific knockout, the percentage of metabolic pathways decreased (53% to 40%) and the percentage of immune/inflammation related pathways increased (10% to 27%) in the pNffAC when compared to p62ffAC. Unlike the total knockout groups, there was no noticeable change in the percentage of signaling pathways enriched in the p62ffAC versus the pNffAC.

Metabolic Dysfunction

In order to determine the metabolic changes associated with the individual or concurrent ablation of p62 and NBR1, we surveyed the expression of genes encoding metabolic enzymes and proteins. A majority of metabolic genes and processes are regulated similarly in the p62KO and DKO groups (FIG3.2A). Out of the 230 metabolic genes considered, 200 are either DE in at least the p62KO or the DKO. Out of the 200 genes, 108 (54%) are either up-regulated in both groups or down-regulated in both groups. It is also important to note that of the 200 genes that are DE in either p62KO or DKO, 161 genes (81%) are “dampened” in the DKO compared to the p62KO (i.e.

the gene is less down-regulated in the DKO compared to the p62KO or less up-regulated in the DKO compared to the p62KO; see Table 3.3). DE genes were identified for DKO vs. p62KO and used for KEGG pathway enrichment analysis. Consistent with the dampening of metabolic genes, 54% of KEGG pathways significantly enriched for DKO vs. p62KO comparison are dampened in the DKO compared to the p62KO (i.e. the pathway is down-regulated in p62KO vs. WT and DKO vs. WT and up-regulated in DKO vs. p62KO OR vice versa, see Table 3.3). Of the dampened pathways, an overwhelming majority (74%) are metabolic pathways (FIG3.2B).

Table 3.3 Metabolic Gene or Pathway Dampening

	p62KO vs. WT	DKO vs. WT	DKO vs. p62KO
Metabolic Gene or Pathway	↑↑↑↑	↑↑	↓↓
Metabolic Gene or Pathway	↓↓↓↓	↓↓	↑↑

In the AlbCre groups, 30/230 genes are DE in p62ffAC and 37/230 genes are DE in pNffAC; of the 61 genes that are DE in at least p62ffAC or pNffAC, 6 genes are regulated similarly in the p62ffAC and pNffAC groups. Also, 29 genes (48%) are dampened in the pNffAC compared to the p62ffAC (FIG3.2A).

Metabolic gene expression is regulated by transcription factors that either directly sense metabolite availability or that are indirectly regulated by other sensors of nutrient availability. In order to elucidate the transcriptional regulation of metabolism we examined gene expression of transcription factors (LXR, RXR, FXR, ESR1, FOXO, SREBP, CEBP, HNF4α, HIF1α, PPAR, and SP-1) that regulate the expression of metabolic genes (glycolysis, TCA cycle, lipid and amino acid metabolism etc.) (FIX3.2C). Our results indicate that there is a changing pattern of transcriptional regulation of metabolism. Many metabolic TFs are uniquely down-regulated in the

p62KO (e.g. CEBPA, CEBPB, HNF4α, NR1H3 (LXRα), NR1H4 (FXR)). Similarly, many metabolic TFs are uniquely up-regulated in the DKO (e.g. NR1H2 (LXRβ), HIF1α, SP-1, and ESR1).

In order to understand the differences in metabolic activities of hepatic stellate cells (HSCs) and the hepatocytes we compared the effect of the p62KO on metabolic gene expression in hepatocytes and HSCs. A previous study by Duran et. al. reports the isolation of HSCs from p62KO and WT mice. Each cell population was cultured and treated with vehicle or calicitriol (VDR agonist) and prepared for RNAseq (NCBI GEO Accession: GSE78760). The untreated (i.e. vehicle treated) sample data was downloaded, analyzed, and incorporated into our study. The number of DE genes identified when comparing the stellate cells obtained from the p62KO mice (hereafter known as p62KO-HSCs) versus the stellate cells obtained from WT mice (hereafter known as WT-HSCs) was 2967 and the number of significantly enriched pathways was 82 FIG3.1A. It is important to note that even though the total knockout captures the gene expression signals from hepatocytes, kupffer cells, stellate cells, and sinusoidal endothelial cells, since the hepatocytes make up 70% of the liver tissue, the majority of the signals observed in the total p62KO can be attributed to the activities of the hepatocytes in response to the DEN and HFD. Therefore, the comparison of the total p62KO and the p62KO-HSCs provides insight into the diverging roles of hepatocytes and HSCs in the development of HCC in the p62KO mice. When comparing these two groups, the main distinction exists in the direction of regulation of many of the major metabolic pathways. Out of the total 230 genes considered, 207 are DE in at least the p62KO or the p62KO-HSCs. The predominant down-regulation of metabolic genes (i.e. 142 down, 32 up) in the p62KO is reversed in the p62KO-HSC samples (i.e. 24 genes down, 75 up). While β-oxidation, ω-oxidation, autophagy, TG synthesis, oxidative phosphorylation, the citric acid cycle,

cholesterol metabolism, FA import and activation, FA synthesis, lipase activation, ketogenesis, chylomicron import, and leukotriene synthesis are down-regulated in the total p62KO condition, many critical rate limiting steps and genes involved in these pathways/processes are up-regulated in HSCs taken from the p62KO liver (FIG3.2A).

There are several notable differences among the 5 knockout groups (p62KO, DKO, p62ffAC, pNffAC, and p62KO-HSC). First, fatty acid synthesis (as marked by the expression of fatty acid synthase, FASN) is up-regulated in the p62KO, down-regulated in the p62KO-HSC and not DE in any other groups. Second, cholesterol synthesis (as marked by MVK, PMVK, MVD, IDI1/2, FDPS, DHCR7, SREBP2) is up-regulated in the DKO and not dramatically regulated in the other groups. Third, serine metabolism (i.e. PHGDH, PSAT1, and PSPH) is strongly up-regulated in the p62KO and DKO and down-regulated in p62ffAC and pNffAC. Fourth, many genes associated with autophagy are uniquely down-regulated in the p62KO (ATG16L1, ATG5, ATG7, ATG9a, GABARAP, GABARAPL2, and MAP1LC3A). Fifth, glucose uptake by glucose transporters (GLUT proteins) are uniquely up-regulated in the DKO (SLC2A1 and SLC2A3). Sixth, TG synthesis genes (GPAT4, AGPAT2/3, LPIN1, and DGAT1/2) are down-regulated in the p62KO. Finally, the expression of chylomicron receptors (LRP1, LRP3, LRP5, and LRP6) are uniquely down-regulated in the p62KO-HSC; many of these and other LRPs (LRP1, LRP5, LRP8, and LRP10) are up-regulated in the DKO (FIG3.2A).

Taken together, there is a significant flux in metabolic regulation in the p62KO, DKO, and p62KO-HSC groups. The overwhelming similarity between p62KO and DKO is somewhat reversed in the HSCs from p62KO. There is a dampening of gene expression in the DKO compared to the p62KO along with differences in select metabolic pathways.

Inflammation & Immune Response

While the measured activation of the innate and adaptive immune response can clear damaged hepatocytes and facilitate the return to homeostasis, the persistent and unchecked activation of inflammation and immune signaling can maintain the toxic microenvironment conducive to tumorigenesis and progression to HCC. In order to characterize the role of p62 and NBR1 in moderating the degree of immune activation we examined the expression of genes encoding interleukins, interleukin receptors, interferon receptors, TGFβ ligands, TGFβ receptors, chemokines, chemokine receptors, complement activation/regulatory genes, MHC-I/II complexes genes, and immunoglobulins from each of the 5 knockout groups (FIG3.3A).

A majority of immune signaling genes (cytokines/cytokine receptors, interleukins/interleukin receptors, interferon receptors, and TGFβ, TGFβ receptors) were DE in all knockout conditions (FIG3.3A). Furthermore, out of 64 immune signaling genes DE in the p62KO, 56 (88%) were up-regulated; similarly, for the DKO (57/60, 95%), p62ffAC (15/27, 56%), pNffAC (25/31, 80%), and p62KO-HSC (31/37, 84%). In p62KO, DKO, and p62KO-HSC, there was a broad activation of interleukins (e.g. IL1A, IL7, IL16 etc.), interleukin receptors (IL10RA, IL17A/D, IL1R2 etc.), interferon receptors (IFNGR1/2 etc.), TGFβ and TGFβ receptors (TGFB1/2/3, TGFBR1/2/3), chemokines (CCL3, CXCL1, CX3CL1 etc.) and chemokine receptors (CCR1, CXCR4 etc.).

Damaged/tumorigenic hepatocytes and activated immune cells present the tumor antigen through the major histocompatibility complex. Genes encoding MHC I and MHC II are up-regulated in p62KO, DKO, pNffAC, and p62KO-HSC. Many genes associated with MHC I and II are down-regulated in the p62ffAC. In addition to presenting the MHC complex, tumorigenic cells

and activated immune cells present antibodies (IGM and IGG) at their surface. IGHG1 is up-regulated in p62KO, NBR1KO, and DKO groups; IGHM is up-regulated in the DKO.

The complement system is an effector function of the immune response. While complement genes are up-regulated in the p62KO, DKO, p62ffAC, pNffAC, and p62KO-HSC each group presents a unique pattern of complement activation. For example, C1Q is up-regulated in p62KO, DKO, p62ffAC, and pNffAC. However, MASP1, C3, C4B, C2, C6, C8A/B, and C9 are uniquely up-regulated in the DKO (FIG3.3A). Additionally, KEGG enrichment analysis (FIG3.3B) suggests up-regulation of the Complement & Coagulation pathway in the p62KO, DKO, and in DKO vs. p62KO groups. This pathway is weakly up in the p62ffAC and strongly down in the pNffAC.

In order to identify the transcriptional control of complement genes we examined Jak/STAT signaling genes (FIG3.2C). JAK1 and JAK2 are up-regulated in both p62KO and DKO, whereas JAK3 is uniquely up-regulated in the DKO. Gene expression for STATs (the downstream target of JAKs) is also shown in FIG 3.2C; notably, STAT3 is uniquely up-regulated in the DKO. Transcription factors of STAT3 expression that are uniquely up-regulated in the DKO are shown in FIG3.2C. EGFR, which can also activate Jak/STAT signaling is uniquely up-regulated in the DKO. Finally, ESR1 can directly activate complement gene expression and is uniquely up-regulated in the DKO.

Taken together, a majority of the immune signals are similarly up-regulated across the different knockout groups with the exception of complement gene expression. (FIG3.2)

Regulation of Fibrosis: p62KO in Hepatic Stellate Cells

Fibrosis is a marker of advanced liver disease and is initiated by activated HSCs (Tsuchida and Friedman, 2017). In order to determine the role of p62 and NBR1 in fibrosis, we examined

known markers of HSC activation in each knockout group (FIG3.3A). Hedgehog signaling (SHH, SMO, and SPP1) was up-regulated in the p62KO and DKO groups. Also, while autophagy, oxidative stress, and ER stress were uniquely up-regulated in the p62KO-HSC group they were either not DE or downregulated in the p62KO and DKO groups. Finally, retinol metabolism (as marked by ADH5 and ADH7) was up-regulated in the p62KO-HSC. Fibrogenic factors such as TGFβ, PDGFRB, and VEGFC were up-regulated in p62KO and p62KO-HSCs.

Consistent with markers of HSC activation, there was an up-regulation of markers of fibrosis (such as actin, collagens, fibronectin, integrins, laminins) in p62KO, DKO, and p62KO-HSC (FIG3.3B). p62KO exhibits the most dramatic up-regulation of structural genes when compared to DKO or p62KO-HSC. Matrix metalloproteinases were strongly induced in p62KO and weakly in the DKO samples; these genes were weakly down-regulated in the p62KO-HSC group. Inhibitors of MMPs (TIMP1/2/3) were up-regulated in the p62KO; TIMP1 was also up-regulated in the p62KO-HSC.

Finally, NBR1KO and AlbCre knockout groups did not display a clear gene signature of HSC activation (FIG3.3A) and, consistently, there was a weak activation of structural genes in these groups (FIG3.3B). The p62ffAC group is characterized by a concurrent up- and down-regulation of structural genes.

Comparison to Human Disease

In order to determine the relevance of the knockout mouse models to human liver disease, we compared our data to publically available human liver disease data (FIG3.5). The number of DE genes for Steatosis vs. Normal (1905 genes), Steatohepatitis vs. Normal (1952 genes), Cirrhosis vs. Normal (8913 genes), p62KO vs. WT (3513 genes), and DKO vs. WT (2569 genes) are shown in FIG3.5A (for the mouse data, only DE genes with known human-mouse orthologues

for Entrez IDs were included). We examined the overlap between each human and mouse DE gene set to determine which stage of liver disease the mouse knockout groups were most similar to (Table 3.4). The number of overlapped genes is bolded; also, the number of overlapped genes that are regulated in the same direction versus the opposite direction is specified. For example, there are 65 overlapping DE genes between p62KO vs. WT and Steatosis vs. Normal groups; of the 65, 31 are either up-regulated in both or down-regulated in both p62KO and Steatosis. On the other hand, 34 of the 65 overlapping DE genes are regulated in opposite directions (i.e. up-regulated in p62KO and down-regulated in Steatosis or vice versa). Similarly, the overlapping genes and their direction of regulation for all other comparisons between p62KO, DKO, Steatosis, Steatohepatitis, and Cirrhosis are specified in Table 3.4.

Table 3.4 Overlapping DE Genes Between Knockout Models and Stages of Human Liver Disease

	Number of Overlapping Genes
(p62KO vs. WT) ∩ (Steatosis vs. Normal)	**65** (31 same direction, 34 opposing direction)
(p62KO vs. WT) ∩ (Steatohepatitis vs. Normal)	**98** (65 same direction, 33 opposing direction)
(p62KO vs. WT) ∩ (Cirrhosis vs. Normal)	**1088** (888 same direction, 200 opposing direction)
(DKO vs. WT) ∩ (Steatosis vs. Normal)	**55** (21 same direction, 23 opposing direction)
(DKO vs. WT) ∩ (Steatohepatitis vs. Normal)	**66** (36 same direction, 30 opposing direction)
(DKO vs. WT) ∩ (Cirrhosis vs. Normal)	**695** (493 same direction, 202 opposing direction)

Given that a substantial number of DE genes were overlapped between the murine knockout samples and the human cirrhosis samples, only these overlapped genes were considered for functional analyses. The 888 and 493 DE genes that were overlapped and regulated in the same direction between p62KO and Cirrhosis and DKO and Cirrhosis, respectively, were used for KEGG and GO enrichment (FIG3.5C, in red). The processes that were regulated in the same

direction between the knockout mouse models and cirrhosis are classical features of liver dysfunction: altered metabolism (e.g. fatty acid degradation and retinol metabolism), immune activation (e.g. tnf signaling pathway and inflammatory response), fibrosis (e.g. extracellular matrix and focal adhesion), angiogenesis (e.g. blood vessel development), and signaling (e.g. PI3K/Akt and PPAR signaling) related pathways. Also, 348 out of 493 genes were also found in the 888 gene set. Enrichment of genes unique to the comparison between the DKO and Cirrhosis (indicated by a * in FIG3.5C) are related to the immune response (e.g. TNF signaling, interleukin-1 mediated signaling, and influenza A).

The 200 and 202 DE genes that were regulated in opposing direction between p62KO and Cirrhosis and DKO and Cirrhosis, respectively, were used for KEGG and GO enrichment (FIG3.5C, in blue). The processes that are divergently regulated between the p62KO and Cirrhosis were mostly related to mitochondrial function and the complement and coagulation pathway. Similarly, the complement and coagulation pathway was significantly enriched as a process that is regulated in opposing directions between the DKO and Cirrhosis. The complement and coagulation genes that were down-regulated in cirrhosis and up-regulated in p62KO and/or DKO are F7, F8, F11, PLG, KNG1, CFI, C1R/C1ra, and SERPINF2; on the other hand, CD59/Cd59a and SERPINA1/Serpina1d are up-regulated in human cirrhosis samples and down-regulated in p62KO and/or DKO. The gene expression for metabolic, immune, and structural processes are shown in FIG3.S2.

3.5 Discussion

In this study we have examined the role of p62 and NBR1 in liver dysfunction and disease. The phenotypic data for each knockout group suggests that the p62KO represents the most advanced disease model as indicated by the fact that the tumors in this group are classified as

hepatocellular carcinomas and by the increase in markers of liver dysfunction (i.e. ALT and TNFα), triglyceride levels, markers of HSC activation (i.e. α-SMA and TGFβ), bridging fibrosis, and increased liver weight. Interestingly, even though NBR1KO did not show any phenotypic differences, the combined knockout of p62 and NBR1 shows markedly decreased disease severity. The phenotypic data from the AlbCre knockout groups suggests that the hepatocyte specific p62-knockout and the joint knockout of p62 and NBR1 protects against tumor progression, highlighting the diverging role of p62 and NBR1 in the hepatocytes and non-hepatocytes. Given the phenotypic signatures of each knockout group, we then examined the transcriptomic signatures of metabolic regulation, immune signaling, and fibrosis to determine the potential mechanisms by which these phenotypes were established.

Metabolic Dysregulation:

The careful control of hepatic metabolism is critical in normal liver function. In our study, all mice were fed a high-fat diet increasing the metabolic load on the liver. The p62KO group is characterized by several aberrant metabolic processes. For example, fatty acid synthase, a marker of liver cancer (Che et al., 2017), is uniquely up-regulated in the p62KO. The accumulation of FAs in the p62KO is further supported by the fact that TG synthesis and lipid oxidation pathways are strongly down-regulated (FIG3.2A) (Berlanga et al., 2014). We report the down-regulation of genes encoding the electron transport chain (ETC) subunits upon treatment with DEN followed by a HFD in the p62KO; this results in impaired glucose metabolism and energy generation and increases fatty acid-mediated oxidative stress (García-Ruiz et al., 2014). While normal avenues of energy generation (ox-phos/TCA cycle) are strongly inhibited, the up-regulation of glycolytic genes suggests a switch to aerobic glycolysis (i.e. the Warburg effect), a hallmark of cancer metabolism (Hsu and Sabatini, 2008) (Liberti and Locasale, 2016) (Wu and Zhao, 2013) (Björnson

et al., 2015). It is important to note that studies characterizing gene signatures of HCC also report the up-regulation of oxidative phosphorylation and the TCA cycle (Nwosu et al., 2017), however, the samples considered in the study by Nwosu et. al. were predominantly viral-mediated HCC unlike the diet induced model of liver dysfunction captured by the p62KO. Next, we examined the transcriptomic control of metabolic gene expression and found that metabolic transcription factors such as PPARG, FOXO1, FOXO3, CEBPA, CEBPB, HNF4A, NR1H3, and NR1H4 were significantly down-regulated in the p62KO (FIG3.2). Additionally, the loss of p62 prevents mTOR activation, resulting in impaired protein-level activation of transcription factors (e.g. SREBF1 and FOXO) that induce the expression of metabolic genes (Duran et al., 2011) (Linares et al., 2013) (Laplante and Sabatini, 2012).

While there are some consistent metabolic gene signatures between the p62KO and DKO (e.g. down-regulation of fatty acid oxidation, oxidative phosphorylation, TCA cycle, and amino acid metabolism) there are many unique features that distinguish the DKO. For example, cholesterol metabolism and chylomicron remnant docking are up-regulated in the DKO; also, TG synthesis and autophagy are de-repressed in the DKO compared to the p62KO. We also explored transcriptional regulation of metabolic gene expression in the DKO. In contrast to the p62KO, our analysis reveals a set of metabolic transcription factors that are either uniquely up-regulated (NR1H2, HIF1A, SP1, PPARD, ESR1, SREBF2, and CEBPD) or de-repressed (CEBPB, HNF4A, NR1H3, and NR1H4) in the DKO (FIG3.2C), suggesting that the concurrent ablation of p62 and NBR1 rewires the transcriptional regulation of metabolism and marginally reverses the effect of the p62KO. The impact of this is seen in the fact that 89% of metabolic genes are dampened in the DKO compared to the p62KO. It is also important to note that the dampening was a unique feature of metabolic processes, suggesting that non-specific changes in the transcriptional and post-

transcriptional mechanisms is unlikely; consistently, a majority of genes encoding RNA polymerase or spliceosome subunits are not differentially expressed (data not shown). There are many protective consequences for the metabolic gene signature present in the DKO. The relative increase in cholesterol biosynthesis and TG synthesis drives lipoprotein assembly limiting steatosis (Nguyen et al., 2008). Also, cholesterol has also been shown to activate mTORC1, which supports the activation of metabolic genes (Castellano et al., 2017) and limits the degree of free fatty acid mediated oxidative stress. Overall, the concurrent ablation of p62 and NBR1 activates protective metabolic activities in the liver.

While metabolic gene expression was significantly down-regulated in the p62KO, many metabolic pathways were up-regulated in the HSCs taken from p62KO mice. This is consistent with the fact that upon damage, the stellate cells are activated and participate in coordinating the progression of fibrosis and inflammation (Tsuchida and Friedman, 2017).

Taken together, the dysregulation of lipid metabolism and down-regulation of autophagy promotes metabolic stress in the p62KO. The concurrent loss of p62 and NBR1 partially de-represses metabolism; how NBR1 may affect the expression of metabolic transcription factors or prevents the activation of FASN require more targeted analyses across multiple metabolic tissues.

Complement Activation & Cancer Immunology

The individual or concurrent loss of p62 and NBR1 was marked by increased activation of innate and adaptive immune genes. There were minor differences in cytokine expression among the 6 knockout conditions (FIG3.3A). We report the up-regulation of MHCI and MCHII genes, suggesting the tumorigenic transformation in the p62KO, DKO, and p62ffAC groups (Herkel et al., 2003). Inflammation and immune signaling is critically important for repairing liver damage and regulating liver regeneration (Robinson et al., 2016) (DeAngelis et al., 2006).

Interestingly, our analysis reveals that the pattern of complement activation is different between p62KO and the DKO. The unique up-regulation of EGFR (Park et al., 1996) and cytokine (Volanakis, 1995) (Schindler et al., 2007) (Rawlings et al., 2004) mediated STAT3 activation as well as ESR1 mediated complement gene expression facilitate a more robust complement activation in the DKO (FIG3.3) (Camporeale et al., 2013) (Buettner et al., 2007) (Divekar et al., 2011) (Couse and Korach, 1999). Additionally, transcription factors up-stream of STAT3 expression that are uniquely up-regulated in the DKO are also shown in FIG3.3C. Furthermore, classical, alternate, and lectin mediated complement pathways (i.e. C3, C1QA/B/C, MASP1) are active in the DKO whereas only markers of the classical pathway are up-regulated in the p62KO (i.e. C1QA/B/C), further supporting the idea that there is a more robust activation of the complement and coagulation pathway in the DKO (Qin and Gao, 2006). Complement activation has been shown to be a link between innate and adaptive immune responses (Dunkelberger and Song, 2010), suggesting that even though there are markers of adaptive immunity (i.e. activation of immunoglobulins) in both the p62KO and the DKO, it is the complete activation of complement in the DKO that bridges the innate and adaptive immune response, resulting in a more efficient clearance of damaged/transformed liver tissue. This is consistent with the phenotypic observation that even though there is an increase in the number of tumors in the DKO, a majority of the tumors are less than 3mm in diameter. In contrast, a majority of the tumors in the p62KO condition are larger than 3mm. Given that C3 deficiency impairs hepatocyte proliferation during liver repair, perhaps the lack of C3 up-regulation in the p62KO perturbs tissue repair and promotes chronic stress conditions (Markiewski et al., 2004).

Fibrosis: HSC Activation

Aberrances in the fibrotic responses can result in excess scar tissue initiating a chronic wound healing response and eventually accelerate the progression from liver dysfunction to HCC (Pellicoro et al., 2014). The initiation of fibrosis is marked by the activation of HSCs (Iredale et al., 2013). On the other hand, our analysis reveals a dramatic induction of fibrosis-related genes in the p62KO (FIG3.4A). Interestingly, this gene signature of fibrosis is significantly attenuated in the p62ffAC but is somewhat maintained in the p62KO-HSC (FIG3.4A), suggesting that the loss of p62 in stellate cells (as opposed to its loss in hepatocytes) drives the activation of HSCs/fibrosis. These results are consistent with recent evidence that p62 located in HSCs promotes VDR and RXR heterodimerization and signaling, which is then able to activate a gene program that inhibits fibrosis (Duran et al., 2016); therefore, p62 activity in HSCs is negatively correlated with fibrosis. It is also important to note that TIMPs are uniquely upregulated in the p62KO, which supports the finding that the lack of ECM clearance propagates stress and disease progression. Finally, our analysis reveals that ADH5 and ADH7 are uniquely up-regulated in the HSCs isolated from p62KO mice, which is a necessary step in retinol metabolism and HSC activation (Lee and Jeong, 2012). Our analysis also highlights differences in hedgehog signaling that may influence p62-mediated HSC activation (Tsuchida and Friedman, 2017). As summarized in FIG3.4A, hedgehog signaling is up-regulated in the p62KO, down-regulated in the HSCs isolated from the p62KO, and not differentially expressed in the p62ffAC (FIG3.4A). Therefore, our analysis suggests that while the loss of p62 in the hepatocytes alone is not sufficient to activate the hedgehog pathway, the total loss of p62 activates hedgehog signaling in hepatocytes, highlighting the paracrine activation hedgehog signaling, leading to the activation of HSCs and promoting fibrosis. These results are in line with previous reports that provide evidence for the inhibition of hedgehog

transcription factors by VDR signaling (Larriba et al., 2014). However, since hedgehog signaling is induced in p62-deficient hepatocytes and somewhat repressed in p62-deficient HSCs, the loss of p62 may perturb VDR signaling in a cell-type specific manner.

The DKO is characterized by a weaker induction of fibrosis related gene expression and HSC activators (HH signaling, markers of ER stress etc); however, enzymes necessary for retinol metabolism are down-regulated or not DE, therefore limiting the degree of fibrosis in the DKO condition. Since the up-regulation of hedgehog signaling, retinol metabolism genes, and markers of ER and oxidative stress are not significantly regulated in the pNffAC group, it is likely that the loss of p62 and NBR1 outside of the hepatocytes regulates the induction of fibrosis.

Taken together, we show that the loss of p62 in hepatocytes HSCs activates HSCs and promotes a pro-fibrogenic gene expression program. The activation of hedgehog signaling in hepatocytes sustains HSC activation and supports chronic fibrosis.

Comparison to Human Samples

The comparison between the mouse knockout models (p62KO and DKO) and the human liver disease samples (Steatosis, Steatohepatitis, and Cirrhosis) revealed a minor overlap between the differentially expressed transcriptomes of the mouse models and Steatosis or Steatohepatitis. On the other hand, there was a sizable overlap between the mouse models and the Cirrhosis samples (FIG3.5). The pro-steatotic, pro-inflammatory, and pro-fibrotic signatures of the p62KO are in line with the p62KO transcriptome being significantly overlapped with the most advanced of the three disease stages (i.e. Cirrhosis). It is important to note that most of the DE genes overlapped and in the same direction in DKO vs. WT ∩ Cirrhosis vs. Normal were also found in the overlap between p62KO and Cirrhosis suggesting that the “Cirrhotic” gene signature in the DKO is predominantly a feature of p62 ablation and not a unique feature of the double knockout.

The down-regulation of complement and coagulation in Cirrhotic samples is consistent with the fact that upon severe liver injury, many of the synthetic functions of the liver (i.e. synthesis of complement and coagulation factors) are impaired (Mammen, 1992) (Thalheimer et al., 2005). The up-regulation of the complement and coagulation pathway and genes in the DKO and the consequential clearance of damaged tissue represents a potentially novel mechanism of protection that is not activated in human hepatic cirrhosis.

It is important to note that neither the total nor the hepatocyte-specific knockout of NBR1 has a dramatic effect on metabolic, immune, or fibrogenic gene expression in liver tissue, suggesting that perhaps NBR1 influences liver function through its activities myeloid cells (Hernandez et al., 2014).

Given the trends in fibrosis, metabolism, and the immune response, it is clear that the robust clearance of damaged tissue and marginal increases in lipid and glucose metabolism along with decreased fibrosis in the DKO rescues the chronic disease phenotype observed in the p62KO.

3.6 Acknowledgements

Chapter 3 is a version of the manuscript in preparation tentatively titled “The Role of p62 and NBR1 in Liver Disease”. Sindhushree Raghunandan, Shakti Gupta, Mano Maurya, Maria Diaz-Meco, Jorge Moscat, Shankar Subramaniam. The author of this dissertation was the primary contributor to the work presented in this chapter.

A

		Number DE Genes ($p < 0.01$ & $\|FC\| > 1.3$)	Number of Enriched KEGG pathways ($p < 0.05$)
Total Knockout	p62KO vs. WT	3625	115
	NBR1 vs. WT	263	23
	DKO vs. WT	2710	116
Hepatocyte Specific Knockout	p62ffAC vs. p62ff	873	58
	pNffAC vs. pNff	428	62
Hepatic Stellate Cells	p62KO-HSC vs. WT-HSC	2967	82

B

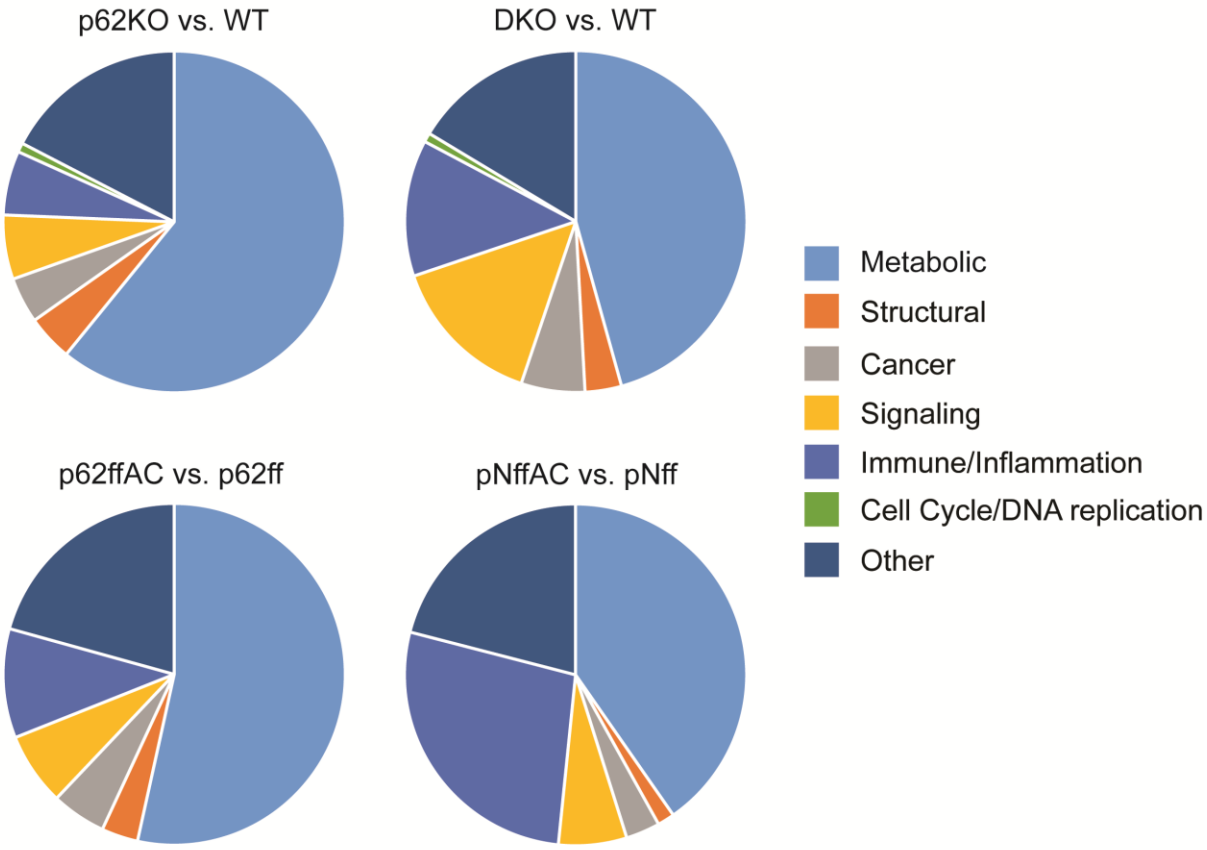

Figure 3.1 Summary of Differential Expression and Functional Enrichment Analysis
A) Summary of the number of DE genes with $p < 0.01$ and $|FC| > 1.3$ and the number of significantly ($p < 0.05$) enriched KEGG pathways in each knockout condition. B) The functional breakdown of enriched pathways for each knockout condition. The legend indicates the functional category corresponding to each color: metabolic (teal), structural (orange), cancer (gray), signaling (yellow), immune signaling/inflammation (light blue), cell cycle/DNA replication (green), and other (dark blue).

Figure 3.2 Transcriptional Regulation of Metabolic Genes and Processes
A) Heatmap of log2(fold-change) of metabolic genes. Gene names are indicated in the first column and functional categories are marked in the right-most column. B) Differentially expressed genes for DKO vs. p62KO were identified and used for KEGG pathway enrichment. Pathway regulation was compared across p62KO vs. WT, DKO vs. WT, and DKO vs. p62KO. If the regulation of a given pathway in p62KO vs. WT and DKO vs. WT was up-regulated and the regulation of the same pathway in DKO vs. p62KO was down-regulated, that pathway was marked as "dampened" in the DKO compared to the p62KO. Similarly, if the regulation of a given pathway in p62KO vs. WT and DKO vs. WT was down-regulated and the regulation of the same pathway in DKO vs. p62KO was up-regulated, that pathway was marked as "dampened" in the DKO compared to the p62KO. The distribution of dampened and non-dampened pathways is shown in the first pie-chart. The second pie-chart indicates the functional distribution of dampened pathways. The colors specify functional groups: metabolic (blue), structural (orange), signaling (gray), and other (yellow). C) The expression of transcription factors that regulate the expression of metabolic genes is shown. For both heatmaps shown the samples from the leftmost column to the right-most column are: p62KO vs. WT, NBR1KO vs. WT, DKO vs. WT, p62ffAC vs. p62ff, pNffAC vs. pNff, and p62KO vs. WT (HSC). Also, expression measurements with $p < 0.05$ are shown; blue indicates down-regulation and red indicates up-regulation.

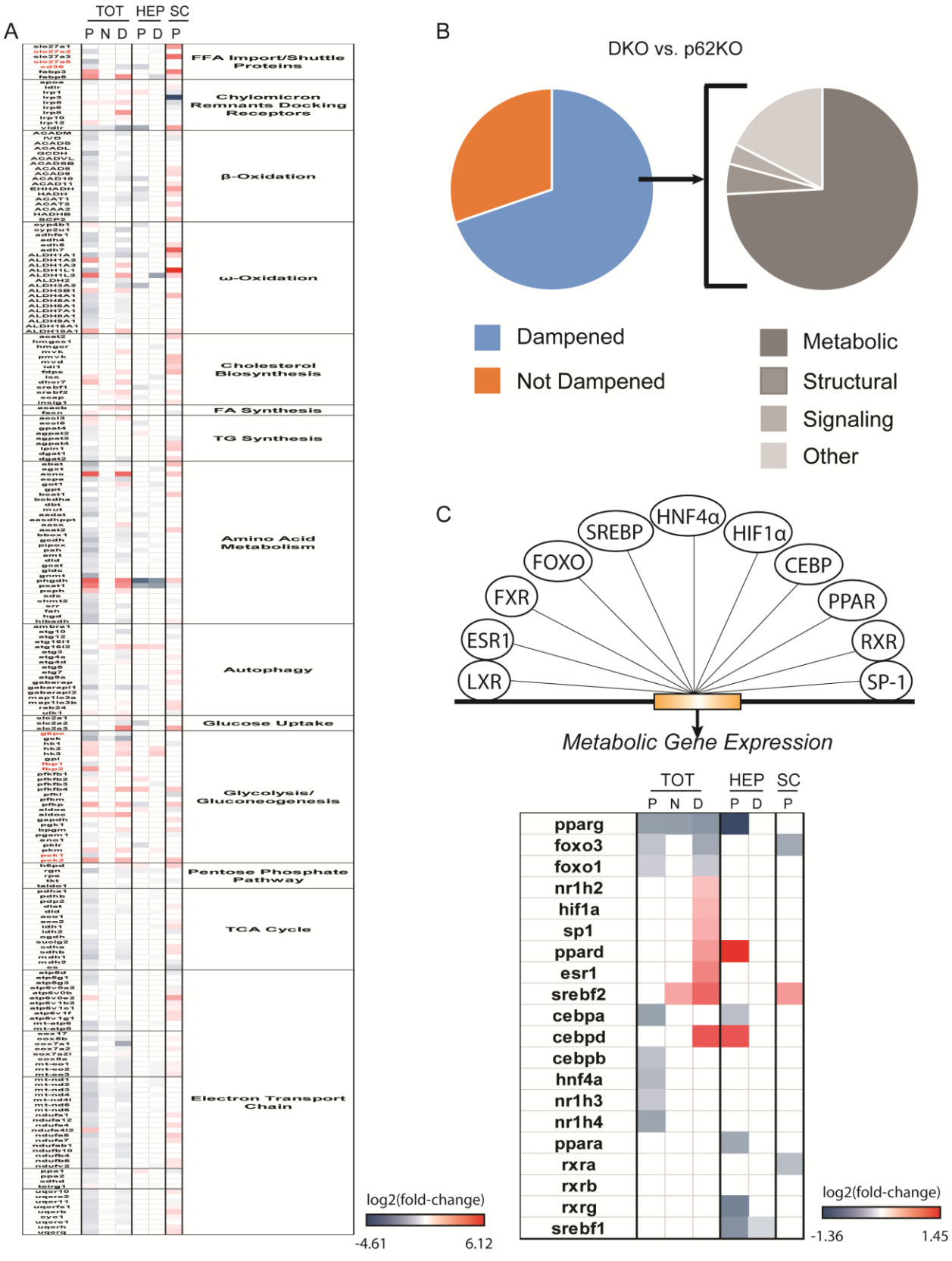
A
TOT HEP SC
P N D P D P
FFA Import/Shuttle Proteins
Chylomicron Remnants Docking Receptors
β-Oxidation
ω-Oxidation
Cholesterol Biosynthesis
FA Synthesis
TG Synthesis
Amino Acid Metabolism
Autophagy
Glucose Uptake
Glycolysis/ Gluconeogenesis
Pentose Phosphate Pathway
TCA Cycle
Electron Transport Chain
log2(fold-change)
-4.61
6.12
B
DKO vs. p62KO
Dampened
Not Dampened
Metabolic
Structural
Signaling
Other
C
HNF4α
SREBP
HIF1α
FOXO
CEBP
FXR
PPAR
ESR1
RXR
LXR
SP-1
Metabolic Gene Expression
TOT HEP SC
P N D P D P
pparg
foxo3
foxo1
nr1h2
hif1a
sp1
ppard
esr1
srebf2
cebpa
cebpd
cebpb
hnf4a
nr1h3
nr1h4
ppara
rxra
rxrb
rxrg
srebf1
log2(fold-change)
-1.36
1.45

Figure 3.3 Transcriptional Regulation of the Innate and Adaptive Immune Response
A) Heatmap of log2(fold-change) of innate and adaptive immune response genes. Gene names are indicated in the first column and functional categories are marked in the right-most column. B) Enrichment of the "Complement and Coagulation" KEGG Pathway is shown. For each knockout group comparison, the number of up/down regulated genes and corresponding p-value of enrichment is shown. C) Transcriptional regulation of JAK/STAT genes, STAT3 transcription factors, and EGFR are shown. For both heatmaps shown the samples from the leftmost column to the right-most column are: p62KO vs. WT, NBR1KO vs. WT, DKO vs. WT, p62ffAC vs. p62ff, pNffAC vs. pNff, and p62KO vs. WT (HSC). Also, expression measurements with $p < 0.05$ are shown; blue indicates down-regulation and red indicates up-regulation.

A

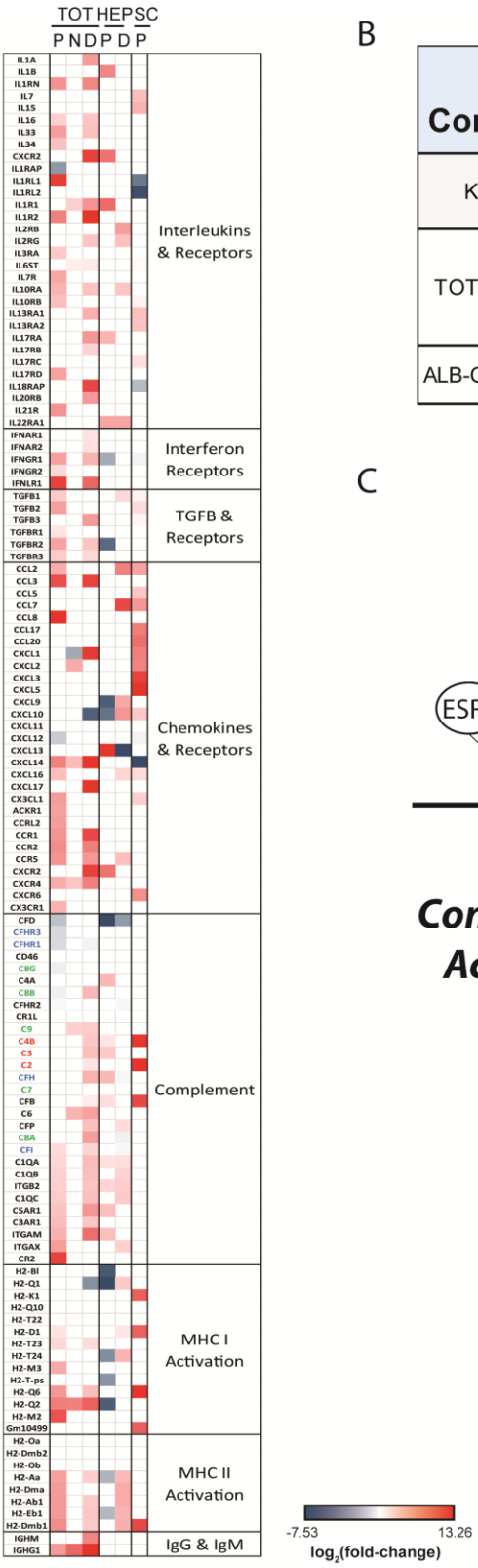

B

KEGG Enrichment: Complement & Coagulation Cascade

Knockout Condition		# genes up	# genes down	p-value
TOTAL	p62KO vs. WT	23	10	2.75E-08
	NBR1KO vs. WT	2	0	0.203448822
	DKO vs. WT	42	2	1.40E-21
	DKO vs. p62KO	28	2	2.64E-15
ALB-CRE	p62ffAC vs. p62ff	7	2	0.002652896
	pNffAC vs. pNff	4	14	1.91E-15

C

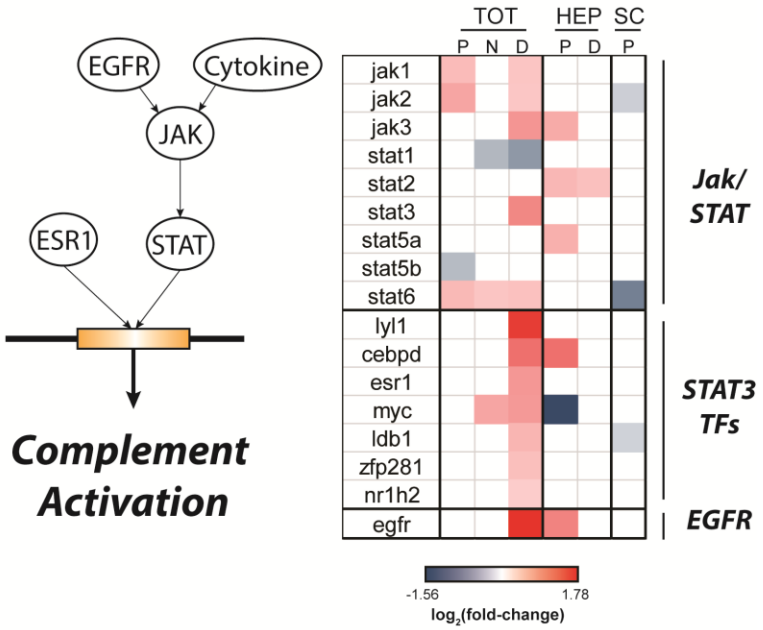

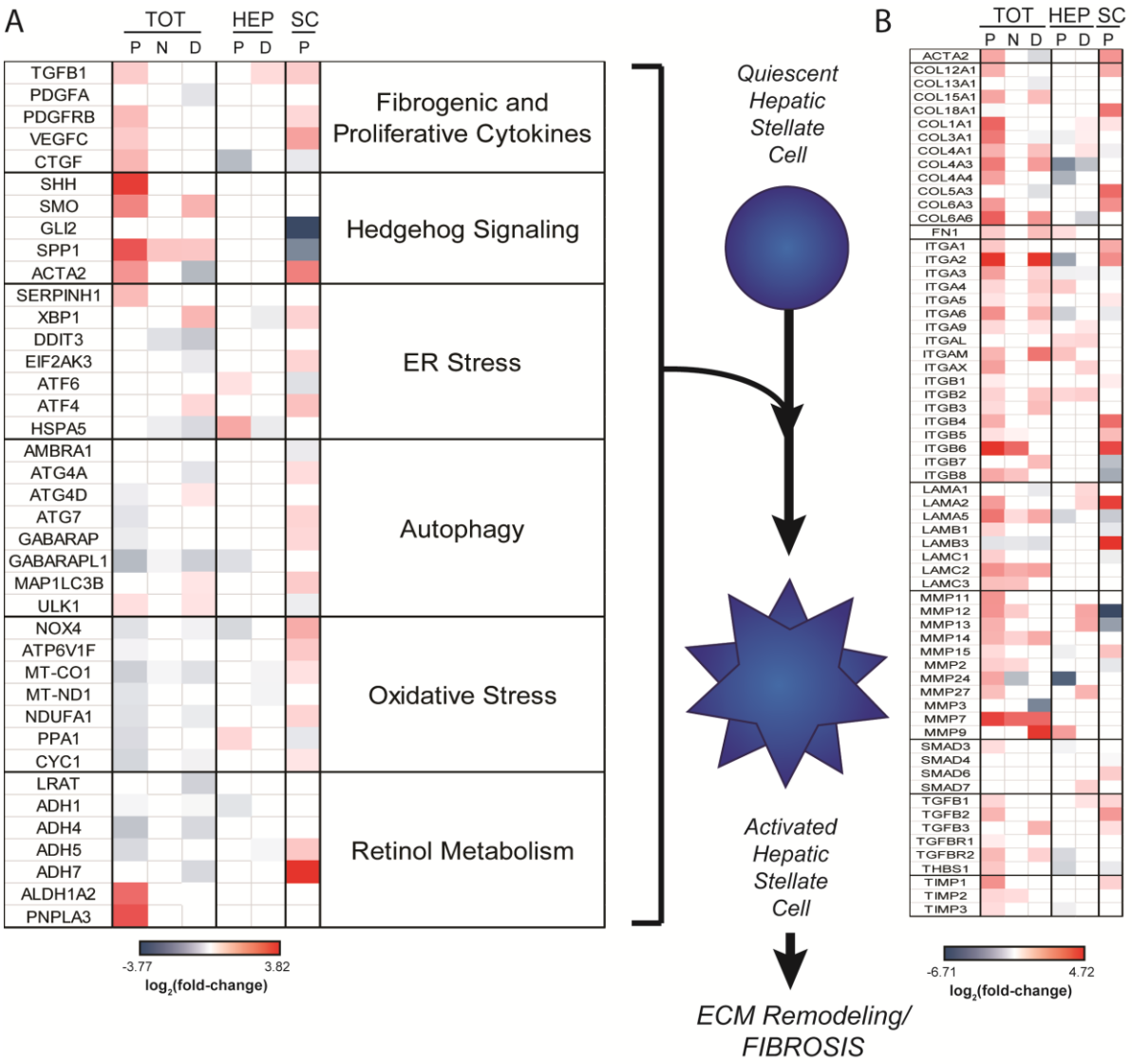

Figure 3.4 Transcriptional Regulation of HSC Activation/Fibrosis

A) Heatmap of log2(fold-change) for genes involved in HSC activation. Functional groups are indicated in the right-most column. B) Heatmap of log2(fold-change) for structural genes involved in ECM remodeling. For both heatmaps shown the samples from the leftmost column to the right-most column are: p62KO vs. WT, NBR1KO vs. WT, DKO vs. WT, p62ffAC vs. p62ff, pNffAC vs. pNff, and p62KO vs. WT (HSC). Also, expression measurements with $p < 0.05$ are shown; blue indicates down-regulation and red indicates up-regulation.

A

	Number of DE genes
Steatosis vs. Normal	1905
Steatohepatits vs. Normal	1952
Cirrhosis vs. Normal	8913
p62KO vs. WT	3513
DKO vs. WT	2569

B

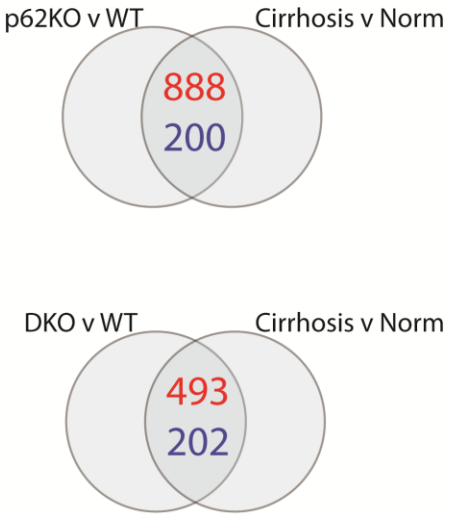

C

Matching Direction of Expression	(p62KO v WT)∩(Cirrhosis v Norm)	(DKO v WT) ∩ (Cirrhosis v Norm)	
GO:0008202~steroid metabolic process	4.93E-06	1.48E-04	
GO:0006635~fatty acid beta-oxidation	6.28E-06	0.03142	
GO:0042632~cholesterol homeostasis	1.09E-05	0.03023	
GO:0019373~epoxygenase P450 pathway	1.30E-05		
KEGG hsa00071:Fatty acid degradation	9.58E-05	1.87E-04	
GO:0001523~retinoid metabolic process	6.97E-04	3.80E-05	
GO:0033539~fatty acid beta-oxidation using acyl-CoA dehydrogenase	0.0014		
KEGG hsa05204:Chemical carcinogenesis	0.00203	1.69E-04	Metabolic
KEGG hsa00072:Synthesis and degradation of ketone bodies	0.00285	0.00508	
GO:0006006~glucose metabolic process	0.01619	0.03587	
GO:0015758~glucose transport	0.02111	0.01195	
KEGG hsa00120:Primary bile acid biosynthesis	0.02238		
GO:0004745~retinol dehydrogenase activity*		3.99E-04	
KEGG hsa00830:Retinol metabolism*		0.02026	
KEGG hsa04668:TNF signaling pathway*		0.0025	
GO:0070498~interleukin-1-mediated signaling pathway*		0.00548	
KEGG hsa05164:Influenza A*		0.01946	
GO:0050900~leukocyte migration	2.20E-08	6.02E-06	Immune
GO:0042060~wound healing	6.60E-06		
GO:0006954~inflammatory response	0.01175		
GO:0001530~lipopolysaccharide binding	0.02034		
GO:0071347~cellular response to interleukin-1	0.0223		
GO:0031012~extracellular matrix	8.23E-23	3.40E-04	
KEGG hsa04512:ECM-receptor interaction	1.07E-15	0.01553	Fibrosis
GO:0007155~cell adhesion	9.43E-14	0.00389	
KEGG hsa04510:Focal adhesion	2.24E-11		
KEGG hsa04514:Cell adhesion molecules (CAMs)	0.01187	0.0393	
GO:0001525~angiogenesis	1.53E-06	0.04209	
GO:0001568~blood vessel development	4.21E-04		
KEGG hsa04151:PI3K-Akt signaling pathway	1.12E-06		
KEGG hsa03320:PPAR signaling pathway	0.03084		Signaling
GO:0043627~response to estrogen*		0.01545	
Oposing Direction of Expression			
GO:0005759~mitochondrial matrix	3.65E-05		
hsa01100:Metabolic pathways	4.98E-05		
hsa04610:Complement and coagulation cascades	2.72E-04	3.03E-05	
GO:0005743~mitochondrial inner membrane	0.00618		
GO:0005739~mitochondrion	0.0103		
GO:0007596~blood coagulation	0.01446	0.00459	
GO:0007597~blood coagulation, intrinsic pathway	0.01562		
hsa00190:Oxidative phosphorylation	0.03054		
	p-value		

Figure 3.5 Comparison to Human Liver Disease

A) Number of differentially expressed genes identified for the human data (Gordon et. al.) and mouse data. The number of DE genes for human samples was determined by ANOVA and the number of DE genes for the mouse samples was determined by DESeq2 ($p < 0.01$). B) The overlap of DE genes from each mouse knockout comparison and Cirrhosis vs. Normal comparison. The number shown in red is the number of overlapping genes regulated in the same direction in both comparisons (e.g. up-regulated in p62KO vs. WT and Cirrhosis vs. Normal or vice versa), whereas the number shown in blue is the number of overlapping genes regulated in the opposite direction in both comparisons (e.g. up-regulated in p62KO vs. WT and down-regulated in Cirrhosis vs. Normal or vice versa). C) The enriched KEGG pathways and GO terms from the overlapping gene lists. Pathways/GO terms shown in red are from overlapping genes that are regulated in the same direction whereas pathways/GO terms shown in blue are from overlapping genes that are regulated in opposite direcitons. The p-value of enrichment in each comparison (i.e. p62KO-Cirrhosis or DKO-Cirrhosis) is shown in the last two columns of the table).

A

		WT			p62KO			NBR1KO			DKO					
TOTAL KNOCKOUT		1	2	5	9	11	13	14	15	18	21	22	23			
	Uniquely mapped paired read%	87.04	83.34	86.51	87.40	86.84	82.75	85.10	82.25	83.36	85.65	83.33	79.82			
		p62ff			p62ffAC			NBR1ffAC			pNff			pNffAC		
HEPATOCYTE SPECIFIC KNOCKOUT		1	2	3	13	16	17	20	25	35	5	6	13	8	10	14
	Uniquely mapped paired read%	74.48	69.80	72.12	67.05	74.76	68.55	85.05	82.31	77.90	83.45	83.24	83.86	83.38	87.56	81.13

B

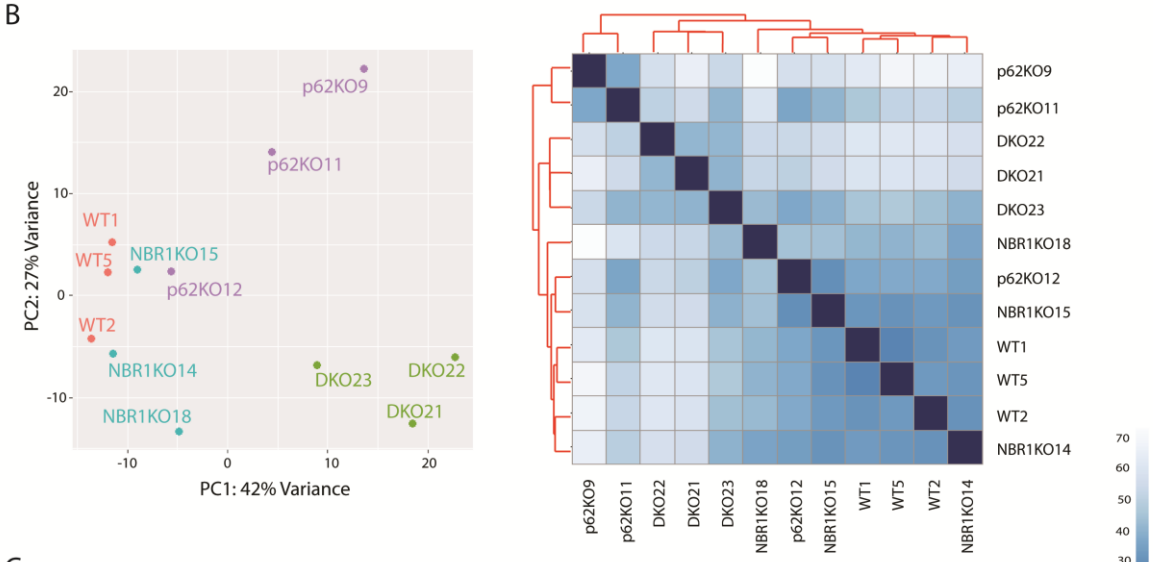

C

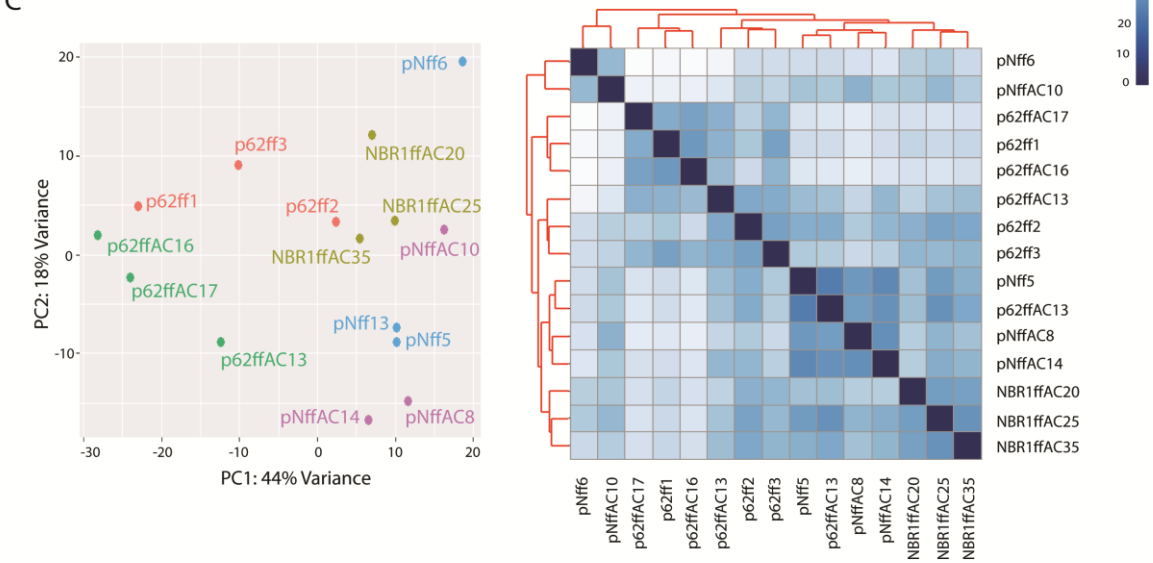

Figure 3.S1 Alignment Summary and Sample Clustering Analysis
A) Uniquely mapped paired alignment percentages shown for each sample. B) Principle Components Analysis (PCA, left) and Euclidean distance clustering (right) for all total knockout samples. C) Principle Components Analysis (PCA, left) and Euclidean distance clustering (right) for all the liver specific (Alb-Cre) knockout samples.

Figure 3.S 2 Heatmap of gene expression in human and mouse data
A) ECM Remodeling/Fibrosis related gene signature. B) Immune response gene signature. C) Metabolic gene signature. Column labels: 1 (Cirrhosis vs. Normal), 2 (Steatohepatitis vs. Normal), 3 (Steatosis vs. Normal), 4 (p62KO vs. WT), 5 (NBR1KO vs. WT), 6 (DKO vs. WT), 7 (p62ffAC vs. p62ff), 8 (pNffAC vs. pNff), 9 (p62KO-HSC vs. WT-HSC). ($p < 0.05$ for all colored tiles; log2(fold-change) legends shown under each panel).

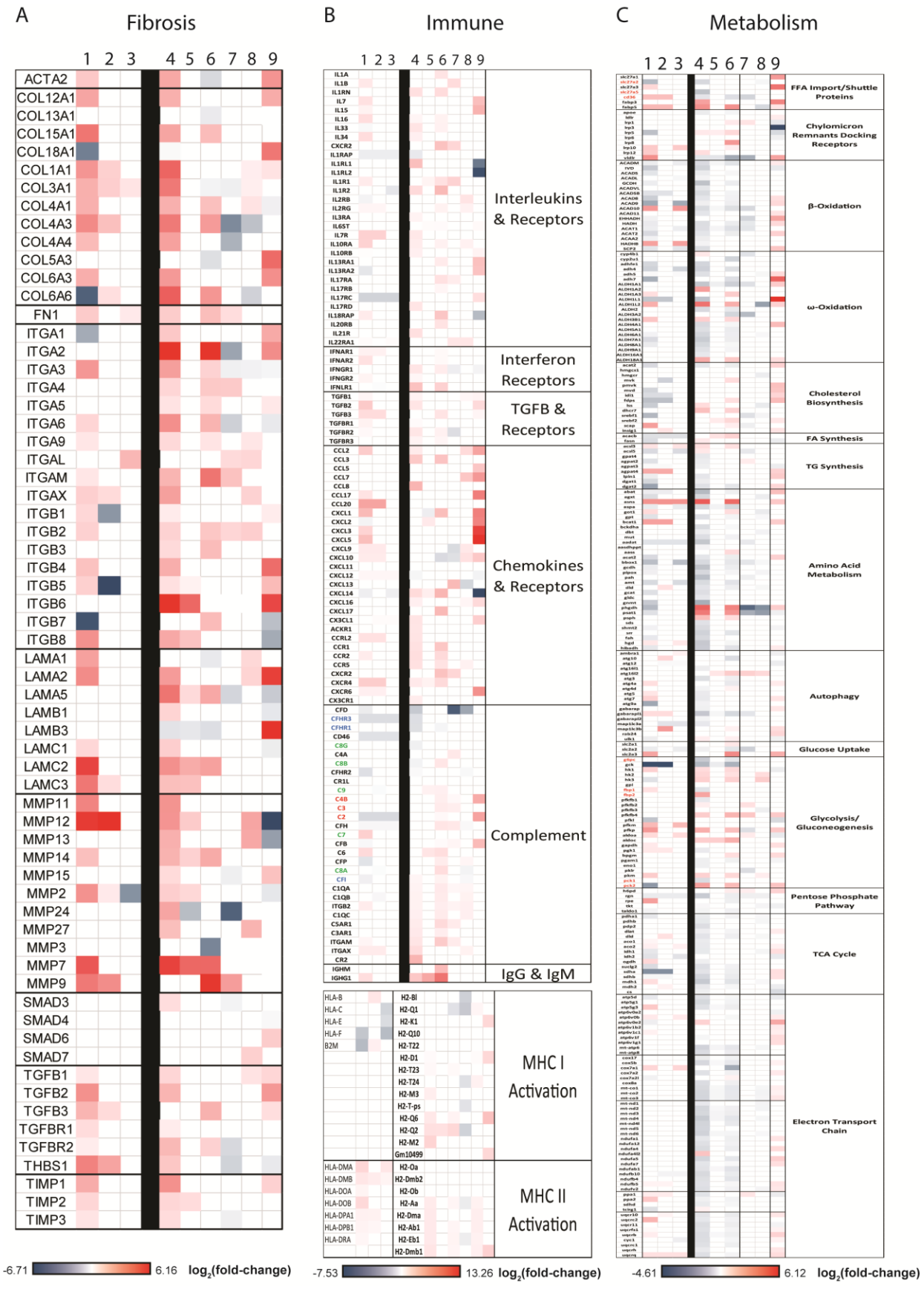
A
Fibrosis
1 2 3 4 5 6 7 8 9
ACTA2
COL12A1
COL13A1
COL15A1
COL18A1
COL1A1
COL3A1
COL4A1
COL4A3
COL4A4
COL5A3
COL6A3
COL6A6
FN1
ITGA1
ITGA2
ITGA3
ITGA4
ITGA5
ITGA6
ITGA9
ITGAL
ITGAM
ITGAX
ITGB1
ITGB2
ITGB3
ITGB4
ITGB5
ITGB6
ITGB7
ITGB8
LAMA1
LAMA2
LAMA5
LAMB1
LAMB3
LAMC1
LAMC2
LAMC3
MMP11
MMP12
MMP13
MMP14
MMP15
MMP2
MMP24
MMP27
MMP3
MMP7
MMP9
SMAD3
SMAD4
SMAD6
SMAD7
TGFB1
TGFB2
TGFB3
TGFBR1
TGFBR2
THBS1
TIMP1
TIMP2
TIMP3
-6.71
6.16
log2(fold-change)
B
Immune
1 2 3 4 5 6 7 8 9
IL1A
IL1B
IL1RN
IL7
IL15
IL16
IL33
IL34
CXCR2
IL1RAP
IL1RL1
IL1RL2
IL1R1
IL1R2
IL2RB
IL2RG
IL3RA
IL6ST
IL7R
IL10RA
IL10RB
IL13RA1
IL13RA2
IL17RA
IL17RB
IL17RC
IL17RD
IL18RAP
IL20RB
IL21R
IL22RA1
Interleukins & Receptors
IFNAR1
IFNAR2
IFNGR1
IFNGR2
IFNLR1
Interferon Receptors
TGFB1
TGFB2
TGFB3
TGFBR1
TGFBR2
TGFBR3
TGFB & Receptors
CCL2
CCL3
CCL5
CCL7
CCL8
CCL17
CCL20
CXCL1
CXCL2
CXCL3
CXCL5
CXCL9
CXCL10
CXCL11
CXCL12
CXCL13
CXCL14
CXCL16
CXCL17
CX3CL1
ACKR1
CCRL2
CCR1
CCR2
CCR5
CXCR2
CXCR4
CXCR6
CX3CR1
Chemokines & Receptors
CFD
CFHR3
CFHR1
CD46
C8G
C4A
C8B
CFHR2
CR1L
C9
C4B
C3
C2
CFH
C7
CFB
C6
CFP
C8A
CFI
C1QA
C1QB
ITGB2
C1QC
C5AR1
C3AR1
ITGAM
ITGAX
CR2
Complement
IGHM
IGHG1
IgG & IgM
HLA-B
HLA-C
HLA-E
HLA-F
B2M
H2-Bl
H2-Q1
H2-K1
H2-Q10
H2-T22
H2-D1
H2-T23
H2-T24
H2-M3
H2-T-ps
H2-Q6
H2-Q2
H2-M2
Gm10499
MHC I Activation
HLA-DMA
HLA-DMB
HLA-DOA
HLA-DOB
HLA-DPA1
HLA-DPB1
HLA-DRA
H2-Oa
H2-Dmb2
H2-Ob
H2-Aa
H2-Dma
H2-Ab1
H2-Eb1
H2-Dmb1
MHC II Activation
-7.53
13.26
log2(fold-change)
C
Metabolism
1 2 3 4 5 6 7 8 9
FFA Import/Shuttle Proteins
Chylomicron Remnants Docking Receptors
β-Oxidation
ω-Oxidation
Cholesterol Biosynthesis
FA Synthesis
TG Synthesis
Amino Acid Metabolism
Autophagy
Glucose Uptake
Glycolysis/ Gluconeogenesis
Pentose Phosphate Pathway
TCA Cycle
Electron Transport Chain
-4.61
6.12
log2(fold-change)

3.7 References

Andrews, S. (2010). FastQC: A quality control tool for high throughput sequence data. Reference Source.

Bataller, R., and Brenner, D.A. (2005). Liver fibrosis. J Clin Invest 115, 209–218.

Bechmann, L.P., Hannivoort, R.A., Gerken, G., Hotamisligil, G.S., Trauner, M., and Canbay, A. (2012). The interaction of hepatic lipid and glucose metabolism in liver diseases. J. Hepatol. 56, 952–964.

Berlanga, A., Guiu-Jurado, E., Porras, J.A., and Auguet, T. (2014). Molecular pathways in non-alcoholic fatty liver disease. Clin Exp Gastroenterol 7, 221–239.

Bilzer, M., Roggel, F., and Gerbes, A.L. (2006). Role of Kupffer cells in host defense and liver disease. Liver Int. 26, 1175–1186.

Björnson, E., Mukhopadhyay, B., Asplund, A., Pristovsek, N., Cinar, R., Romeo, S., Uhlen, M., Kunos, G., Nielsen, J., and Mardinoglu, A. (2015). Stratification of Hepatocellular Carcinoma Patients Based on Acetate Utilization. Cell Rep 13, 2014–2026.

Buettner, R., Huang, M., Gritsko, T., Karras, J., Enkemann, S., Mesa, T., Nam, S., Yu, H., and Jove, R. (2007). Activated signal transducers and activators of transcription 3 signaling induces CD46 expression and protects human cancer cells from complement-dependent cytotoxicity. Mol. Cancer Res. 5, 823–832.

Camporeale, A., Marino, F., Papageorgiou, A., Carai, P., Fornero, S., Fletcher, S., Page, B.D.G., Gunning, P., Forni, M., Chiarle, R., Morello, M., Jensen, O., Levi, R., Heymans, S., Poli, V. (2013). STAT3 activity is necessary and sufficient for the development of immune-mediated myocarditis in mice and promotes progression to dilated cardiomyopathy. EMBO Mol Med 5, 572–590.

Castellano, B.M., Thelen, A.M., Moldavski, O., Feltes, M., van der Welle, R.E.N., Mydock-McGrane, L., Jiang, X., van Eijkeren, R.J., Davis, O.B., Louie, S.M., Perera, R.M., Covey, D.F., Nomura, D.K., Ory, D.S., Zoncu, R. (2017). Lysosomal cholesterol activates mTORC1 via an SLC38A9-Niemann-Pick C1 signaling complex. Science 355, 1306–1311.

Che, L., Pilo, M.G., Cigliano, A., Latte, G., Simile, M.M., Ribback, S., Dombrowski, F., Evert, M., Chen, X., and Calvisi, D.F. (2017). Oncogene dependent requirement of fatty acid synthase in hepatocellular carcinoma. Cell Cycle 16, 499–507.

Cohen, J.C., Horton, J.D., and Hobbs, H.H. (2011). Human fatty liver disease: old questions and new insights. Science 332, 1519–1523.

Couse, J.F., and Korach, K.S. (1999). Estrogen Receptor Null Mice: What Have We Learned and Where Will They Lead Us? Endocr Rev 20, 358–417.

Dash, S., Chava, S., Chandra, P.K., Aydin, Y., Balart, L.A., and Wu, T. (2016). Autophagy in hepatocellular carcinomas: from pathophysiology to therapeutic response. Hepat Med 8, 9–20.

DeAngelis, R.A., Markiewski, M.M., and Lambris, J.D. (2006). Liver regeneration: a link to inflammation through complement. Adv. Exp. Med. Biol. 586, 17–34.

DeAngelis, R.A., Markiewski, M.M., Kourtzelis, I., Rafail, S., Syriga, M., Sandor, A., Maurya, M.R., Gupta, S., Subramaniam, S., and Lambris, J.D. (2012). A complement-IL-4 regulatory circuit controls liver regeneration. J. Immunol. 188, 641–648.

Desvergne, B., Michalik, L., and Wahli, W. (2006). Transcriptional regulation of metabolism. Physiol. Rev. 86, 465–514.

Divekar, S.D., Storchan, G.B., Sperle, K., Veselik, D.J., Johnson, E., Dakshanamurthy, S., Lajiminmuhip, Y.N., Nakles, R.E., Huang, L., and Martin, M.B. (2011). The role of calcium in the activation of estrogen receptor-alpha. Cancer Res. 71, 1658–1668.

Dong, W., Simeonova, P.P., Gallucci, R., Matheson, J., Fannin, R., Montuschi, P., Flood, L., and Luster, M.I. (1998). Cytokine expression in hepatocytes: role of oxidant stress. J. Interferon Cytokine Res. 18, 629–638.

Dowman, J.K., Tomlinson, J.W., and Newsome, P.N. (2010). Pathogenesis of non-alcoholic fatty liver disease. QJM 103, 71–83.

Dunkelberger, J.R., and Song, W.-C. (2010). Complement and its role in innate and adaptive immune responses. Cell Res. 20, 34–50.

Durán, A., Serrano, M., Leitges, M., Flores, J.M., Picard, S., Brown, J.P., Moscat, J., and Diaz-Meco, M.T. (2004). The atypical PKC-interacting protein p62 is an important mediator of RANK-activated osteoclastogenesis. Dev. Cell 6, 303–309.

Duran, A., Amanchy, R., Linares, J.F., Joshi, J., Abu-Baker, S., Porollo, A., Hansen, M., Moscat, J., and Diaz-Meco, M.T. (2011). p62 is a key regulator of nutrient sensing in the mTORC1 pathway. Mol Cell 44, 134–146.

Duran, A., Hernandez, E.D., Reina-Campos, M., Castilla, E.A., Subramaniam, S., Raghunandan, S., Roberts, L.R., Kisseleva, T., Karin, M., Diaz-Meco, M.T., Moscat, J. (2016). p62/SQSTM1 by binding to vitamin D receptor inhibits hepatic stellate cell activity, fibrosis and liver cancer. Cancer Cell 30, 595–609.

Elpek, G.Ö. (2014). Cellular and molecular mechanisms in the pathogenesis of liver fibrosis: An update. World J Gastroenterol 20, 7260–7276.

Elpek, G.Ö. (2015). Angiogenesis and liver fibrosis. World J Hepatol 7, 377–391.

Fatehi-Hassanabad, Z., and Chan, C.B. (2005). Transcriptional regulation of lipid metabolism by fatty acids: a key determinant of pancreatic β-cell function. Nutr Metab (Lond) 2, 1.

García-Ruiz, I., Solís-Muñoz, P., Fernández-Moreira, D., Grau, M., Colina, F., Muñoz-Yagüe, T., and Solís-Herruzo, J.A. (2014). High-fat diet decreases activity of the oxidative phosphorylation complexes and causes nonalcoholic steatohepatitis in mice. Dis Model Mech 7, 1287–1296.

Gissen, P., and Arias, I.M. (2015). Structural and functional hepatocyte polarity and liver disease. J Hepatol 63, 1023–1037.

Gorden, D.L., Myers, D.S., Ivanova, P.T., Fahy, E., Maurya, M.R., Gupta, S., Min, J., Spann, N.J., McDonald, J.G., Kelly, S.L., Duan, J., Sullards, M.C., Leiker, T.J., Barkley, R.M., Quehenberger, O., Armando, A.M., Milne, S.B., Mathews, T.P., Armstrong, M.D., Li, C., Melvin, W.V., Clements, R.H., Washington, M.K., Mendonsa, A.M., Witztum, J.L., Guan, Z., Glass, C.K., Murphy, R.C., Dennis, E.A., Merril, A.H., Russell, D.W., Subramaniam, S., Brown, A. (2015). Biomarkers of NAFLD progression: a lipidomics approach to an epidemic. J Lipid Res 56, 722–736.

Herkel, J., Jagemann, B., Wiegard, C., Lazaro, J.F.G., Lueth, S., Kanzler, S., Blessing, M., Schmitt, E., and Lohse, A.W. (2003). MHC class II-expressing hepatocytes function as antigen-presenting cells and activate specific CD4 T lymphocyutes. Hepatology 37, 1079–1085.

Hernandez, E.D., Lee, S.J., Kim, J.Y., Duran, A., Linares, J.F., Yajima, T., Müller, T.D., Tschöp, M.H., Smith, S.R., Diaz-Meco, M.T., Moscat, J. (2014). A macrophage NBR1-MEKK3 complex triggers JNK-mediated adipose tissue inflammation in obesity. Cell Metab. 20, 499–511.

Hsu, P.P., and Sabatini, D.M. (2008). Cancer cell metabolism: Warburg and beyond. Cell 134, 703–707.

Hu, J., Ge, H., Newman, M., and Liu, K. (2012). OSA: a fast and accurate alignment tool for RNA-Seq. Bioinformatics 28, 1933–1934.

Iredale, J.P., Thompson, A., and Henderson, N.C. (2013). Extracellular matrix degradation in liver fibrosis: Biochemistry and regulation. Biochim. Biophys. Acta 1832, 876–883.

Kanehisa, M., and Goto, S. (2000). KEGG: kyoto encyclopedia of genes and genomes. Nucleic Acids Res. 28, 27–30.

Kanehisa, M., Sato, Y., Kawashima, M., Furumichi, M., and Tanabe, M. (2016). KEGG as a reference resource for gene and protein annotation. Nucleic Acids Res. 44, D457-462.

Kanehisa, M., Furumichi, M., Tanabe, M., Sato, Y., and Morishima, K. (2017). KEGG: new perspectives on genomes, pathways, diseases and drugs. Nucleic Acids Res. 45, D353–D361.

Kawano, Y., and Cohen, D.E. (2013). Mechanisms of hepatic triglyceride accumulation in non-alcoholic fatty liver disease. J Gastroenterol 48, 434–441.

Koo, S.-H. (2013). Nonalcoholic fatty liver disease: molecular mechanisms for the hepatic steatosis. Clin Mol Hepatol 19, 210–215.

Lahiri, P., Schmidt, V., Smole, C., Kufferath, I., Denk, H., Strnad, P., Rülicke, T., Fröhlich, L.F., and Zatloukal, K. (2016). p62/Sequestosome-1 Is Indispensable for Maturation and Stabilization of Mallory-Denk Bodies. PLoS ONE 11, e0161083.

Laplante, M., and Sabatini, D.M. (2012). mTOR signaling in growth control and disease. Cell 149, 274–293.

Larriba, M.J., González-Sancho, J.M., Bonilla, F., and Muñoz, A. (2014). Interaction of vitamin D with membrane-based signaling pathways. Front Physiol 5.

Lee, Y.-S., and Jeong, W.-I. (2012). Retinoic acids and hepatic stellate cells in liver disease. J. Gastroenterol. Hepatol. 27 Suppl 2, 75–79.

Lewis, J.R., and Mohanty, S.R. (2010). Nonalcoholic fatty liver disease: a review and update. Dig. Dis. Sci. 55, 560–578.

Liberti, M.V., and Locasale, J.W. (2016). The Warburg Effect: How Does it Benefit Cancer Cells? Trends Biochem Sci 41, 211–218.

Linares, J.F., Duran, A., Yajima, T., Pasparakis, M., Moscat, J., and Diaz-Meco, M.T. (2013). K63 Polyubiquitination and Activation of mTOR by the p62-TRAF6 Complex in Nutrient-Activated Cells. Mol Cell 51, 283–296.

Long, M., Li, X., Li, L., Dodson, M., Zhang, D.D., and Zheng, H. (2017). Multifunctional p62 Effects Underlie Diverse Metabolic Diseases. Trends Endocrinol. Metab. 28, 818–830.

Love, M.I., Huber, W., and Anders, S. (2014). Moderated estimation of fold change and dispersion for RNA-Seq data with DESeq2. Genome Biology 15, 550.

Lu, B., Bridges, D., Yang, Y., Fisher, K., Cheng, A., Chang, L., Meng, Z.-X., Lin, J.D., Downes, M., Yu, R.T., Liddle, C., Evans, R.M., Saltiel, A.R. (2014). Metabolic crosstalk: molecular links between glycogen and lipid metabolism in obesity. Diabetes 63, 2935–2948.

Mammen, E.F. (1992). Coagulation abnormalities in liver disease. Hematol. Oncol. Clin. North Am. 6, 1247–1257.

Markiewski, M.M., Mastellos, D., Tudoran, R., DeAngelis, R.A., Strey, C.W., Franchini, S., Wetsel, R.A., Erdei, A., and Lambris, J.D. (2004). C3a and C3b activation products of the third component of complement (C3) are critical for normal liver recovery after toxic injury. J. Immunol. 173, 747–754.

Matys, V., Kel-Margoulis, O.V., Fricke, E., Liebich, I., Land, S., Barre-Dirrie, A., Reuter, I., Chekmenev, D., Krull, M., and Hornischer, K. (2006). TRANSFAC® and its module TRANSCompel®: transcriptional gene regulation in eukaryotes. Nucleic Acids Research 34, D108–D110.

Min, J.S., DeAngelis, R.A., Reis, E.S., Gupta, S., Maurya, M.R., Evans, C., Das, A., Burant, C., Lambris, J.D., and Subramaniam, S. (2016). Systems analysis of the complement-induced priming phase of liver regeneration. J Immunol 197, 2500–2508.

Moscat, J., and Diaz-Meco, M.T. (2009). p62 at the crossroads of autophagy, apoptosis, and cancer. Cell 137, 1001–1004.

Moscat, J., and Diaz-Meco, M.T. (2012). p62: a versatile multitasker takes on cancer. Trends Biochem. Sci. 37, 230–236.

Müller, T.D., Lee, S.J., Jastroch, M., Kabra, D., Stemmer, K., Aichler, M., Abplanalp, B., Ananthakrishnan, G., Bhardwaj, N., Collins, S., Divanovic, S., Endele, M., Finan, B., Gao, Y., Harbegger, K.M., Hembree, J., Hepper, K.M, Hofmann, S., Holland, J., Kuchler, D., Krishna, R., Lehti, M., Oelkrug, R., Ottaway, N., Perez-Tilve, D., Raver, C., Walch, A.K., Schriever, S.C., Speakman, J., Tseng, Y.H., Diaz-Meco, M., Pfluger, P.T., Moscat, J., Tschop, M.H. (2013). p62 links β-adrenergic input to mitochondrial function and thermogenesis. J. Clin. Invest. 123, 469–478.

Nguyen, P., Leray, V., Diez, M., Serisier, S., Bloc'h, J.L., Siliart, B., and Dumon, H. (2008). Liver lipid metabolism. Journal of Animal Physiology and Animal Nutrition 92, 272–283.

Nwosu, Z.C., Megger, D.A., Hammad, S., Sitek, B., Roessler, S., Ebert, M.P., Meyer, C., and Dooley, S. (2017). Identification of the Consistently Altered Metabolic Targets in Human Hepatocellular Carcinoma. Cellular and Molecular Gastroenterology and Hepatology 4, 303–323.e1.

Park, O.K., Schaefer, T.S., and Nathans, D. (1996). In vitro activation of Stat3 by epidermal growth factor receptor kinase. Proc Natl Acad Sci U S A 93, 13704–13708.

Paschos, P., and Paletas, K. (2009). Non alcoholic fatty liver disease and metabolic syndrome. Hippokratia 13, 9–19.

Pellicoro, A., Ramachandran, P., Iredale, J.P., and Fallowfield, J.A. (2014). Liver fibrosis and repair: immune regulation of wound healing in a solid organ. Nat. Rev. Immunol. 14, 181–194.

Pettinelli, P., Obregón, A.M., and Videla, L.A. (2011). Molecular mechanisms of steatosis in nonalcoholic fatty liver disease. Nutr Hosp 26, 441–450.

Pio, R., Ajona, D., and Lambris, J.D. (2013). Complement inhibition: a promising concept for cancer treatment. Semin Immunol 25, 54–64.

Poli, G., Albano, E., and Dianzani, M.U. (1987). The role of lipid peroxidation in liver damage. Chem. Phys. Lipids 45, 117–142.

Qin, X., and Gao, B. (2006). The complement system in liver diseases. Cell. Mol. Immunol. 3, 333–340.

Radisky, D.C., Kenny, P.A., and Bissell, M.J. (2007). Fibrosis and Cancer: Do Myofibroblasts Come Also From Epithelial Cells Via EMT? J Cell Biochem 101, 830–839.

Rawlings, J.S., Rosler, K.M., and Harrison, D.A. (2004). The JAK/STAT signaling pathway. J. Cell. Sci. 117, 1281–1283.

Reis, E.S., Mastellos, D.C., Ricklin, D., Mantovani, A., and Lambris, J.D. (2017). Complement in cancer: untangling an intricate relationship. Nat. Rev. Immunol.

Rensen, S.S., Slaats, Y., Driessen, A., Peutz-Kootstra, C.J., Nijhuis, J., Steffensen, R., Greve, J.W., and Buurman, W.A. (2009). Activation of the complement system in human nonalcoholic fatty liver disease. Hepatology 50, 1809–1817.

Reuter, S., Gupta, S.C., Chaturvedi, M.M., and Aggarwal, B.B. (2010). Oxidative stress, inflammation, and cancer: how are they linked? Free Radic. Biol. Med. 49, 1603–1616.

Robinson, M.W., Harmon, C., and O'Farrelly, C. (2016). Liver immunology and its role in inflammation and homeostasis. Cell Mol Immunol 13, 267–276.

Rodriguez, A., Durán, A., Selloum, M., Champy, M.-F., Diez-Guerra, F.J., Flores, J.M., Serrano, M., Auwerx, J., Diaz-Meco, M.T., and Moscat, J. (2006). Mature-onset obesity and insulin resistance in mice deficient in the signaling adapter p62. Cell Metab. 3, 211–222.

Rowell, D.L., Eckmann, L., Dwinell, M.B., Carpenter, S.P., Raucy, J.L., Yang, S.K., and Kagnoff, M.F. (1997). Human hepatocytes express an array of proinflammatory cytokines after agonist stimulation or bacterial invasion. Am. J. Physiol. 273, G322-332.

Rui, L. (2014). Energy metabolism in the liver. Compr Physiol 4, 177–197.

Schindler, C., Levy, D.E., and Decker, T. (2007). JAK-STAT signaling: from interferons to cytokines. J. Biol. Chem. 282, 20059–20063.

Shen, H., French, B.A., Liu, H., Tillman, B.C., and French, S.W. (2014). Increased activity of the complement system in the liver of patients with alcoholic hepatitis. Exp Mol Pathol 97, 338–344.

Soardo, G., Donnini, D., Domenis, L., Catena, C., De Silvestri, D., Cappello, D., Dibenedetto, A., Carnelutti, A., Bonasia, V., Pagano, C., Sechi, L.A. (2011). Oxidative stress is activated by free fatty acids in cultured human hepatocytes. Metab Syndr Relat Disord 9, 397–401.

Stumptner, C., Heid, H., Fuchsbichler, A., Hauser, H., Mischinger, H.-J., Zatloukal, K., and Denk, H. (1999). Analysis of intracytoplasmic hyaline bodies in a hepatocellular carcinoma: demonstration of p62 as major constituent. The American Journal of Pathology 154, 1701–1710.

Stumptner, C., Fuchsbichler, A., Zatloukal, K., and Denk, H. (2007). In vitro production of Mallory bodies and intracellular hyaline bodies: the central role of sequestosome 1/p62. Hepatology 46, 851–860.

Thalheimer, U., Triantos, C.K., Samonakis, D.N., Patch, D., and Burroughs, A.K. (2005). Infection, coagulation, and variceal bleeding in cirrhosis. Gut 54, 556–563.

Tsuchida, T., and Friedman, S.L. (2017). Mechanisms of hepatic stellate cell activation. Nat Rev Gastroenterol Hepatol 14, 397–411.

Volanakis, J.E. (1995). Transcriptional regulation of complement genes. Annu. Rev. Immunol. 13, 277–305.

Weiskirchen, R., and Tacke, F. (2014). Cellular and molecular functions of hepatic stellate cells in inflammatory responses and liver immunology. Hepatobiliary Surg Nutr 3, 344–363.

Wu, W., and Zhao, S. (2013). Metabolic changes in cancer: beyond the Warburg effect. Acta Biochim Biophys Sin (Shanghai) 45, 18–26.

Yang, J.-Q., Liu, H., Diaz‐Meco, M.T., and Moscat, J. (2010). NBR1 is a new PB1 signalling adapter in Th2 differentiation and allergic airway inflammation in vivo. The EMBO Journal 29, 3421–3433.

Younossi, Z.M., Koenig, A.B., Abdelatif, D., Fazel, Y., Henry, L., and Wymer, M. (2016). Global epidemiology of nonalcoholic fatty liver disease-Meta-analytic assessment of prevalence, incidence, and outcomes. Hepatology 64, 73–84.

Zatloukal, K., Stumptner, C., Fuchsbichler, A., Heid, H., Schnoelzer, M., Kenner, L., Kleinert, R., Prinz, M., Aguzzi, A., and Denk, H. (2002). p62 Is a common component of cytoplasmic inclusions in protein aggregation diseases. The American Journal of Pathology 160, 255–263.

CHAPTER 4 : CONCLUSIONS & FUTURE DIRECTION

In this thesis we have explored the mechanisms of stress response using a systems biology approach. In Chapters 2 and 3, we identified key sensors, transducers, and transcriptional regulators of the oxidative stress response in endothelial cells and high-fat diet and carcinogen mediated liver toxicity. The use of high-throughput measurements across varying doses, times, and cell-types has guided a holistic approach to characterizing cellular dysfunction and identifying novel mechanisms of stress response. While this approach has progressed our understanding of endothelial and liver pathologies, there are several biological and technical challenges that limit our understanding of the cellular stress response. Additionally, the high-level comparison of the *in vitro* study presented in Chapter 2 and the *in vivo* study presented in Chapter 3 highlights important biological and technical parameters that are important to consider in characterizing mechanisms of stress response.

4.1 Biological & Technical Challenges in Characterizing the Oxidative Stress Response

Endothelial cells (ECs) make up the barrier between circulating blood and the surrounding tissues. They not only regulate the passage of signaling molecules and immune cells into the surrounding tissue but are the first line of defense against toxins and pathogens. While the fundamental role of endothelial cells (ECs) throughout the body is well defined, there are site-specific and context-specific variations in endothelial function that should be taken into account when characterizing mechanisms of stress response using ECs from a particular source (Aird, 2012) (Chiu and Chien, 2011). This is critically important in understanding the role of angiogenesis in promoting cancer (Aird, 2009). Also, oxidative stress (whether it's exogenous or endogenous) is often present with other stressors such as paracrine factors secreted by the surrounding smooth muscle cells or adherent immune cells. Therefore, studies should optimize

media and culture conditions such that the artificial environment *in vitro* closely mimics the disease state (Truskey, 2010).

While each of the possible endogenous and exogenous sources of reactive oxygen species connote different biochemical/physiological circumstances, the addition of hydrogen peroxide to cell culture is the preferred method of inducing oxidative stress since it is the easiest and most cost-effective method *in vitro* (Zhou et al., 2013) (Csordas et al., 2006) (Wen et al., 2013) (Gong et al., 2010) (Clément et al., 1998) (Xu et al., 2013) (van Gorp et al., 1999) (Nadeev et al., 2015) (Messner et al., 2012). The instability of hydrogen peroxide and the generation of exogenous hydrogen peroxide by components of the cell culture media (Long et al., 2010) should be taken into account when optimizing the effective treatment dose for *in vitro* studies and therapeutic parameters for *in vivo* models of oxidative stress.

Chapter 2 also highlights the importance of temporal dynamics in stress response. Collecting time-series measurements allows us to cluster samples from each time point in order to identify clear temporal phases of stress response. This is highly dependent on the inter-replicate variance. Our analysis highlights mechanisms present at the nexus between the acute response and the chronic response, which is critically important in understanding the initiation of chronic stress states and identifying early biomarkers of disease. Additionally, the concurrent activation of pro-death and pro-survival mechanisms summarized in our temporal model reiterates the complexity and stochasticity in cell fate decisions (Flusberg and Sorger, 2015). Given that many of the proteins involved in cell fate decisions have functions separate from coordinating cell fate, it is important to consider the pleiotropic functions of proteins and the diversity of protein function derived by spliced variants when interpreting transcriptomic data.

The use of Systems Biology allows us to address some of these challenges. High-throughput measurements taken from multiple types of endothelial cells in parallel cultures may provide valuable insight on endothelial heterogeneity. Similarly, the use of time-course experiments that are informed by dose-dependent measurements allow us to identify phenotypically relevant inflection points. Taken together, the development of more sophisticated co-culture models and the inclusion of dose- and time-series high-throughput measurements will further support our efforts to characterize stress response.

4.2 Biological and Technical Challenges in Characterizing Liver Toxicity

Chapter 3 examines the complexity of stress response due to the coordinated effort by multiple cell types and organs. It is important to note that p62 is a central autophagic protein and signaling scaffold in many tissues, however, the effect of p62 ablation in each tissue has a different effect (Long et al., 2017). For example, while in hepatocytes the loss of p62 is protective (Umemura et al., 2016), p62 ablation in stellate cells results in the activation of pro-fibrogenic programs (Duran et al., 2016). An added layer of complexity is introduced by the fact that many cells are transformed into myofibroblast like cells in case of chronic hepatic stress, making it more challenging to identify the true distribution of cell types in a given tissue sample.

Interestingly, we found that there was a marginal de-repression of metabolic gene expression in the DKO compared to the p62KO. This highlights that not all stress response processes are binary transitions from active to inactive states. Additionally, this emphasizes the importance of using high-throughput measurements such that global changes in gene expression (however subtle at the gene level) can be identified and characterized. Another critical question that arises when thinking about metabolic dampening is whether the dampening is due to inherent changes in the transcriptional regulation of metabolism or due to a change in the fraction of

tumorigenic vs. healthy hepatocytes in the liver. Sorting by cell type and/or using single-cell sequencing techniques would be very useful in untangling the cell-type specific mechanisms of stress response. Taken together, it is clear that there are many challenges in understanding the sometimes diverging role of a given protein across various tissues in coordinating the progression or prevention of disease. The continued development of tissue specific gene ablation models and use of high-throughput measurements will provide a greater understanding of stress response in various diseases.

4.3 Future Directions: Implications for Designing Therapeutics

First, the mechanistic insights gained from the systems level analyses of stress response in both models of stress provide exciting avenues of therapeutic design for cardiovascular and liver diseases. Additionally, this analysis has reinforced many principles of stress response such as dose- and time-dependence, the heterogeneity of transcriptional regulation at the nexus between cell fates, and paracrine effects on stress response and disease progression. It is also important to note that in both studies we identified gatekeepers of global transcriptional regulation in response to stress; this suggests the importance of testing the effect of therapeutics on the function of the known global stress regulators in order to minimize off-target effects. The differences found in the comparison of mouse data to human data provides support for using mouse models to recapitulate human diseases and highlights key species-specific differences that are important to consider when designing therapies.

4.4 References

Aird, W.C. (2009). Molecular heterogeneity of tumor endothelium. Cell Tissue Res. 335, 271–281.

Aird, W.C. (2012). Endothelial Cell Heterogeneity. Cold Spring Harb Perspect Med 2.

Chiu, J.-J., and Chien, S. (2011). Effects of disturbed flow on vascular endothelium: pathophysiological basis and clinical perspectives. Physiological Reviews 91, 327–387.

Clément, M.-V., Ponton, A., and Pervaiz, S. (1998). Apoptosis induced by hydrogen peroxide is mediated by decreased superoxide anion concentration and reduction of intracellular milieu. FEBS Letters 440, 13–18.

Csordas, A., Wick, G., and Bernhard, D. (2006). Hydrogen peroxide-mediated necrosis induction in HUVECs is associated with an atypical pattern of caspase-3 cleavage. Experimental Cell Research 312, 1753–1764.

Duran, A., Hernandez, E.D., Reina-Campos, M., Castilla, E.A., Subramaniam, S., Raghunandan, S., Roberts, L.R., Kisseleva, T., Karin, M., Diaz-Meco, M.T., Moscat, J. (2016). p62/SQSTM1 by binding to vitamin D receptor inhibits hepatic stellate cell activity, fibrosis and liver cancer. Cancer Cell 30, 595–609.

Flusberg, D.A., and Sorger, P.K. (2015). Surviving apoptosis: life-death signaling in single cells. Trends Cell Biol 25, 446–458.

Gong, G., Qin, Y., Huang, W., Zhou, S., Yang, X., and Li, D. (2010). Rutin inhibits hydrogen peroxide-induced apoptosis through regulating reactive oxygen species mediated mitochondrial dysfunction pathway in human umbilical vein endothelial cells. European Journal of Pharmacology 628, 27–35.

van Gorp, R.M., Broers, J.L., Reutelingsperger, C.P., Bronnenberg, N.M., Hornstra, G., van Dam-Mieras, M.C., and Heemskerk, J.W. (1999). Peroxide-induced membrane blebbing in endothelial cells associated with glutathione oxidation but not apoptosis. American Journal of Physiology-Cell Physiology 277, C20–C28.

Long, L.H., Hoi, A., and Halliwell, B. (2010). Instability of, and generation of hydrogen peroxide by, phenolic compounds in cell culture media. Arch. Biochem. Biophys. 501, 162–169.

Long, M., Li, X., Li, L., Dodson, M., Zhang, D.D., and Zheng, H. (2017). Multifunctional p62 Effects Underlie Diverse Metabolic Diseases. Trends Endocrinol. Metab. 28, 818–830.

Messner, B., Frotschnig, S., Steinacher-Nigisch, A., Winter, B., Eichmair, E., Gebetsberger, J., Schwaiger, S., Ploner, C., Laufer, G., and Bernhard, D. (2012). Apoptosis and necrosis: two different outcomes of cigarette smoke condensate-induced endothelial cell death. Cell Death Dis 3, e424.

Nadeev, A.D., Kudryavtsev, I.V., Serebriakova, M.K., Avdonin, P.V., Zinchenko, V.P., and Goncharov, N.V. (2015). [DUAL PROAPOPTOTIC AND PRONECROTIC EFFECT OF HYDROGEN PEROXIDE ON HUMAN UMBILICAL VEIN ENDOTHELIAL CELLS]. Tsitologiia 57, 909–916.

Truskey, G.A. (2010). Endothelial Cell Vascular Smooth Muscle Cell Co-Culture Assay For High Throughput Screening Assays For Discovery of Anti-Angiogenesis Agents and Other Therapeutic Molecules. International Journal of High Throughput Screening 2010, 171.

Umemura, A., He, F., Taniguchi, K., Nakagawa, H., Yamachika, S., Font-Burgada, J., Zhong, Z., Subramaniam, S., Raghunandan, S., Duran, A., Linares, J.F., Reina-Campos, M., Umemura, S., Valasek, M.A., Seki, E., Yamaguchi, K., Koike, K., Itoh, Y., Diaz-Meco, M.T., Moscat, J., Karin,

M.. (2016). p62, upregulated during preneoplasia, induces hepatocellular carcinogenesis by maintaining survival of stressed HCC-initiating cells. Cancer Cell 29, 935–948.

Wen, Y.-D., Wang, H., Kho, S.-H., Rinkiko, S., Sheng, X., Shen, H.-M., and Zhu, Y.-Z. (2013). Hydrogen sulfide protects HUVECs against hydrogen peroxide induced mitochondrial dysfunction and oxidative stress. PLoS One 8, e53147.

Xu, M.-C., Shi, H.-M., Wang, H., and Gao, X.-F. (2013). Salidroside protects against hydrogen peroxide-induced injury in HUVECs via the regulation of REDD1 and mTOR activation. Molecular Medicine Reports 8, 147–153.

Zhou, X., Yuan, D., Wang, M., and He, P. (2013). H2O2-induced endothelial NO production contributes to vascular cell apoptosis and increased permeability in rat venules. Am. J. Physiol. Heart Circ. Physiol. 304, H82-93.